A GUIDE TO REGIONAL GROUNDWATER FLOW IN FRACTURED ROCK AQUIFERS

Peter G. Cook
CSIRO Land and Water, Glen Osmond, SA, Australia

Inquiries should be made to:
Seaview Press
PO Box 234
Henley Beach, South Australia 5022
Telephone 08 8235 1535; fax 08 8235 9144
E-mail: seaview@seaviewpress.com.au
Web site: http://www.seaviewpress.com.au

Printed by:
CM Digital
234 Currie Street
Adelaide, South Australia 5000

Cover Photo. Fractured Ordovician metasediments, Wagga Wagga, New South Wales. Author's photo

National Library of Australia Cataloguing-in-Publication entry
Cook, P. G. (Peter G.).
A guide to regional groundwater flow in fractured rock aquifers.

Bibliography.
ISBN 1 74008 233 8.

1. Groundwater - Australia. 2. Aquifers - Australia.
3. Water chemistry - Australia. I. Title.

553.790994


CSIRO


Land & Water
AUSTRALIA

LIST OF CONTRIBUTORS

The following people assisted in compiling this volume:

Mike Williams
Department of Land and Water Conservation, NSW, Australia

Craig Simmons
Flinders University of South Australia, SA, Australia

Andrew Love
Department of Water, Land and Biodiversity Conservation, SA, Australia

Todd Halihan
Oklahoma State University, OK, USA

Graham Herbert
Department of Natural Resources and Mines, Qld, Australia

Graham Heinson
Adelaide University, SA, Australia

PREFACE

The purpose of this guidebook is to describe field methods that can be used for characterising groundwater flow in fractured rocks, and to discuss some of the problems inherent with several of the traditional techniques that are routinely applied in porous media aquifers. Much of the research into groundwater flow in fractured rocks has been focused on the contaminant-remediation and nuclear-waste-disposal industries. In contrast, this book concentrates on characterisation of groundwater flow for regional groundwater resource assessment, which has received relatively little attention. The book also focuses on groundwater quantity, and does not discuss water quality or hydrochemistry, except where this can be used to quantify groundwater flows or aquifer recharge rates.

The book draws heavily on the results of three recent studies into groundwater quantity sustainability in fractured rock aquifers in Australia. These studies, in part funded by Land and Water Australia, took place in the Clare Valley, South Australia, Atherton Tablelands, Queensland, and Wagga Wagga, New South Wales. The studies provided an opportunity to develop and test various methods for characterising groundwater flow in fractured rock systems. However, this book is not limited to these studies, but also includes examples from a number of studies carried out in different parts of the world. In the interests of readability, we have not included a complete and in-depth discussion of any of the techniques that are presented. Instead, we refer the reader to other reports and papers for this information. Our intended audience is practising hydrogeologists in government agencies and private consulting firms, who are required to conduct studies on fractured rock systems. The book is thus a practical guide, and not a theoretical treatment of the topic. It also assumes that the reader is familiar with methods for estimating groundwater flow in porous media.

TABLE OF CONTENTS

LIST OF CONTRIBUTORS iv

PREFACE v

1. BASIC PRINCIPLES 1

1.1. INTRODUCTION 1
1.1.1. Classification of fractured rock aquifers 1
1.1.2. Fracture and matrix porosity 2
1.1.3. Types of fractures 2
1.1.4. Water flow and solute transport 3
1.2. FLOW AND TRANSPORT THROUGH A SINGLE PLANAR FRACTURE 4
1.3. THE PARALLEL PLATE MODEL 5
1.3.1. Groundwater flow 5
1.3.2. Solute transport 8
1.4. FROM PARALLEL PLATES TO FRACTURED ROCK AQUIFERS 10

2. MAJOR ROCK TYPES 14

2.1. CRYSTALLINE ROCKS 14
2.2. VOLCANIC ROCKS 15
2.3. CARBONATE ROCKS 18
2.4. CLASTIC FORMATIONS 21
2.5. DYKES AND SILLS 23

3. GEOLOGICAL CHARACTERISATION 25

3.1. INTRODUCTION 25
3.2. CHARACTERISING FRACTURES 25
3.2.1. Number of sets 25
3.2.2. Orientation 26
3.2.3. Spacing 29
3.2.4. Fracture length 31
3.2.5. Fracture connectivity 31
3.2.6. Aperture 31
3.2.7. Surface roughness 33
3.3. CHARACTERISING THE ROCK MATRIX 34
3.3.1. Matrix porosity 34
3.3.2. Matrix permeability 35
3.3.3. Matrix diffusion coefficients 35
3.4. IDENTIFYING FRACTURES FROM BOREHOLE LOGGING 37
3.5. LINEAMENT MAPPING 40

4. AQUIFER HYDRAULICS 42

4.1. MEASUREMENT OF HYDRAULIC HEAD 42
4.2. MEASUREMENT OF AQUIFER HYDRAULIC CONDUCTIVITY 46
4.2.1. Introduction 46
4.2.2. Pumping tests 47
4.2.3. Borehole flowmeters 52
4.2.4. Tracer approaches 52
4.3. SURFACE GEOPHYSICS FOR MAPPING RADIAL ANISOTROPY 55

5. GROUNDWATER FLOW, AQUIFER RECHARGE AND DISCHARGE 59

5.1. INTRODUCTION 59
5.2. DARCY'S LAW 59
5.3. POINT DILUTION AND WELL DILUTION METHODS 62
5.3.1. Introduction 62
5.3.2. Point dilution 62
5.3.3. Radon 63
5.3.4. Well dilution 67
5.4. APPLIED TRACER TESTS 70
5.5. GROUNDWATER DATING 71
5.6. INFERRING RECHARGE FROM HYDROGRAPH RESPONSE 74
5.7. CHLORIDE MASS BALANCE 77
5.8. GROUNDWATER DISCHARGE 80

6. GROUNDWATER MODELLING 83

6.1. INTRODUCTION 83
6.2. CONCEPTUAL AND MATHEMATICAL MODELS 83
6.3. EQUIVALENT POROUS MEDIUM APPROACH 85
6.4. DUAL-POROSITY MODELS 86
6.5. DISCRETE FRACTURE NETWORK MODELS 87
6.6. STOCHASTIC MODELS 91
6.7. ANALYTICAL SOLUTIONS 91
6.8. COMPARISON OF APPROACHES 92
6.9. CONCLUSION 98

7. REFERENCES 100

1. BASIC PRINCIPLES

1.1. Introduction

All aquifers contain some degree of heterogeneity. In many cases, the degree of heterogeneity is relatively low, and does not need to be explicitly considered in groundwater investigations. Where aquifer heterogeneity is more pronounced, however, it can have important implications for how we measure groundwater processes. The fundamental characteristic of fractured rock aquifers is extreme spatial variability in hydraulic conductivity, and hence groundwater flow rate. Hydraulic properties can also be highly anisotropic, so that hydraulic properties must be defined in conjunction with directional information. Water velocities through individual fractures can be extremely high, but the fractures usually occupy only a very small fraction of the aquifer. Thus, even when water velocities through individual fractures may be high, average volumetric flow rates through the aquifer can be quite low. Because of this heterogeneity, a number of methods that are traditionally used for characterising porous media aquifer systems are of limited value in fractured rock aquifers.

1.1.1. Classification of fractured rock aquifers

All aquifers can be considered to fall on a continuum between porous media systems and conduit systems (Fig. 1.1). In *homogeneous porous media* aquifers (Fig. 1.1a), groundwater flows through gaps between the sand grains. In *heterogeneous porous media* aquifers (Fig. 1.1b), systematic variation in the size of the sand grains leads to the existence of preferential flow zones. At the other extreme, in *purely fractured media* (Fig. 1.1e) groundwater flows only in conduits, and the aquifer matrix between the conduits is impermeable and has no porosity. In *fractured porous media* water is also stored in the aquifer matrix between the conduits. In some cases, the matrix permeability is negligible (Fig. 1.1d), although in other cases it can contribute significantly to flow (Fig. 1.1c). In reality, most fractured rock aquifers are of the fractured porous media type. Models of groundwater flow, however, usually assume either homogeneous porous media or purely fractured media. Furthermore, models of groundwater flow in purely fractured systems usually assume that fractures are planar and parallel and many also assume that the fractures are identical. While these assumptions are unlikely to be true in reality, they provide a useful starting point for our understanding of groundwater behaviour in fractured rocks.

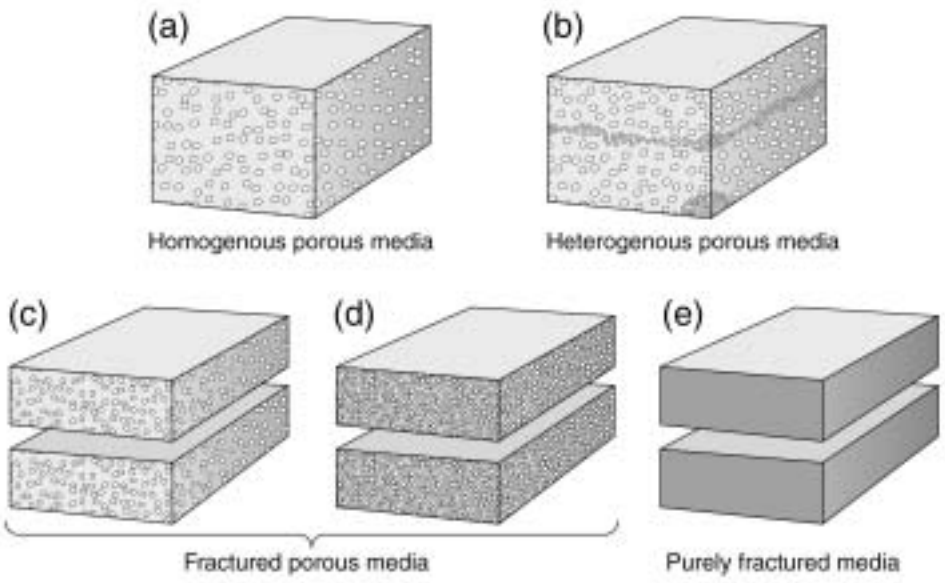

Figure 1.1. Classification of porous and fractured rocks: a) homogeneous porous media, b) heterogeneous porous media, c) fractured porous media with significant permeability in the aquifer matrix, d) fractured porous media with significant porosity, but negligible permeability in the aquifer matrix, e) purely fractured media, with zero porosity and zero permeability within the aquifer matrix.

1.1.2. Fracture and matrix porosity

Fractured rock aquifers are comprised of a network of fractures that cut through a rock matrix. Characterisation of fractured rock aquifers thus requires information on the nature of both the fractures and the rock matrix. Fractures can be characterised in terms of their dimensions (aperture, length, width), their location (orientation, spacing, etc) and the nature of the fracture walls (e.g., surface roughness). The rock matrix is characterised by its pore size distribution, often expressed in terms of porosity and hydraulic conductivity.

The *fracture porosity* (β_f) is defined as the total volume of the aquifer occupied by open fractures. The *matrix porosity* (β_m) is the porosity of the rock matrix. In most cases, $\beta_m >> \beta_f$. The *total porosity* is given by:

$$-_t = -_f + -_m\left(1 - -_f\right) \qquad (1.1)$$

1.1.3. Types of fractures

Fractures (or *joints*) are planes along which stress has caused partial loss of cohesion in the rock. Conventionally, a fracture or joint is defined as a plane where there is hardly any visible movement parallel to the surface of the fracture; otherwise, it is classified as a fault. In practice, however, a precise distinction may be difficult, as at times within one set of fractures some planes

may show some displacement whereas others may not exhibit any movement. Fractures can be classified in several ways based on their geometric relationship with bedding or foliation. Strike joints are those that strike parallel to the strike of the bedding or foliation of the rock. In dip joints, the strike direction of joints runs parallel to the dip direction of the rock. Oblique or diagonal joints strike at an angle to the strike of the rock. Bedding joints are parallel to the bedding plane. Further, depending upon the strike trend of fractures with respect to the regional fold axis, fractures are designated as longitudinal (parallel), transverse (perpendicular) or oblique (Singhal & Gupta, 1999). The relationship between fractures and the stresses that form them is discussed in most structural geology texts.

Sheeting joints are generally flat, or somewhat curved and nearly parallel to the topographic surface, and often develop due to release of overburden stress in granitoid rocks. They are closely developed near to the surface and their spacing increases with depth. *Columnar joints* are generated due to shrinkage in rocks; igneous rocks contract on cooling, whereas mud and silt shrink because of desiccation. As a result, polygonal and columnar joints develop. The columns are often five- or six-sided, generally range from a few centimetres to a metre in diameter, and are several metres high.

1.1.4. Water flow and solute transport

In some cases, fractures become filled with minerals or clay deposits. Where they remain open, however, they can form channels for groundwater flow. Because frictional forces operate along the fracture walls, the velocity of water moving through a fracture will be greatest toward the middle of the fracture. If the hydraulic gradient is constant, then the mean water velocity through a fracture (averaged over the fracture width) will increase as the distance between the walls increases. The mean velocity will also be greater if the fracture walls are flat and smooth, rather than irregular and rough.

While groundwater flow in fractured porous media occurs mainly through fractures, much of the water contained within these aquifers is stored within the matrix. This has important implications for the movement of contaminants or other dissolved substances. Even if the permeability of the matrix is very low, diffusion will cause mixing of solutes in water flowing through the fractures with those in the relatively immobile water in the rock matrix. In practice, this means that dissolved substances usually appear to travel more slowly than water. Experimental studies have observed that very large particles (glass beads and bacteriophage) may travel very quickly (because they move through the fractures and do not readily enter the small pores within the matrix), while smaller solutes (including most ions) move more slowly. For example, in fractured shale near Oak Ridge, Tennessee, velocities

of small glass beads have been measured to be up to 200 m day^{-1} (McKay *et al*., 2000). In southern Ontario, Canada, bacteriophage have been observed to travel at 4 m day^{-1}, while dissolved bromide travels at only 4 cm day^{-1} (McKay *et al.*, 1993). This movement of solutes between the fractures and the matrix is referred to as *matrix diffusion*. It causes smaller molecules to appear to move more slowly than larger molecules, depending on their diffusion coefficients.

1.2. Flow and transport through a single planar fracture

We can represent a fracture as a planar void with two flat parallel surfaces. The hydraulic conductivity of this fracture is defined as:

$$K_f = (2b)^2 \frac{\rho g}{12\mu} \qquad (1.2)$$

where *2b* is the fracture aperture, β is the density of water, *g* is acceleration due to gravity and μ is the viscosity of water.[1] The mean groundwater velocity through the fracture, V_w, can be calculated as the product of the fracture hydraulic conductivity and the hydraulic gradient:

$$V_w = K_f \frac{\delta i}{\delta z} \qquad (1.3)$$

where $\beta i/\beta z$ is the hydraulic gradient. The transmissivity of an individual fracture is then:

$$T_f = (2b)^3 \frac{\rho g}{12\mu} \qquad (1.4)$$

If the aquifer matrix is impermeable, then the transmissivity of any interval of aquifer is calculated by summing the transmissivities of the fractures within that interval. Where an interval contains only a single fracture, the transmissivity of the interval is simply equal to the transmissivity of that fracture.

If the aquifer matrix is impermeable but has significant porosity, then solute transport is affected by matrix diffusion. Suppose that water within a fracture initially has a solute concentration of zero, and we then release a conservative tracer into the fractures, at a concentration that we will denote by c_0, and that this release continues over time. The distance that the tracer will have moved after a given period of time, *t*, can be expressed:

$$x = V_w b \sqrt{\frac{t}{D\theta_m}} \qquad (1.5)$$

---

[1] For freshwater at 20°C, β = 1.00 g cm^{-3}, and μ = 1.00 mPa s, and so

$\frac{\rho g}{\mu}$ = 8.6 ρ 10^6 $m^{\rho 1}s^{\rho 1}$ = 7.4 ρ 10^{11} $m^{\rho 1}day^{\rho 1}$

where V_w is the water velocity within the fractures and D is the effective diffusion coefficient within the matrix.[2,3] Thus for a water velocity in the fractures of 35 m day^{-1}, fracture aperture of $2b$ = 250 µm, matrix porosity β_m = 0.05 and diffusion coefficient $D = 10^{-4}$ m^2 yr^{-1}, the solute will travel 1386 m in 1 year. This is much less than the travel distance of the water, which is approximately 13 km (V_w β t). Whereas in porous media the distance travelled by a solute is directly proportional to the travel time, the distance travelled through a fracture is proportional to the square root of time. This means that if the solute travels 10 m in the first year, it will travel a further 4 m (and not 10 m) in the following year.

1.3. The parallel plate model

1.3.1. Groundwater flow

Consider a system of evenly spaced, identical, planar, parallel fractures in an impermeable rock matrix. The hydraulic conductivity of the medium in the direction parallel to the fractures can be expressed:

$$K = \frac{(2b)^3}{2B}\frac{\rho g}{12\mu} \qquad (1.6)$$

where $2B$ is the fracture spacing.[4] In any other direction, the hydraulic conductivity is zero. This equation is sometimes referred to as the *cubic law*, because of the nature of the dependence of hydraulic conductivity on fracture aperture. A doubling of fracture aperture results in a factor-of-eight increase in hydraulic conductivity. The relationship is shown graphically in Figure 1.2. For example, a fractured media with a fracture spacing of $2B$ = 1 m and fracture aperture of $2b$ = 250 µm, will have a hydraulic conductivity of approximately 10^{-5} m s^{-1}, similar to that of a coarse sand. It will also have the same hydraulic conductivity as a fractured media with a fracture spacing of 10 cm, and fracture aperture of 115 µm (Fig. 1.3).

---

[2] This equation describes the distance along the fracture where the concentration is equal to $c_0/2$. It is simplified from Equation 3.6 of Lever and Bradbury (1985).

[3] The diffusion coefficient in the matrix is defined by $D = D_0\beta_m\beta$, where D_0 is the free solution diffusion coefficient for the particular solute species, β_m is the matrix porosity and β is the tortuosity within the matrix.

[4] The quantity $\frac{(2b)^3}{12(2B)}$ is often referred to as the permeability, and has units of m^2 or Darcy.

For flow in freshwater, a permeability of 1 Darcy = 10^{-12} m^2 is equivalent to an hydraulic conductivity of 0.75 m day^{-1} (8.6 β 10^{-6} m s^{-1})

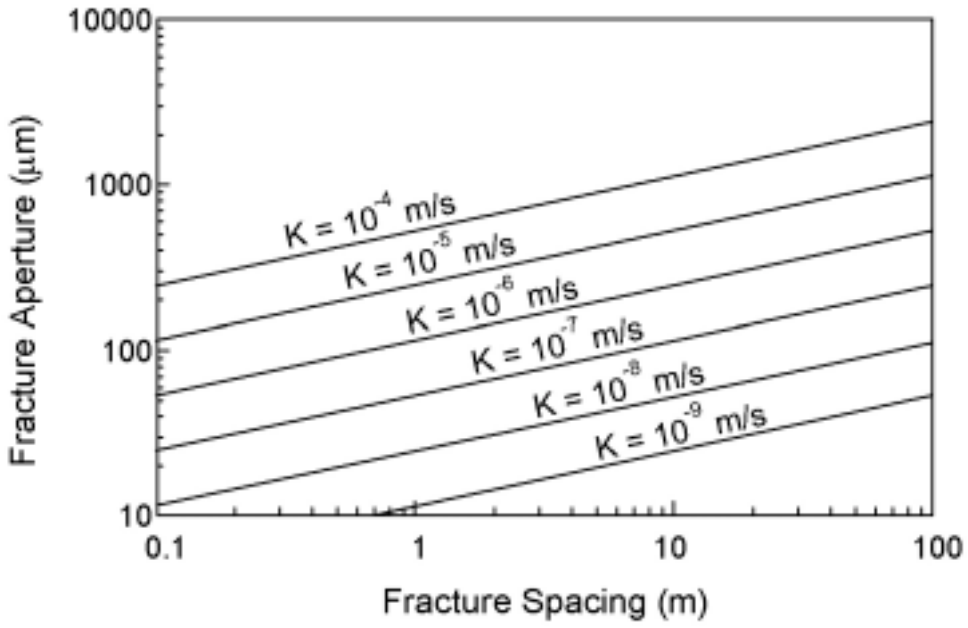

Figure 1.2. Relationship between fracture aperture, fracture spacing and aquifer hydraulic conductivity, for an aquifer consisting of planar, parallel uniform fractures. This figure can be simply derived using Equation 1.6.

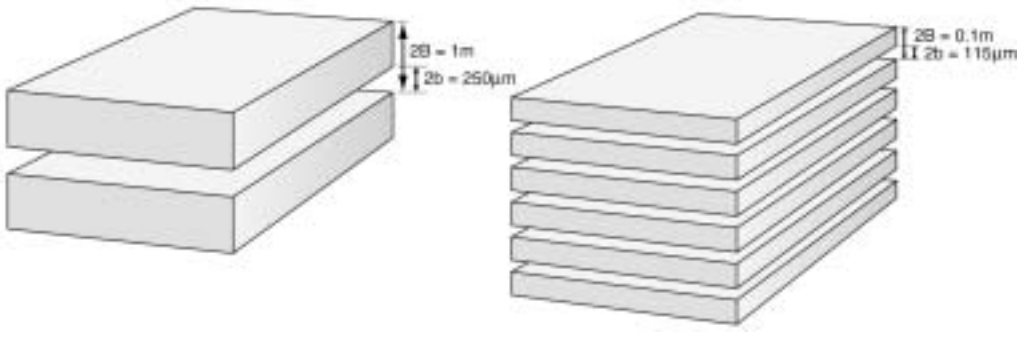

Figure 1.3. Two different fractured rock systems with identical hydraulic conductivities (10^{-5} m s^{-1}). a) aquifer comprising identical planar, parallel fractures, with fracture aperture of 250 µm and fracture spacing of 1 m, b) aquifer comprising identical planar, parallel fractures, with fracture aperture of 115 µm, and fracture spacing of 0.1 m.

The mean groundwater flow rate (sometimes called the Darcy velocity), q, is the amount of water that the aquifer transmits, per unit cross-sectional area. It is given by Darcy's law:

$$q = K\frac{\delta i}{\delta z} \qquad (1.7)$$

where $\beta i/\beta z$ is the hydraulic gradient. In a homogeneous porous media, the groundwater flow rate is related to the groundwater velocity by $q = v\theta$, where β is the porosity of the porous media. In a purely fractured media, the groundwater flow rate will be related to the water velocity within the fractures, V_w, by

$$q = V_w\theta_f = V_w bB^{\theta 1} \qquad (1.8)$$

While groundwater velocities in porous media are often very low (typically between 1 and 100 m yr^{-1}), velocities in discrete fractures can be much higher. They are often measured in metres per day, rather than metres per year.

Assuming a hydraulic conductivity of 10^{-5} m s^{-1} and a hydraulic gradient of 10^{-2}, Equation 1.7 gives a groundwater flow rate of approximately 3 m yr^{-1}. If the fracture spacing is 1 m and the fracture aperture is 250 µm, then the water velocity in the fractures will be 35 m day^{-1} (*see* Box 1.1). Figure 1.4 shows the water velocity that will occur through fractures of various apertures as a function of hydraulic gradient. The water velocity in the fracture is proportional to the square of the fracture aperture, while the flow rate is proportional to the cube of the fracture aperture.

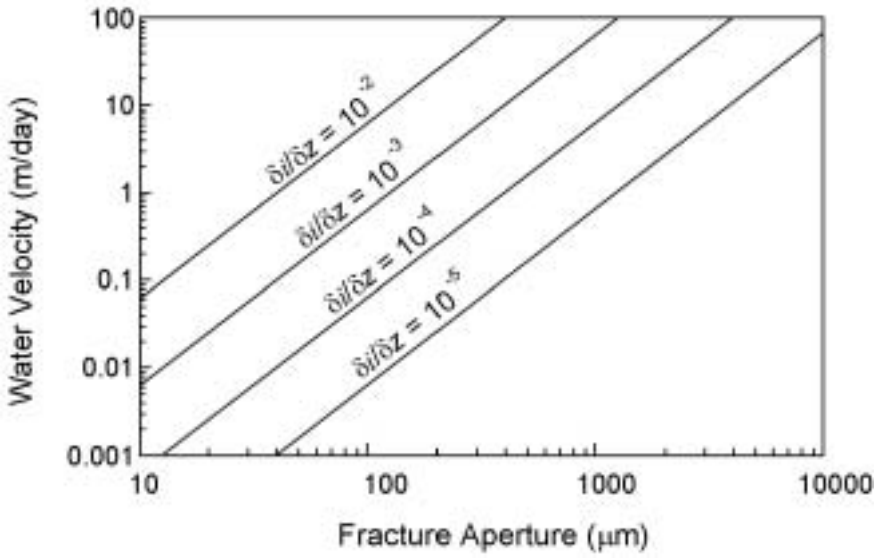

Figure 1.4. Water velocity within planar fractures as a function of fracture aperture and hydraulic gradient. This figure can be simply derived using Equations 1.6, 1.7 and 1.8.

Box 1.1. Calculation of flow rates and solute transport distances in a fractured porous media with negligible matrix permeability.

Fracture Spacing $2B$ = 1.0 m
Fracture Aperture $2b$ = 250 μm
Hydraulic Gradient $\beta i/\beta x = 10^{-2}$
Matrix Porosity $\beta_m = 0.05$
Effective Diffusion Coeff $D = 10^{-4}$ m^2/yr
Hydraulic Conductivity $K = 10^{-5}$ m/s (Equation 1.6)
Flow rate q = 3.1 m/yr (Equation 1.7)
Water velocity in fracture V_w = 35 m/day (Equation 1.8)
Travel distance of water in
t = 1 year x = 12.8 km
t = 2 years x = 25.6 km
Travel distance of solute in
t = 1 year x = 1386 m (Equation 1.5)
t = 2 years x = 1960 m

1.3.2. Solute transport

If the rock matrix is impermeable, then solute transport will be characterised by advection through the fractures, with diffusion into the immobile water in the matrix. An understanding of the relationship between water velocities and apparent solute velocities can be gained by considering two end-member scenarios. Firstly, suppose that there is no diffusion into the matrix. In this case, the apparent velocity of a tracer is equal to the water velocity through the fractures (Fig. 1.5a). On the other hand, suppose that diffusion is very rapid and that fractures are spaced very closely together, so that after a period of time diffusion of solute into the matrix may result in the solute concentration throughout the matrix being identical to the concentration within the fracture (Fig. 1.5d). (We say that fracture and matrix concentrations have equilibrated.) Even though the water is moving only through the fracture, because of this equilibration it will appear as if the solute is moving evenly through the fracture and the matrix. In this case, the apparent tracer velocity, V_a, is related to the velocity of the water in the fractures, V_w, by the ratio of the total porosity, β_t, to the fracture porosity, β_f, The tracer velocity will be equal to the groundwater flow rate divided by the total porosity:

$$V_a = V_w \frac{\theta_f}{\theta_t} = \frac{q}{\theta_t} \qquad (1.9)$$

This condition is sometimes referred to as *equivalent porous media* (*EPM*) for solute transport, and will occur when Dt/B^2 is large (Van der Kamp, 1992; Cook *et al.*, 1996).

In between these two end-members (Fig. 1.5b,c), the apparent solute velocities, V_a, will be less than the water velocity in the fractures, but greater than the EPM velocity

$$V_w \frac{\theta_f}{\theta_t} < V_a < V_w \qquad (1.10)$$

If the fracture spacing is large relative to the matrix diffusion coefficient, then diffusion into the matrix from one fracture penetrates less than half-way to the adjacent fractures (Figure 1.5b). This special case will be discussed in later sections, and is referred to as *large fracture spacings*.

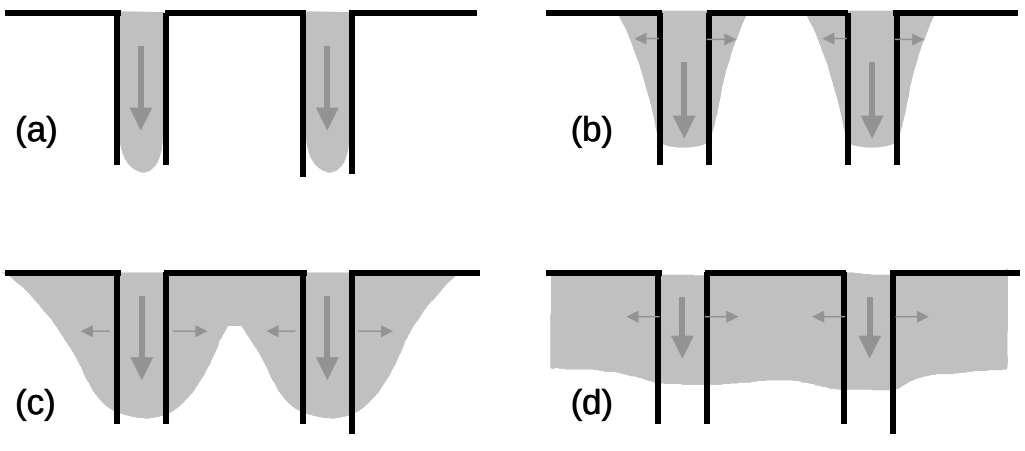

Figure 1.5. Schematic representation of tracer movement through fractured rocks. (a) No diffusion into the rock matrix. (b) Partial exchange between fracture and matrix concentrations, but with diffusion penetrating less than half-way between adjacent fractures. (c) Partial exchange between fracture and matrix concentrations, with diffusion penetrating more than half-way between adjacent fractures. (d) Complete equilibration of fracture and matrix concentrations (*equivalent porous media*).

Figure 1.6 shows the decrease in apparent solute velocity with time as a result of the matrix diffusion process. Initially, where diffusion penetrates less than half-way between adjacent fractures, the velocity is inversely related to the square root of time, as given by Equation 1.5. As matrix diffusion continues, the velocity approaches a constant value. Once equivalent porous media conditions are reached, then the distance travelled by a solute will increase directly with time (as is the case for porous media aquifers), rather than with the square root of time, and the apparent velocity will be given by Equation 1.9.

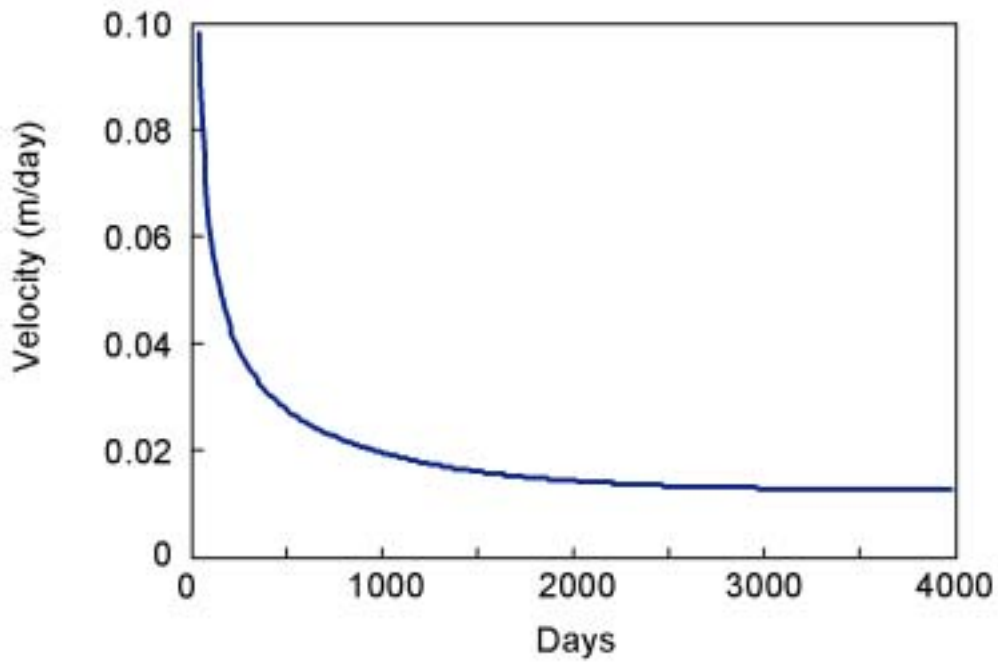

Figure 1.6. Apparent velocity of a tracer in fractured rock. Initially, the tracer velocity appears to decrease with time as solute diffuses into the rock matrix. At very late times, diffusion may result in equivalent tracer concentrations within the fractures and the aquifer matrix. When this occurs, the tracer velocity will not change with time. The curve shown is for V_w = 500 m/year, β_m = 0.1, B = 0.05 m, b = 50 μm, $D = 10^{-5}$ m^2/yr.

1.4. From parallel plates to fractured rock aquifers

In Section 1.3 we developed simple equations relating groundwater flow and solute transport to fracture characteristics, for simple systems comprising identical, planar, parallel and evenly spaced fractures of infinite length. We can build on this model, by considering flow through aquifers comprising more than one set of parallel fractures, by allowing the matrix to have some permeability, and by allowing fractures to have a finite length. For example, Figure 1.7 shows the anisotropy that develops where a series of parallel, finite fractures are imbedded in a matrix of finite permeability. In all cases, the hydraulic conductivity normal to the fracture planes is equal to that of the unfractured formation. For $\beta = 1$, the fractures are vanishingly small and the hydraulic conductivity parallel to the fracture planes is also equal to the unfractured formation conductivity, so that the anisotropy ratio is one. For $\beta < 1$, the anisotropy increases as *W/H* increases (Prats, 1972).

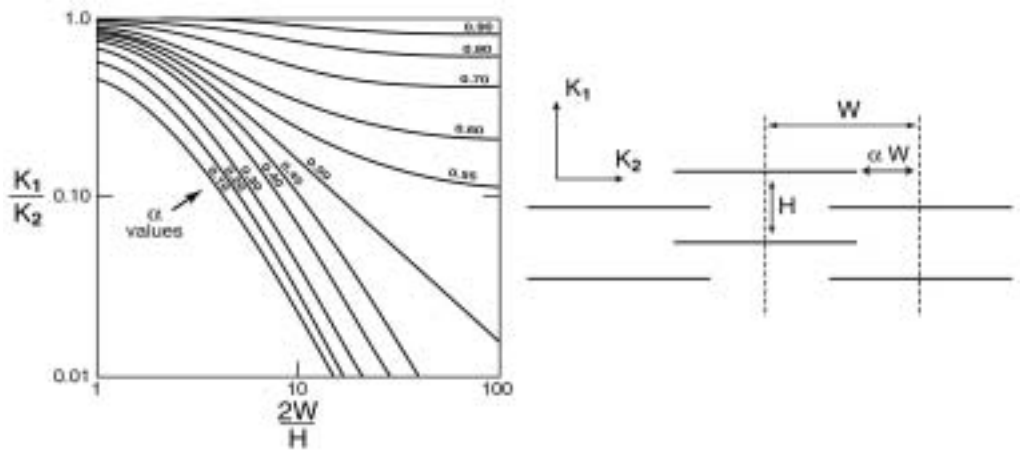

Figure 1.7. Anisotropy of hydraulic conductivity in a system of identical, planar, parallel finite fractures in a permeable matrix. (After Prats, 1972).

When the distribution of fractures is irregular, zones of high and low fracture density usually develop. Figure 1.8 shows the frequency distribution of hydraulic conductivity measured from injection tests in 3-m packed sections of granite aquifers in Aspo, Sweden. At this site, the hydraulic conductivity ranges over seven orders of magnitude. A similarly large distribution of hydraulic conductivity has been measured in the Clare Valley, South Australia, where hydraulic conductivity measured in pumping tests also ranges over seven orders of magnitude (Love *et al.*, 2002). Such variation in conductivity is largely due to spatial variations in fracture aperture, fracture density, fracture length and fracture connectivity.

There has been some discussion about how hydraulic conductivity in fractured rock aquifers varies with the scale of investigation. Consider a system of evenly spaced, identical fractures. Clearly, at very small scales the hydraulic conductivity varies between that of the matrix, K_m, and that of the fractures, K_f. However, when measurements are made at scales much larger than the fracture spacing, then the variability of hydraulic conductivity will be greatly reduced. At these scales, each measurement will return a value equal to the aquifer hydraulic conductivity. The scale beyond which the hydraulic conductivity approaches a constant value is referred to as the *representative elementary volume* (*REV*). However, when fractures are not evenly spaced and identical, then it is no longer clear that an *REV* exists. A number of people have argued that the hydraulic conductivity continues to increase as the scale of investigation increases because the probability of intersecting larger fractures increases. The basis of this proposition is that aquifers comprise a large number of very small fractures and a small number of large fractures. However, others have argued that above a certain scale of measurement, permeability begins to decrease with increasing scale, as fracture connectivity

is reduced. This proposed decrease in conductivity at large scales is a consequence of fractures having finite lengths. The maximum hydraulic conductivity occurs at the scale that is just great enough for a single large cluster of fractures to form that spans the entire network (Renshaw, 1998). Whether or not an *REV* exists for a fracture network is very important for groundwater modelling and is discussed further in Chapter 6.

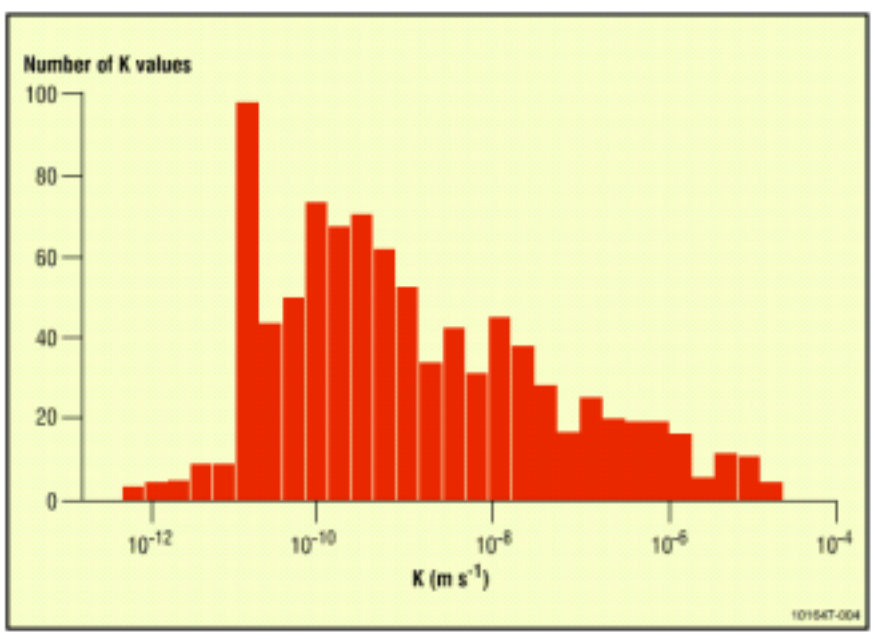

Figure 1.8. Distribution of hydraulic conductivity measured from injection tests in 3-m packed sections of granite aquifers in Aspo, Sweden. (After Tsang *et al.*, 1996).

As fracture networks become complex, it is no longer practical to characterise the system properties as the sum of individual fractures. Even for the simple parallel plate model, with identical planar fractures, characterisation of groundwater flow and solute transport requires estimates of fracture orientation, fracture spacing, fracture aperture, matrix porosity and matrix diffusion coefficient. Many of these parameters are difficult to measure accurately. Because of this, approaches that aim to measure large-scale properties that integrate the small-scale variability are more likely to be successful than those that aim to characterise the small-scale variation. Furthermore, field approaches should focus on measurement of aquifer properties that are most closely related to the properties of interest. For example, if the investigator is interested in knowing the groundwater flow rate, then it is preferable to use methods that measure groundwater flow

directly, rather than infer it from indirect methods (such as measurements of velocity or hydraulic conductivity). Similarly, if the investigator is interested in predicting the velocity of contaminants, it is preferable to perform tracer tests that measure solute velocities than to attempt to infer solute velocities from measurements of groundwater flow rate. In many cases, approximate direct methods may prove to be more useful than more accurate indirect methods.

2. MAJOR ROCK TYPES

2.1. Crystalline rocks

Crystalline rocks include intrusive igneous rocks (e.g., granite, diorite, granodiorite, gabbro, dolerite, pegmatite) and metamorphic rocks (e.g., gneiss, quartzite, marble, schist, slate, phyllite). Many of the intrusive igneous rocks (e.g., granite, diorite, granodiorite, gabbro) form large intrusive bodies (plutons) while others (e.g., dolerite, pegmatite) tend to occur as linear features of restricted extent, such as dykes and sills. (The latter are discussed in Section 2.5.) The crystalline rocks are characterised by very low primary porosity and permeability, although this can be significantly increased by weathering and fracturing. As such, the climate, topography and rock structure are often more important in accounting for differences in well yield than the rock type. The weathered layer, in particular, can be an important source of groundwater, and thick, areally extensive weathered layers can form reliable aquifers. While in arid and semi-arid regions the weathered layer is usually thin (< 1 m), in humid tropical regions its thickness may reach 100 m (Singhal & Gupta, 1999).

Generally, coarse-grained, quartz-rich rocks such as granite and quartzite are more brittle than slates and schists, and have a coarse-grained weathering product, therefore they tend to develop and preserve open joint systems. Weathering products of phyllite, schist and slate include clay minerals that tend to fill the fractures. Snow (1968) calculated fracture apertures in granite, gneiss and metavolcanic rocks from measurements of permeability derived from packer tests in drill holes. Computed apertures ranged from 75–400 µm in the upper 10 m of bedrock, decreasing to 50–100 µm at 15–60 m depth. Similarly, Gale *et al.* (1982) estimated fracture apertures between 5 and 20 µm at depths of several hundred metres in granites at Stripa, Sweden. Rocha and Barroso (1971) measured the apertures of open fractures in granite using a specially designed coring method. The average fracture aperture was 400 µm at 2.5–4.5 m depth into the bedrock, decreasing to 100 µm at 13.5 – 14.5 m (Trainer, 1988).

Clauser (1992) compiled data on hydraulic conductivity of crystalline rocks measured at a variety of spatial scales (Fig. 2.1). An increase in average permeability of about 3 orders of magnitude from the laboratory scale to the borehole scale is observed. Core material for laboratory measurements is usually derived from unfractured samples, and may be biased towards the lower end of a rock's permeability range. Hydraulic conductivities measured at the borehole scale generally range between 10^{-2} and 10^{-7} m^2 day^{-1}

(permeability of 10^{-14}–10^{-19} m^2). The porosity of unweathered crystalline rock usually varies between 0.1% and 1%.

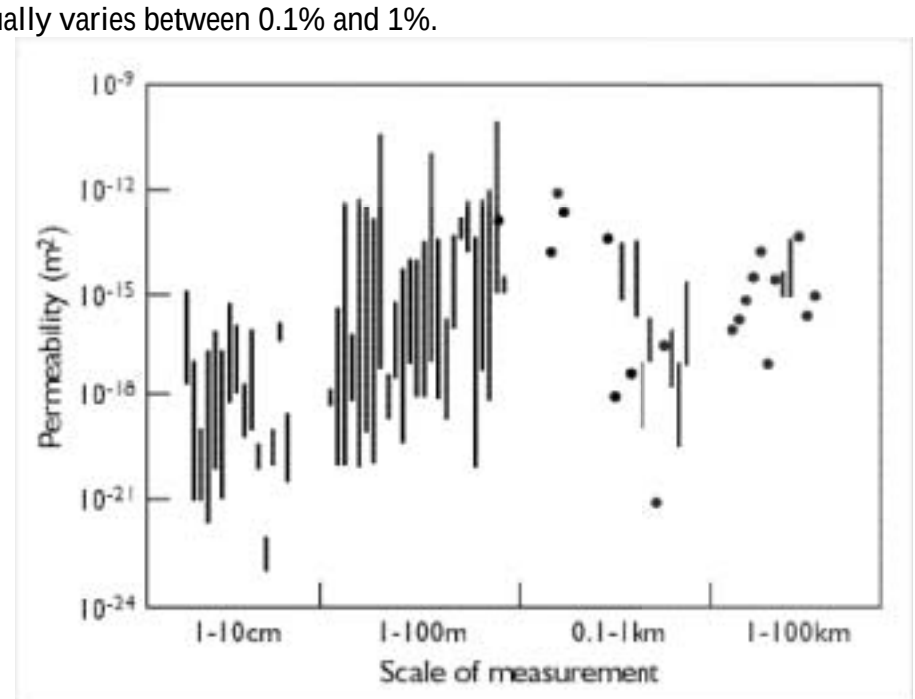

Figure 2.1. Permeabilities of crystalline rocks measured at different scales. Bars mark the permeability range when several individual values are reported; circles represent individual values. (After Clauser, 1992).

2.2. Volcanic rocks

Volcanic rocks are formed by the solidification of magma at or near the ground surface. Acidic lava (e.g., rhyolite, dacite, andesite) is viscous and, therefore, restricted in extent, often forming steep-sided bulbous domes. Basic lava (basalt) has lower viscosity, and spreads over large areas forming thin, aerially extensive sheets. The lateral extent of individual flows may vary from a few tens of metres to as much as hundreds of kilometres. The thickness may range from less than 1 m to more than 30 m, most being between l0–30 m (Walker, 1973). Many lava flows develop a brecciated upper surface that is progressively pushed beneath the flow as it advances (Fig. 2.2), and this tends to produce a relatively permeable top and base to many lava flow units. Basalts typically exhibit hexagonal columnar jointing (Fig. 2.3), which form during cooling and can lead to high vertical hydraulic conductivity. However high hydraulic conductivity zones in basalts usually form horizontal layers, either as brecciated zones along basalt flow contacts, or interbedded pyroclastic deposits (Fig. 2.4). These zones may be locally confined, or may form perched aquifers underlain by denser basalt units or intruded sills of lower permeability.

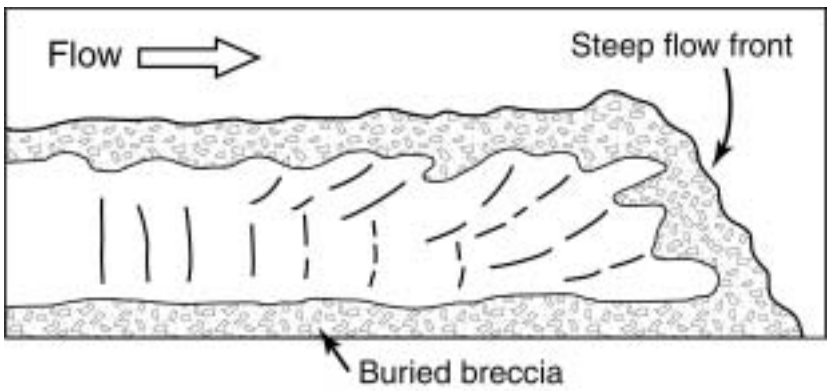

Figure 2.2. Development of brecciated material on the top surface of lava flow and its burial due to downward sliding along the steep-moving front. (From Singhal & Gupta, 1999).

Figure 2.3. Groundwater-fed springs flowing over columnar basalt sequence in Gum Creek at Dalwood Falls, Alstonville, NSW. Photo courtesy of R.T. Green, DLWC.

Figure 2.4. Pyroclastic deposit near the crater rim, Mount Quincan, Atherton Tablelands. Layers are approximately 20–30 cm thick, and consist of basaltic scoria, ash and peridotite clasts. The coarser layers are highly porous and permeable. (From Buck, 1999).

Tuffs are fine-grained pyroclastic deposits, generally comprising volcanic glass fragments of less than 4 mm in diameter. Ash-flow tuffs are deposited from a turbulent mixture of gas and pyroclastic material, and are generally unstratified, poorly sorted, and at least partially welded. Deposits from individual volcanic eruptions are usually restricted in extent to a few hundred square kilometres or less, but repeated eruptions can create deposits that may be ten of metres thick and cover thousands of square kilometres. Air-fall tuffs are very fine-grained, well-sorted and distinctly bedded. Individual air-fall tuffs generally thin rapidly away from their source, but may still cover thousands of square kilometres. Unlike ash flows, air-fall tuffs are generally thin, of relatively uniform thickness, and tend to parallel the surface topography (Wood & Fernandez, 1988).

Primary porosity and permeability in volcanic rocks depend on the rate of cooling, the extent of degassing during cooling, and on the viscosity of the magma. Total porosity in basalts ranges from close to zero to more than 75%, with values less than 15% being most common. Figure 2.5 shows the range of values of hydraulic conductivity determined on volcanic rocks from field and

laboratory studies, with values ranging over 16 orders of magnitude (Wood & Fernandez, 1988). Horizontal hydraulic conductivity in basalts is usually several times greater than vertical hydraulic conductivity due to the presence of interflow spaces and horizontal fractures. In Gran Canaria, Spain, the ratio of K_h/K_v is reported to be between 20 and 100 (Custudio, 1985). (*See* also Box 4.2.) In some cases, however, columnar jointing may impart high vertical conductivity. Basalts at Box Canyon, Idaho, are characterised by a columnar joint spacing ranging from 0.3 m at the upper surface of the basalt flow, to 1.5–2.0 m towards the centre of the flow (a depth of 8 m; Faybishenko *et al.*, 1999).

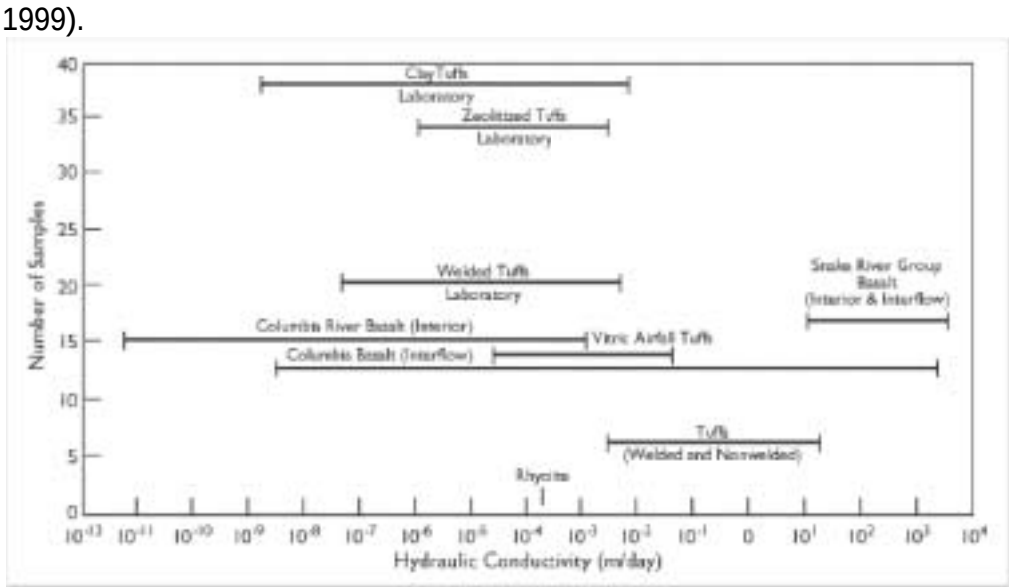

Figure 2.5. Range in hydraulic conductivity of volcanic rocks. (From Wood & Fernandez, 1988).

The hydraulic conductivity of pyroclastic deposits depends on the degree of consolidation and welding. Non-welded tuffs typically have porosities between 30 and 40%. Welded tuffs, formed at high temperatures by the fusion of rock fragments, have low porosity and very low conductivity. The porosity of welded tuffs typically averages between 10 and 20% (Wood & Fernandez, 1988).

2.3. Carbonate rocks

Carbonate rocks are sedimentary rocks containing more than 50% carbonate minerals, usually calcite, $CaCO_3$, and dolomite, $CaMg(CO_3)_2$. The term limestone is used for those rocks that contain more than 90% carbonate, with calcite as the dominant mineral. If the rock contains more than 50% but less than 90% carbonate, it is termed arenaceous limestone or argillaceous limestone, depending upon the relative amounts of quartz and clay minerals.

Chalk is a fine-grained limestone, which is soft and white in colour. The term dolomite is used for carbonate rock with a high proportion of dolomite minerals.

Figure 2.6. Horizontal fractures in Paleozoic limestone from Montreal, Canada. Photograph courtesy of Rene Therrien, Laval University.

Carbonate rocks are soluble in water rich in carbonic acid. In some carbonate rocks, dissolution of matrix material by water flowing through fractures can enlarge apertures, resulting in large conduits for groundwater flow and leading to the development of karst topography. Figure 2.7 depicts the generalised porosity — pore size — hydraulic conductivity relationship for several types of carbonate rocks. Also shown is a speculative boundary differentiating conditions favourable to the development of karst. This boundary originates at a rock pore size of 10 µm, a value believed to be the lower threshold necessary for significant flow and solvent action by water (Brahana *et al.*, 1988). Porosity in carbonate rocks can vary from less than 1% in marbles and some massive limestones to as high as 45% in some chalks and calcareous tuffs. Dolomites are usually more porous than limestones due to reduction in volume as a result of dolomitisation (the replacement of calcite by dolomite). Chalk and some limestones may have high porosity, but since the pores are small (usually < 10 µm), primary permeability is low and specific

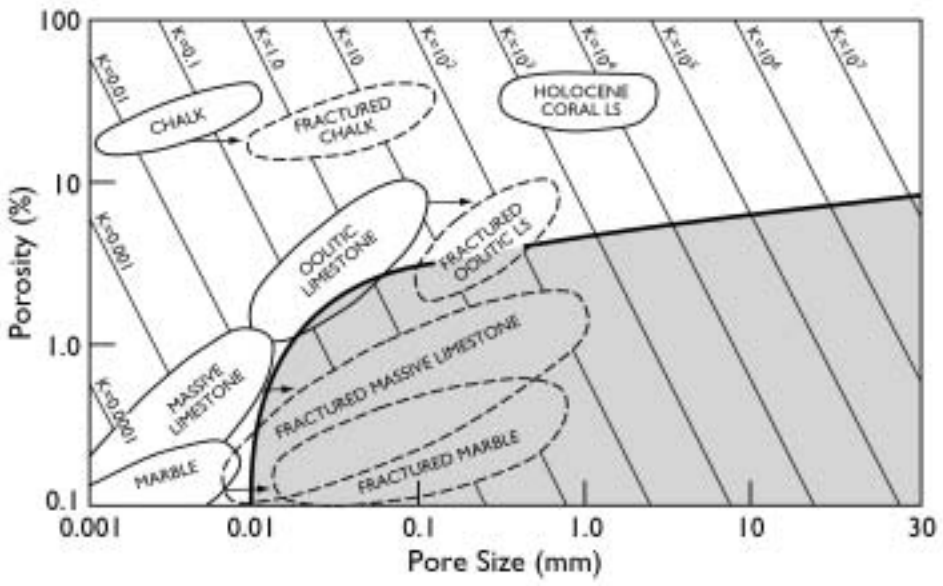

Figure 2.7. Porosity, pore size, and theoretical hydraulic conductivity (m/day) of unfractured (solid ellipses) and fractured (broken ellipses) carbonate rocks. The shaded area depicts conditions favourable for the development of karst features. (From Brahana *et al.*, 1988).

retention is high. For example, the mean interconnected porosity of the Lincolnshire Limestone is 15%, while the mean matrix hydraulic conductivity is only 10^{-9} m s^{-1} (10^{-4} m day^{-1}) (Greswell *et al.*, 1998). However, the rock may acquire high secondary porosity and permeability, depending on fracturing and dissolution of mineral matter. For the Lincolnshire Limestone, groundwater flow is largely restricted to the fractures. The aquifer hydraulic conductivity determined from pumping tests ranges between approximately 20-100 m day^{-1} (Bishop & Lloyd, 1990), which is more than five orders of magnitude greater than the matrix hydraulic conductivity. The San Antonio segment of the Edwards aquifer in Texas, USA consists of Cretaceous limestones and dolomites that have undergone multiple periods of karstification. The mean aquifer hydraulic conductivity, based on over 900 well tests, is approximately 7 m day^{-1} (permeability of 8.8 β 10^{-12} m^2), while the mean matrix hydraulic conductivity is approximately 10^{-3} m day^{-1}. The aquifer includes a number of wells with very high discharge rates, including one well with a discharge rate of 1.6 m^3 s^{-1} (Halihan *et al.*, 2000). In central Queensland, Pearce (1982) reports transmissivity values for Devonian limestone from the Mt Larcom district ranging from 10 m^2 day^{-1} in poorly fractured areas, to 3000 m^2 day^{-1} for bores that tap solution channels. The Gambier Limestone, southeastern South Australia, is a porous limestone with significant primary porosity and permeability, and also containing a secondary

fracture porosity from dissolution of the rock matrix along structurally weak zones. Transmissivity determined from pumping tests ranges from 200 m^2 day^{-1} to more than 10 000 m^2 day^{-1}. Porosities measured from rock outcrop range from 50 to 60%. Despite karstic development, however, it is believed that the solution channels do not form a large interconnected network, and that regional groundwater flow occurs predominantly as inter-granular flow (Love *et al.*, 1993). In contrast, the Murray Group Limestone in South Australia is a fine to coarse, highly fossiliferous limestone which is also highly porous but with no significant karst development. The mean hydraulic conductivity is approximately 1.0 m day^{-1}, which is largely attributed to matrix flow.

2.4. Clastic formations

Coarse-grained, unconsolidated sediments usually have high hydraulic conductivity and porosity. Because of their incoherent nature, they do not readily fracture. However, on consolidation, these rocks become more elastic and can be prone to fracturing. Unconsolidated fine-grained deposits (such as clays and glacial tills) have primary porosity and permeability which can be increased by fracturing.

The hydraulic properties of sandstones depend on their textural characteristics, which are determined by the depositional environment along with post-depositional changes due to cementation, consolidation and fracturing. The hydraulic conductivity of sandstones is typically 1–3 orders of magnitude lower than that of unconsolidated sediments (Davis & De Wiest, 1966). This decrease in hydraulic conductivity is mostly due to the reduction in pore space due to cementation. Davis (1988) reports hydraulic conductivities for sandstones between approximately 0.003–5 m day^{-1}. Poorly cemented sandstones may have porosity of about 35%, but this typically decreases to 5–25% on cementation. Stratification of sandstones can impart anisotropy, with the hydraulic conductivity parallel with the bedding plane usually higher than perpendicular to it. In Berea Sandstone, USA, permeability parallel to the bedding was found approximately four times higher than that perpendicular to the bedding (Lee & Farmer, 1993).

Fine-grained argillaceous rocks (e.g., shale, siltstone) are formed by compaction and lithification of clay and mud deposits. The porosity of freshly deposited clays and muds is usually high (50% to 80%), but is usually reduced to less than 30% by compaction following burial. Shales usually have porosities in the range of 1% to 3%. Intergranular permeabilities in shales and siltstones are usually low (between 10^{-13} and 10^{-9} m s^{-1}), although fracturing can significantly increase hydraulic conductivity. Singhal and Gupta (1999) suggest typical hydraulic conductivities of fractured siltstones and shales of

10^{-7} to 10^{-4} m s^{-1}. In a heterogeneous sedimentary sequence, thin incompetent beds, such as shales, will be more intensely fractured as compared with thicker units of strong and resistant formations, such as mudstones. Within units of the same lithology, an increase in fracture spacing with depth is frequently observed. Devonian siltstones of the Appalachian plateau, New York, USA, exhibit two sets of fractures — subhorizontal bedding plane fractures and vertical fractures. The spacing of bedding plane fractures increases from 3–8 cm at shallow depths (< 7 m) to more than one metre below 45 m depth. Slug tests in these siltstones indicate that closer spacing of bedding plane fractures at shallow depths impart hydraulic conductivities ($4 \beta 10^{-7}$ to $2 \beta 10^{-6}$ m s^{-1}) which are 100 times greater than those obtained from deeper wells ($4 \beta 10^{-9}$ to $2 \beta 10^{-8}$ m s^{-1}) (Merin, 1992). Average fracture spacing in weathered Nolichucky Shale, Oak Ridge, Tennessee is 0.005–0.03 m (Fig. 2.8), compared with 0.2 m in fresh rock. Hydraulic conductivities in the intensively weathered zone (<10 m depth) are 10^{-6} to 10^{-5} m s^{-1} (Cook *et al.*, 1996).

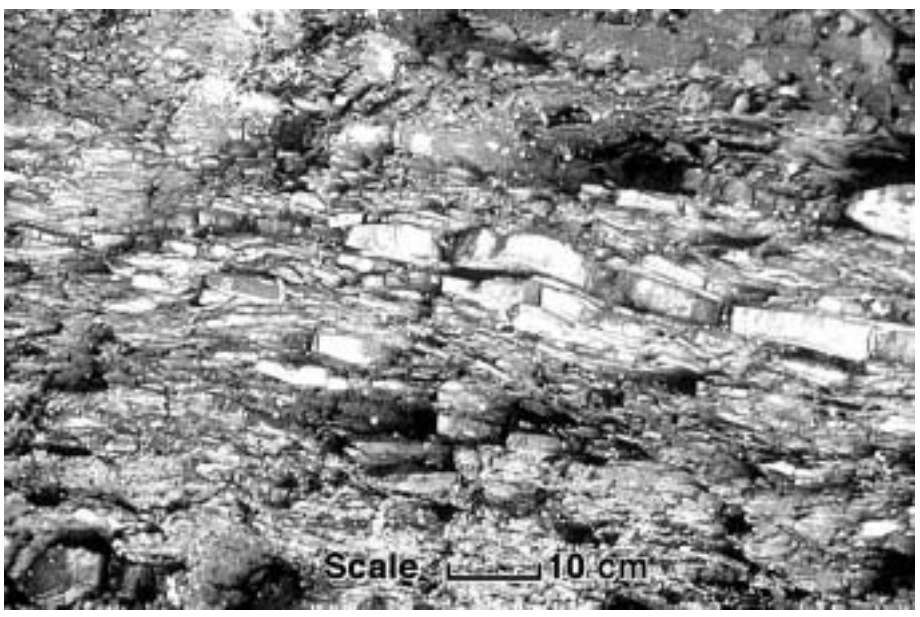

Figure 2.8. Weathered Nolichucky Shale, Oak Ridge, Tennessee. Photograph courtesy of William Sanford, Colorado State University.

Glacial tills are ice-transported sediments that are typically unstratified and poorly sorted, containing material from clay to boulder-size. In some areas tills are thick and unfractured but, wherever fractured, they provide active hydraulic connections and potential contaminant pathways (Hendry, 1982; Ruland *et al.*, 1991). Fracture spacing in clay deposits usually increases with depth thereby effecting the vertical distribution of permeability (Fig. 2.9). Shallow fractures are regarded to be a result of alternate cycles of wetting and

drying, freezing and thawing. McKay *et al.* (1993) measured a mean fracture aperture of 10 µm from clay-rich tills in southern Ontario, based on hydraulic testing and application of the cubic law.

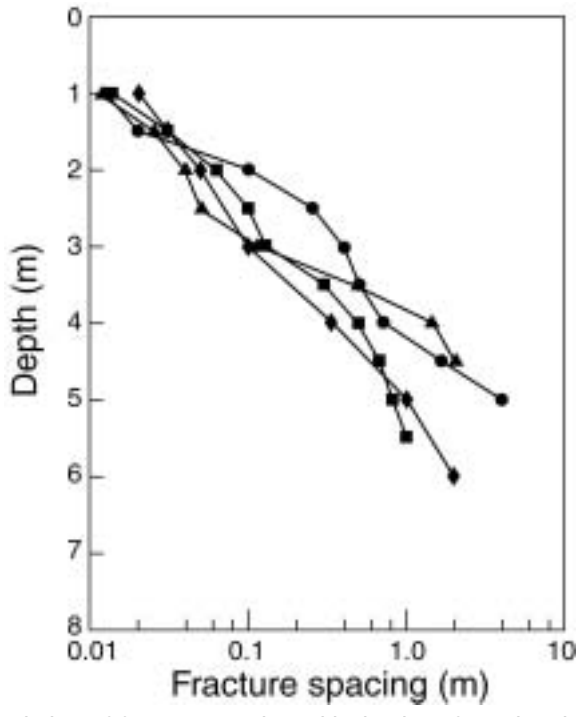

Figure 2.9. Variation of fracture spacing with depth at four sites in glacial till in southern Ontario. (From Ruland *et al.*, 1991).

2.5. Dykes and sills

Dykes are vertical or steeply inclined intrusive igneous bodies that cut across the pre-existing rocks. They vary in thickness from a few decimetres to hundreds of metres, with widths of l–10 m being most common. They may be from a few metres to several kilometres long and represent feeders for the lava flows. Massive and unweathered dykes can form barriers to lateral groundwater movement. In the Witwatersrand goldfields area of South Africa, a series of north-south trending dykes between 6 and 60 m in thickness that intrude volcanic and sedimentary rocks have created a series of isolated aquifer compartments. Recharge to the compartments occurs from rainfall while discharge occurs through springs located at the downstream contact of the dolomite and the intrusive dykes. In south-western Australia, dolerite dykes can impede the lateral flow of groundwater, forcing it to the surface where evaporation can cause salinisation (Engel *et al.*, 1989).

Fractured dykes may form good aquifers. One of the dykes in the Palaghat Gap, India, extends for a strike length of about 14 km and is highly fractured. The discharges from some of the wells in this dyke are between 240 and 840 m^3 day^{-l} (Singhal & Gupta, 1999). Due to thermal effects, dykes can also cause fracturing of adjacent rock. In particular, Sami (1996) found the yield of bores adjacent to dolerite dykes intruding the fractured sandstone/mudstone Karoo Aquifer, South Africa, to be significantly higher than elsewhere in the basin. Pumping tests in Botswana indicate that dykes which are thicker than 10 m serve as groundwater barriers, but those of smaller width are permeable as they develop cooling joints and fractures (Bromley *et al.*, 1994).

Sills are nearly horizontal tabular bodies that commonly follow the bedding of enclosing sedimentary rocks or lava flows. Some of the sills are very thick and extend over large areas. Due to their low permeability, except when fractured, sills may support perched water bodies.

3. GEOLOGICAL CHARACTERISATION

3.1. Introduction

Characterisation of geological material is important for building up a conceptual understanding of the hydrogeological processes operating in any region. Information on fracture distributions can be obtained at a number of scales. The most detailed information can be collected from outcrop exposures, although the availability of outcrops is often limited, and they can be affected by weathering. Shallow fractures might not be representative of conditions at greater depth. Some fracture information can be obtained from boreholes, either from examination of core material, or using geophysical logging methods. At larger scales, the locations of major fracture zones and faults can sometimes be obtained from aerial photography and remote sensing. Information on characteristics of the rock matrix can usually be reliably determined only by using core samples taken from drilling or from surface exposures.

3.2. Characterising fractures

Fracture properties can be measured directly in mine openings, surface outcrop exposures, and on core samples. However, results need to be interpreted with some caution, because they may be affected by stress release. Furthermore, the orientation of boreholes and outcrop surfaces will influence the number of fractures with different orientations that can be observed. This may bias any interpretation. In particular, vertical boreholes will not intercept vertical fractures, and will preferentially intercept horizontal fractures relative to high angle (inclined) fractures. Methods for characterising fractures are described in LaPointe and Hudson (1985) and Singhal and Gupta (1999). Some of the more common measurements are briefly described in the following sections.

3.2.1. Number of sets

Fracture sets are groups of fractures or discontinuities with preferred orientations. While data on fracture characteristics (e.g., orientation, spacing, length, aperture) should be collected for all fractures on an outcrop, it is sometimes convenient to present the results as average values for each of the sets. The outcrop exposure shown in Figure 3.1 contains five sets of fractures: four steeply dipping sets and one gently dipping set.

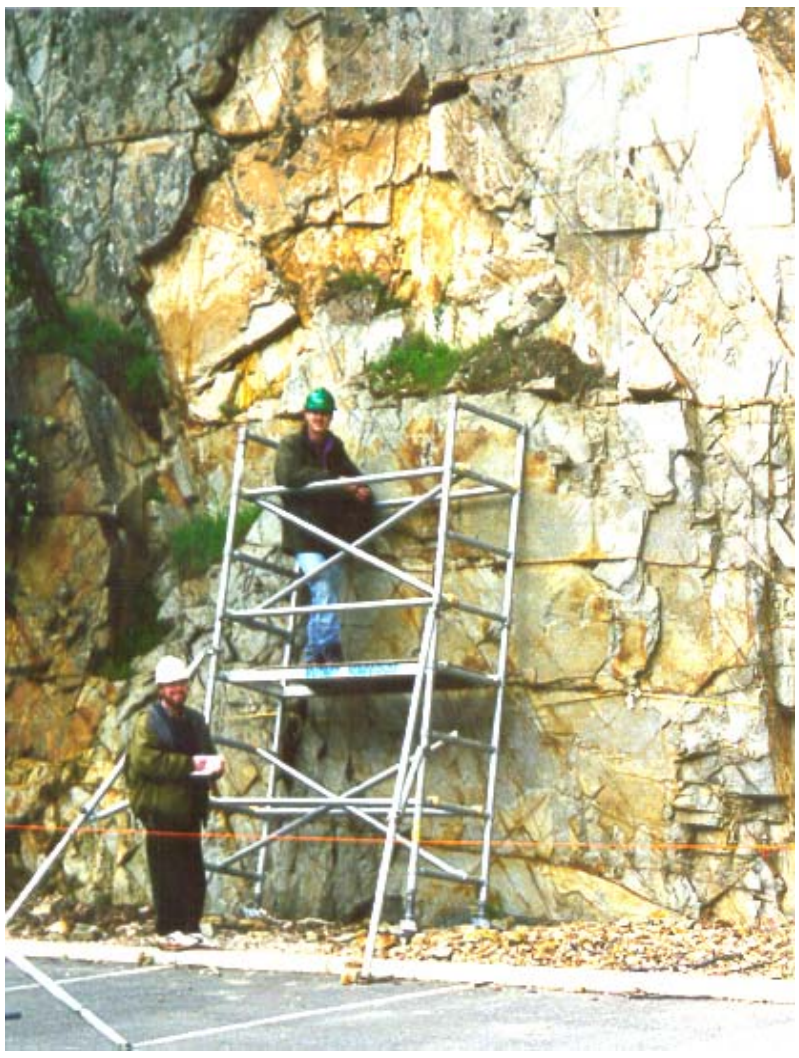

Figure 3.1. Mapping fracture properties in an exposure in the Mintaro Shale, Clare Valley, South Australia. Five sets of fractures are present, four steeply dipping sets and one gently dipping set. This site is located on the limb of a major syncline, with the bedding planes oriented vertically. The bedding comprises one vertically dipping fracture set that strikes 151°. (The cliff face is the bedding plane.) A second set of vertical fractures strikes 59°. A set of conjugate shear fractures has the same trend as the second set of vertical fractures with dips of approximately 60°. The only shallow dipping fracture set has a strike of 345° and a dip of 27°.

3.2.2. Orientation

Orientation data for fractures can be collected either from oriented boreholes or surface exposures, although it should be noted that considerable bias is

introduced by the orientation of the borehole or the surface from which the fracture data are collected. Methods for correcting for this bias are discussed by LaPointe and Hudson (1985). Of course, fracture orientation data can be obtained from core data only if the orientation of cores can be determined. The most practical method is to compare fracture locations in cores with the results of images of the borehole wall derived from downhole geophysical logging (*see* Section 3.4).

The orientation of the fracture plane is defined in terms of dip direction (angle with respect to north) and dip amount (angle from horizontal). The orientation is expressed in terms of a pair of numbers, such as 25°/N 330°, implying a plane dipping at 25° in the direction 330° measured clockwise from the north. The fracture strike is perpendicular to the dip direction. It should be noted, however, that calculation of mean fracture orientation for a fracture set is not as simple as averaging values for strikes, dip directions and dip amounts. Suppose that we want to describe the average orientation of two fractures: 85°/N 416° and 87°/N 238°. It must be realised that 85°/N 416° is equivalent to 95°/N 236°, and so the average orientation is 91°/N 237° or 89°/N 57° (and not 86°/N 327°).

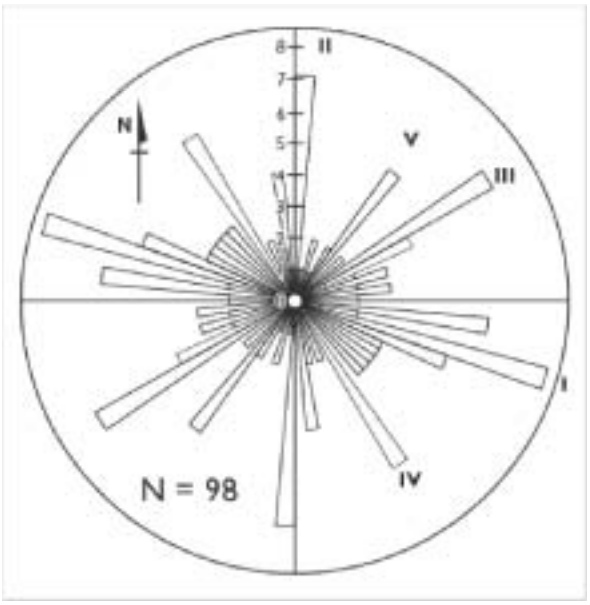

Figure 3.2. Rose diagram of orientations of 98 vertical fractures observed in drill core samples of the Eramosa member, a dolostone, Smithville, Ontario. Vertical fractures can be subdivided into five different sets. Set I appears to be the most dominant. Set II is roughly orthogonal to Set I. (From Novakowski *et al.*, 1999).

A number of graphical methods have been developed for displaying data on fracture orientation collected from rock units. *Rose diagrams* (Fig. 3.2) can be constructed for parameters such as length or number of joints in a particular

Box 3.1. Mapping fracture orientations, Wagga Wagga, New South Wales.

The orientation of major fractures in Ordovician metasediments in the Wagga Wagga region have been mapped in an outcrop exposure in the Southern Roadbase Quarry. Three fracture sets are recognised, one set of bedding plane fractures, and two shear sets (Cook *et al.*, 2001b).

Table 3.1. Measurements of strike and dip on individual fractures in an exposure of Ordovician metasediments near Wagga Wagga. By convention, dip direction is 90° clockwise of the strike. (Note that the mean orientations are not simply the means of the individual strike and dip values.)

	Bedding		Shear 1		Shear 2	
No	Strike	Dip	Strike	Dip	Strike	Dip
1	326	90	164	48	30	49
2	326	90	169	42	35	65
3	328	85	201	25	38	85
4	332	89	203	75	41	61
5	332	82	229	40	48	67
6	336	79	233	38	48	55
7	148	87	255	31	50	53
8	148	86	270	82	51	86
9	155	85	283	70	52	46
10			295	47	52	59
11			318	51	54	80
12			320	50	55	58
13					55	56
14					56	61
15					58	52
16					59	65
17					60	49
18					68	47
19					69	40
20					90	77
Mean	**330**	**88**	**216**	**35**	**53**	**60**

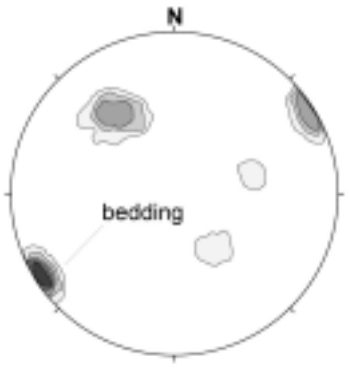

Figure 3.3. Contour diagram of poles to fracture planes. Contours near edges of the diagram indicate steeply dipping fractures. Horizontal fractures would lie in the centre of the circle.

direction, with the directions often grouped into 5° or 10° intervals. The length of petals becomes a measure of relative dominance of the trend and the resulting strike petals have a mirror image about the centre of the rose. (Data on the amount of dip cannot be incorporated in the diagram.) *Spherical projections* are used for representing the orientation of geological planar surfaces. These include great-circle plots and β-pole plots, information on which can be found in most structural geology texts. The pole-plotting method has a relative advantage over the great-circle method in that clusters of poles and their relative concentrations can be readily ascertained on such plots by contouring. Contours near edges of the diagram indicate steeply dipping fractures, while those near the centre of the circle indicate horizontal fractures (Box 3.1).

3.2.3. Spacing

The joints belonging to a particular fracture set are often parallel and roughly equidistant. The fracture spacing describes the average perpendicular distance between two adjacent fractures of the same set. The average apparent spacing between fractures of a set can be measured by spreading a tape in any convenient direction on an outcrop face, although this measurement has to be corrected for angular distortion to give the value of true fracture interval, perpendicular to the fracture orientation (LaPointe & Hudson, 1985).

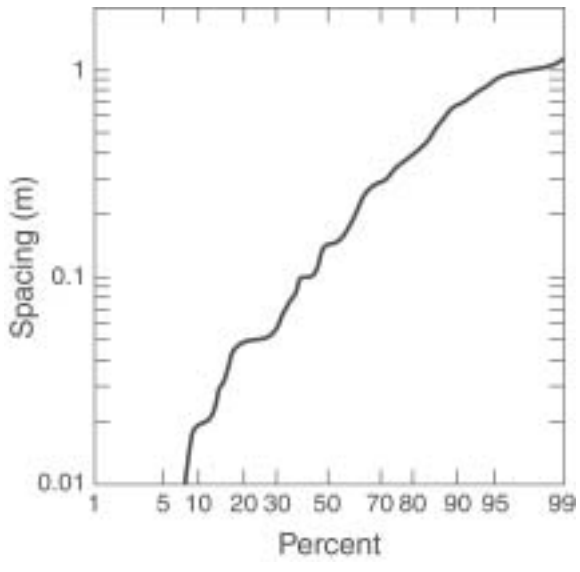

Figure 3.4. Distribution of fracture spacings measured along a horizontal scanline in an exposure of Mintaro Shale, Clare Valley, South Australia (*see* Fig. 3.1). The x-axis refers to the number of fractures that are less than the specified value. Thus, for example, 70% of fractures spacings are smaller than 0.3 m (Halihan, unpublished.)

Box 3.2. Fracture properties in granite, schist and pegmatite, mapped on a roadcut near Mirror Lake, New Hampshire.

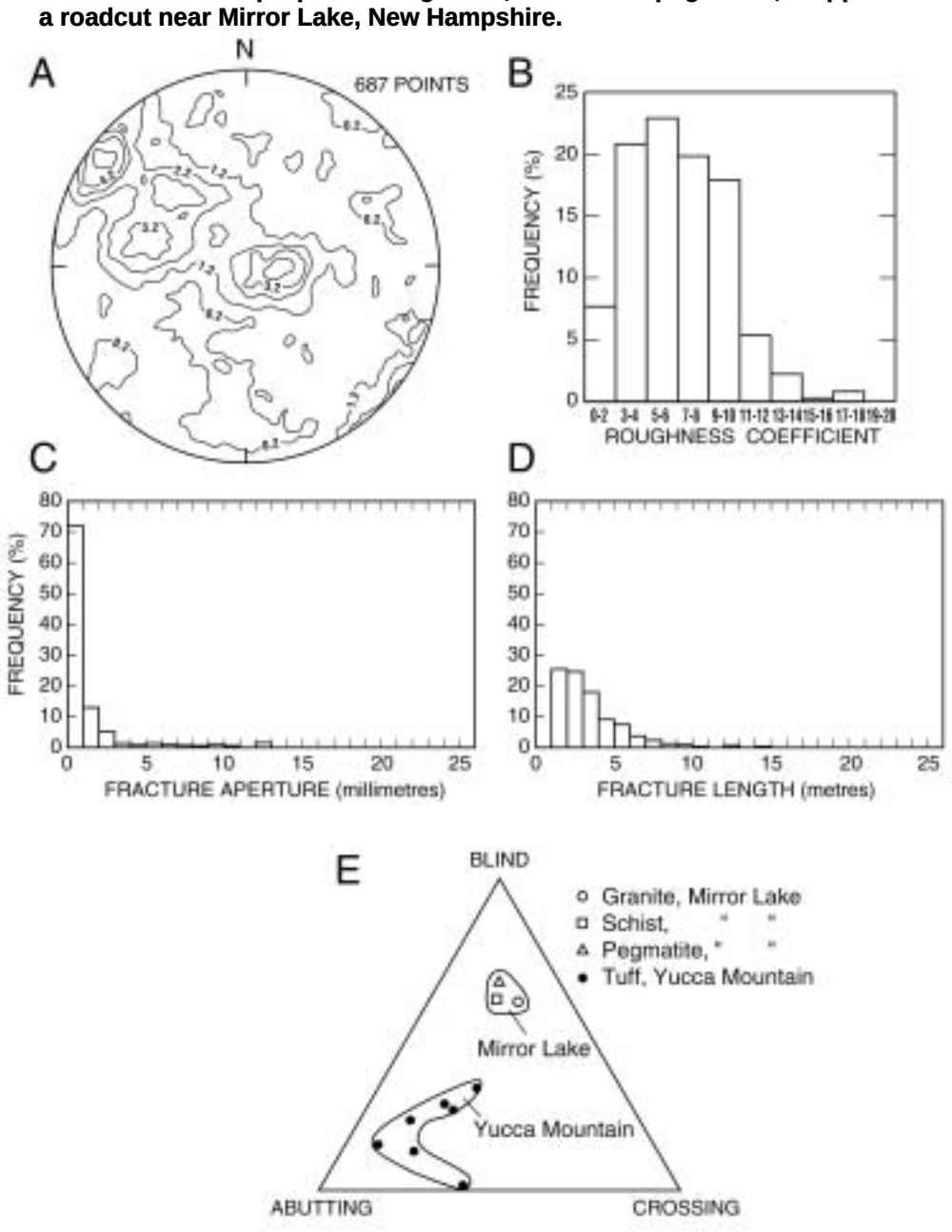

Figure 3.5. Fracture properties in granite, schist and pegmatite, mapped on a roadcut near Mirror Lake, New Hampshire. (a) Contoured lower hemisphere projection of poles to fractures. (b) Histogram of roughness coefficient. (c) Histogram of fracture aperture. (d) Histogram of fracture length. (e) Ternary diagram of percentages of fracture intersections and terminations. Data from sites at Yucca Mountain, Nevada are shown for comparison. (From Barton, 1996).

3.2.4. Fracture length

Fracture length can be rather difficult to quantify, as it will differ in the dip and strike directions. It can be measured by observing the discontinuity trace length in an exposure, in both dip and strike directions. The observed trace length may be only an apparent value of the true trace length due to various types of bias creeping into the data during measurements in exposures. Figure 3.5d shows the distribution of fracture trace length in a roadcut near Mirror Lake, New Hampshire. The distribution is cut off at both the upper and lower ends. The upper limit is imposed by the size of the outcrop being used for mapping. The lower limit is imposed by the decision to ignore fractures below a critical size (in this case 1 m).

3.2.5. Fracture connectivity

The ability of fractures to act as conduits for groundwater flow is affected by the degree to which the fractures are interconnected. Fracture connectivity increases with increasing fracture length and fracture density, as the chance of fracture intersection increases (Fig. 3.6). Connectivity can be represented by the ratios of three types of fracture termination: (1) blind fractures that terminate in the rock matrix; (2) fractures that cross other fractures; and (3) fractures that abut other fractures (Fig. 3.6). Figure 3.5e displays the relative proportions of different fracture terminations on a ternary diagram. The high proportion of blind endings at Mirror Lake compared with Yucca Mountain suggests that the fracture network at this site is relatively poorly interconnected. Thus groundwater flow is expected to occur through highly tortuous pathways. If fracture apertures and densities were similar, then poor fracture connectivity would result in relatively low aquifer permeability.

3.2.6. Aperture

Aperture is the perpendicular distance separating the adjacent rock walls of an open fracture, in which the intervening space is air- or water-filled. Measurement of apertures in surface exposures can be made with a vernier or gauge (Fig. 3.7). However, some caution needs to be applied when interpreting measurements of fracture apertures from surface excavations, because they may have been affected by the release of overburden pressures. More often, fracture aperture is calculated indirectly, from measurement of fracture transmissivity (Equation 1.4).

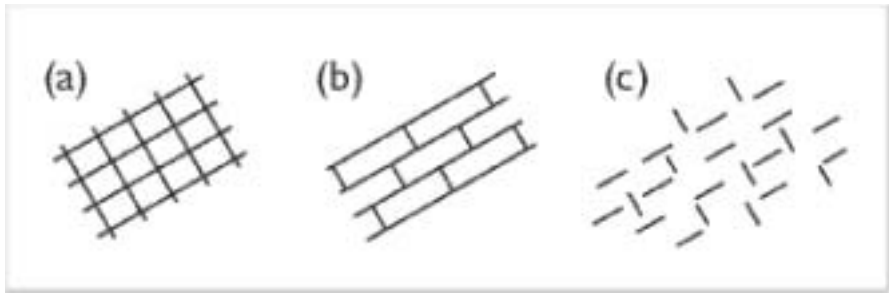

Figure 3.6. The influence of fracture length on fracture connectivity. a) Fracture length is large relative to fracture spacing, and all fracture terminations are *crossing*; b) One set of fractures has fracture length greater than fracture spacing, while the other set has fracture spacing greater than fracture length. All fracture terminations are *abutting*; c) Both sets of fractures have fracture spacing greater than fracture length, and all fracture terminations are *blind*. (After Singhal & Gupta, 1999).

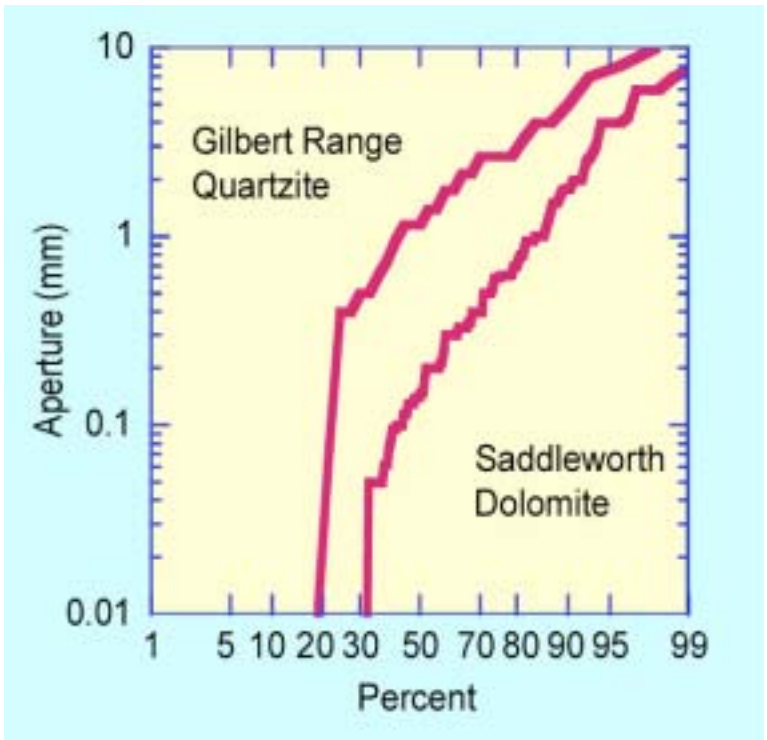

Figure 3.7. Distribution of fracture apertures measured with a feeler gauge on exposures of the Gilbert Range Quartzite and Saddleworth Dolomite, Clare Valley, South Australia. The x-axis refers to the proportion of apertures that are less than the specified value. Thus, for example, in the Saddleworth Dolomite, 90% of fracture apertures are less than 2 mm. The distributions are truncated at the lower end, because of the inability to measure very small fractures. (From Love *et al.*, 2002).

3.2.7. Surface roughness

Fracture walls are not flat parallel smooth surfaces, but contain irregularities. Rough surfaces of fractures reduce fluid flow and lead to a local channelling effect of preferential flow. Surface roughness is measured by comparing the profile of an exposed, unweathered fracture surface with a standard set of profiles. The *joint roughness coefficient* (*JRC*) is usually defined on a scale from 0 to 20 (Barton & Choubey, 1977; Fig. 3.8). Roughness coefficient values at Mirror Lake range from 0 to 18, with a mode of 5-6 (Fig. 3.5b).

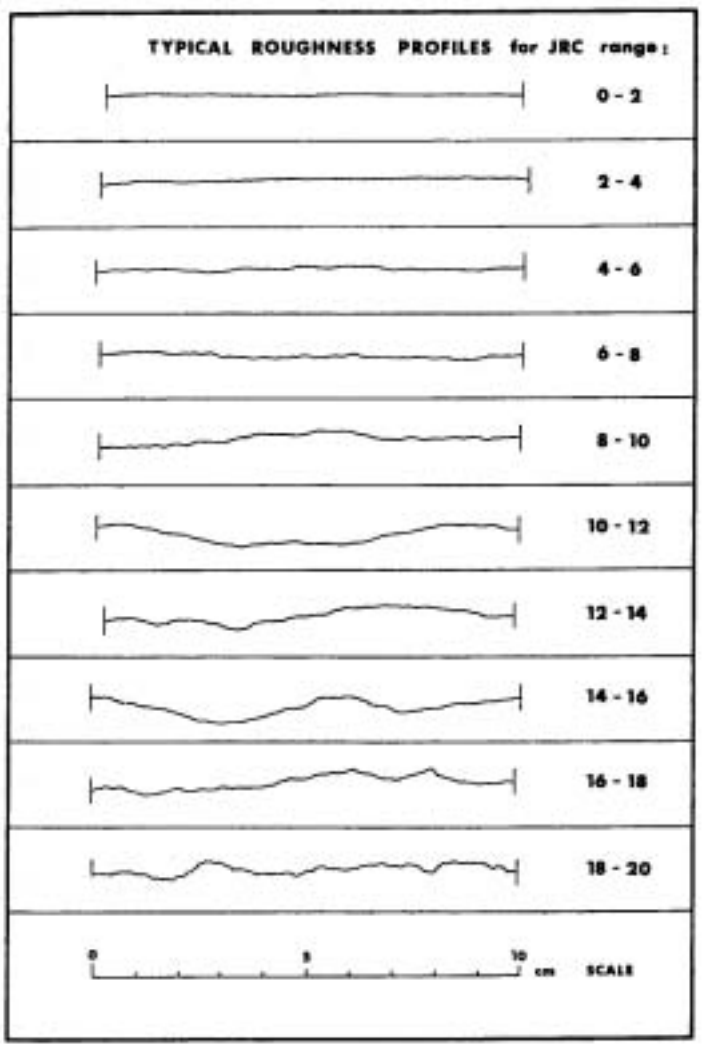

Figure 3.8. Typical roughness profiles, defining the *joint roughness coefficient* range from 0 through 20. (From Barton & Choubey, 1977).

3.3. Characterising the rock matrix

Measurements of matrix porosity and permeability may help determine the extent to which fractures are likely to dominate groundwater flow. Where matrix permeability is low, fracture permeability is likely to exceed matrix permeability, and fractures will dominate groundwater flow. Where fracture aperture and spacing data is also available, direct comparison between fracture and matrix hydraulic conductivities can be made. Measurements of matrix diffusion coefficients determine the extent to which solutes will be retarded relative to water movement.

Where measurements of rock matrix properties are carried out on surface samples (such as those obtained from outcrop exposures), the results can be seriously affected by weathering. Weathering will increase porosity, permeability and the matrix diffusion coefficient. It is important therefore to obtain core samples from depth within the aquifer for these measurements.

3.3.1. Matrix porosity

There are a number of different methods that can be used for estimating the porosity of the rock matrix. One of the simplest is the *water saturation* (or *water absorption*) method. Skagius and Neretnieks (1986) describe a method whereby rock core samples are first kept under vacuum at 90° C for three days to dry them, after which their weight is recorded. The samples are subsequently placed in a pan of distilled water in a vacuum chamber, which is held at a pressure close to the boiling point of water at ambient temperature (~ 25 mm Hg). Samples are removed and weighed at approximately weekly intervals until the sample weight reaches a constant value. The total increase in weight is used to calculate the porosity. Despite its simplicity, however, water saturation is less accurate than some of the other methods, and consistently yielded lower results than other methods in a comparison on ceramic materials (Andreola *et al.*, 2000).

In *helium pycnometry*, the pore volume is calculated from the observed pressure change between two chambers, one of which contains the rock sample. With no sample present, the pressure in each chamber is the same. When the sample is present, the change in pressure allows the volume of the rock matrix to be determined. The pore volume can be determined from the rock matrix volume and the bulk density. The sample can also be ground to allow determination of closed as well as open porosity.

The *mercury intrusion* method allows determination of the pore size distribution of rock samples, in addition to the total porosity. Mercury is forced into the rock sample, and the volume of mercury accepted by the rock is measured as the pressure is increased. Greater pressures are required for the

mercury to penetrate smaller pores, and the pressure required is dependent on the size of the pore opening. Pore diameters greater than approximately 0.003 µm can be measured (Andreola *et al.*, 2000). The specific yield of the rock matrix can be estimated from the difference in water content at saturation and field capacity.

3.3.2. Matrix permeability

Measurements of matrix permeability are made in the laboratory using a permeameter. In the constant head permeameter, a constant flow of fluid through a cylindrical core sample is induced under constant hydraulic gradient. The volume of fluid that flows through per unit time is then used to determine the hydraulic conductivity. In the falling head permeameter there is a decreasing flow through the sample due to a falling head difference.

Because hydraulic conductivities of many rocks are very low, standard methods that are used for determining hydraulic conductivities of soil samples usually do not have sufficient precision to be used for low porosity rocks, and the time required for these tests to be carried out would be very long. Therefore, the test method is usually varied, so that fluid is forced into the rock material under large pressures.

One method that is used in the petroleum industry involves saturating the core with one fluid, and then displacing this (under pressure) with a second fluid. (Gas displacing water is referred to as drainage, whereas water displacing gas is referred to as imbibition.) Produced volumes of both fluids are monitored and recorded as a function of time, and are used to determine hydraulic conductivity of the core material.

3.3.3. Matrix diffusion coefficients

Matrix diffusion coefficients have been measured on intact core samples by measuring rates of diffusion of solutes through rock samples. Intrinsic diffusion coefficients for other species can be calculated if the appropriate free water diffusion coefficients are known. In the *double reservoir method*, two reservoirs of water are connected only via a rock sample. Solute is added to one reservoir, and the solute concentration is monitored in the second reservoir. The rate of increase of solute concentration in the second reservoir is used to calculate the diffusion coefficient for the solute in the rock sample. The rate of decrease in solute concentration in the first reservoir can also be monitored as a check upon the method (Greswell *et al.*, 1998). In the *radial diffusion method*, a small diameter hole is drilled through the centre of a core sample (parallel to the core axis), and this is filled with fluid having a different solute concentration to the saturated core material. Solute concentration within the hole is monitored, and the diffusion coefficient of the rock is determined from the rate of change of concentration (Novakowski & van der Kamp,

1996). Estimates of diffusion coefficient can also be made from measurements of electrical resistance of core samples that are saturated with a fluid of known electrical conductivity.

Diffusion coefficients in consolidated sedimentary rocks mostly range between 10^{-11} and 10^{-14} m^2 s^{-1} (Parker *et al.*, 1994). Figure 3.9 shows the relationship between solute diffusion coefficient and matrix porosity for core samples of Lincolnshire Limestone. The diffusion coefficient for KBr varies between approximately 10^{-12} and 10^{-10} m^2 s^{-1} for porosity values between 4% and 25%. The mean diffusion coefficients for NaCl in Athabasca Formation sandstone (mean porosity 9%) was measured to be 1.5 β 10^{-11} m^2 s^{-1}, which plots close to the data shown in Figure 3.11 (Feenstra *et al.*, 1984). Iodide ion diffusion coefficients on unweathered granites range between 1 β 10^{-14} and 2 β 10^{-12} m^2 s^{-1} for porosities between 0.05 and 2.5% (Bradbury & Green, 1985; Skagius & Neretnieks, 1986). Significantly higher diffusion coefficients of approximately 1.3 β 10^{-10} m^2 s^{-1} for Na_2SO_4 in clay-rich till (porosity 31%) and 1.7 β 10^{-10} m^2 s^{-1} for organic dye in Ordovician limestone were measured by Novakowski and van der Kamp (1996).

A number of studies have observed increased matrix porosities and diffusion coefficients in weathered rock adjacent to fractures. For example, matrix diffusion coefficients and matrix porosity values for granite samples were found to be significantly higher at the fracture surface than at a distance of 5 cm from the fracture (Bradbury & Green, 1985). A zone of increased porosity of 10–20 cm was measured either side of a fracture in the Lincolnshire Limestone (Greswell *et al.*, 1998).

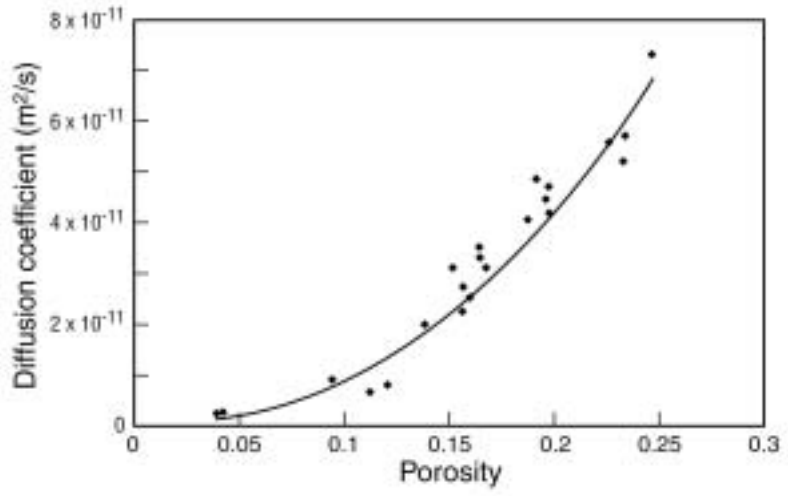

Figure 3.9. Relationship between solute diffusion coefficient for KBr and matrix porosity for core samples of Lincolnshire Limestone. (From Greswell *et al.*, 1998).

3.4. Identifying fractures from borehole logging

Borehole geophysical methods reveal information on a range of aquifer properties that may be related to the potential for groundwater flow. *Gamma logs* measure natural concentrations of radioactive elements (mainly K, U and Th), which tend to concentrate in fine-grained units. The technique has been widely used for lithological mapping, with shales and shaly sandstones usually having highest radioactivity. The logs are sometimes useful for locating fractures, as soluble radioactive minerals (e.g., uranium oxide) may precipitate in joints and fractures. *Density* and *neutron* logs provide information on the porosity of aquifer material. In some cases, they can provide information about the presence of fracture zones. *Neutron logs* are most sensitive to the presence of hydrogen ions and hence the amount of fluid present. *Sonic logs* record amplitude, velocity and attenuation of different compression and shear waves, which can be interpreted in terms of fractures. *Resistivity logs* aim to measure the resistivity of the formation material. This will be influenced by aquifer mineralogy, porosity, pore geometry and conductivity of pore fluids. The *calliper log* provides an approximate measure of the diameter of the borehole. It can identify zones of weak and fractured rock. Fractured horizons sometimes show an increase in borehole size, although individual fractures are often too small to be detected.

Dipmeters measure the formation micro-conductivity using an array of sondes that slowly rotate in the borehole as it is winched up or down. The images that are produced can be used to determine the dip angle and direction of bedding planes that intersect the borehole. Higher resolution methods involving a larger number of resistivity sensors can be used to detect fractures.

The *borehole televiewer* (BHTV) is often the most useful of the geophysical logs for locating fractures, although is less widely available than the more conventional borehole geophysical tools. The tool comprises a video image, a source of acoustic energy and a magnetometer. It is slowly rotated at uniform speed; the changes in the uniformity of the bore walls such as fractures are reflected as changes in picture intensity. Fractures perpendicular to the hole appear as horizontal traces, whereas fractures intersecting at an angle show as sinusoidal images. Fracture strike and dip can be determined from BHTV images, and qualitative information can be obtained on fracture frequency and aperture size.

Fluid temperature and conductance logs provide information on exchange of fluid between the borehole and the aquifer. In many cases, evidence of fluid movement is amplified in the temperature gradient log (the rate of change of temperature with depth). Sudden shifts in fluid properties with depth indicate exchange of fluid between the well and the surrounding aquifer. In the Clare

Valley, South Australia, electrical conductivity profiles have a step-like appearance, with sudden changes in concentration over small vertical distances, but little variation between these depths. The spacing of the steps is mostly of the order of 10–30 m, and their location usually corresponds to temperature anomalies (Box 3.3). However, these stratified profiles were not apparent immediately after the bore was drilled, presumably due to mixing during the drilling process. Similarly, the profiles may become distorted during pumping, and so the presence of fractures may be indicated from such data only after the bore has remained undisturbed for a period of several months.

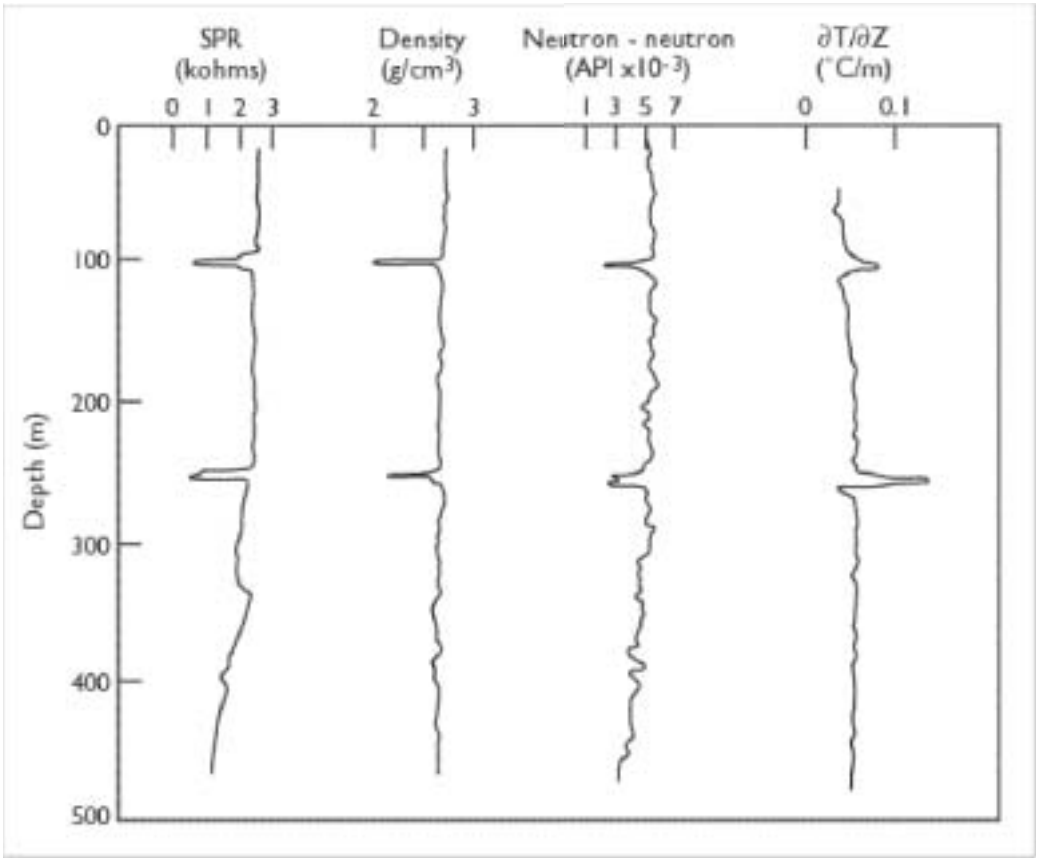

Figure 3.10. Comparison of some conventional geophysical logs obtained from a borehole in fractured granite, Manitoba, Canada. Anomalies at 100 m and 252 m are clearly correlated among single-point resistance (SPR), density, neutron (neutron-neutron) and differential temperature logs. (After Drury, 1989.)

Figure 3.10 shows the correlation between conventional geophysical logs and differential temperature obtained from a borehole in fractured granite in Manitoba, Canada. Anomalies at 100 m and 252 m can be clearly seen in single-point resistance, density, neutron and differential temperature logs, and

Box 3.3. Identifying fractures with bore fluid EC and temperature logs.

Temperature and bore fluid electrical conductivity logs have been used to identify the location of major flowing fractures in uncased bores within the Clare Valley, South Australia. Step-like changes in EC occur over vertical distances of only 1-3 m. The changes in electrical conductivity indicate movement of water into the borehole, and are believed to mark the locations of the major, flowing fractures. Anomalies in the temperature profile were apparent at the same depth as the changes in electrical conductivity. Such profiles probably indicate that flow is largely confined to discrete, well-spaced features. However, it is clear from investigations elsewhere in the region that significant groundwater flows occur through fractures which are not apparent from these logs.

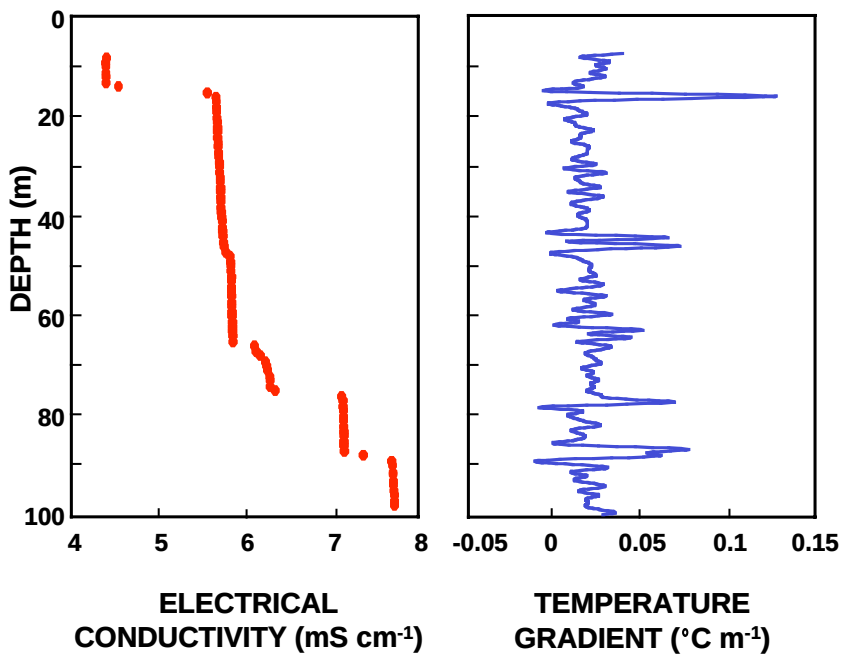

Figure 3.11. Electrical conductivity and temperature gradient logs for an uncased borehole in metasiltstone, Clare Valley, South Australia. The temperature profile was measured at 0.1 m intervals, with a resolution of 0.004°C. The temperature gradient was calculated from this data, and smoothed using a cubic spline routine. Step-like increases in electrical conductivity are correlated with temperature gradient anomalies, and locate major, flowing fractures. (From Cook *et al.*, 1999).

are interpreted as indicating the locations of major flowing fractures (Drury, 1989). It should be noted, however, that fractures cannot always be identified using geophysical logging methods, and results as unambiguous as those shown in Figure 3.10 are rare. It has usually been found that BHTV methods are most effective in locating fractures within boreholes, and they have the added advantage of also providing information on fracture orientation. In a geophysical study of three boreholes in fractured biotite gneiss at a contaminated site in Massachusetts, it was found that single point resistance logs identified only 50% of fractures that had been identified with BHTV logs, while neutron logs and calliper logs were able to identify only 35% and 25% of fractures, respectively (Dearborn, 1988). Furthermore, a number of the geophysical logs are not able to distinguish between open fractures and fractures that are filled with clay materials. Many of the methods are strongly affected by properties of the rock matrix, which can hinder their ability to detect fractures. The advantage of bore fluid conductivity logging is that variations in the measured signal can be due only to groundwater flow into the borehole.

3.5. Lineament mapping

Lineaments (or *fracture traces*) are natural linear features that can be mapped from aerial photography or remote sensing images. These features might include light or dark lines in the soil, alignment of vegetation, aligned gaps in ridges or straight reaches of streams. Such features often reflect subsurface geology, and may denote the presence of faults or major fractures. For example, Bradbury and Muldoon (1992) describe fractures that are visible in alfalfa fields using aerial photography, and use these photographs to determine fracture orientation and density. Electromagnetic profiling and vertical electrical sounding have also been used to identify faults and fracture zones (Kumar *et al.*, 2000; Bromley *et al.*, 1994). In Western Australia, Engel *et al.* (1989) used magnetic surveys to locate dolerite dykes that formed barriers to groundwater flow.

Statistical analysis of lineament data can provide regional-scale information on fracture density and orientation. Singhal and Gupta (1999) describe some simple methods for describing lineament density: (1) the number of lineaments per unit area; (2) the total length of lineaments per unit area; and (3) the number of lineament intersections per unit area. To measure lineament intersections, the intersection of two or more lineaments are plotted as points, and the number of points falling within a specified grid area is counted. Contouring the data gives a map of intersection density, which may reflect regional-scale fracture density. Analysis of lineament direction may be

plotted as rose diagrams (Section 3.2.2), and may provide useful information on fracture orientation. Buck (1999) mapped lineament direction on the Atherton Tablelands, North Queensland based on stream reaches (Fig. 3.12), but this information was not directly related to the hydrogeology.

It is often been found that wells located on lineaments, and particularly on the intersection of lineaments, produce higher bore yields than those located elsewhere. For example, Kellgren and Sander (2000) used satellite remote sensing to increase the success rate of bores in the semi-arid northeastern region of South Africa. Bores drilled at lineaments identified by remote sensing had median yields of 1.2 L s^{-1}, compared with a median yield of 0.5 L s^{-1} for bores drilled without prior lineament analysis. The yield of wells located along lineaments in phyllites and quartzites in Andhra Pradesh, India, was four orders of magnitude higher than elsewhere in similar rock types (Waters *et al.*, 1990).

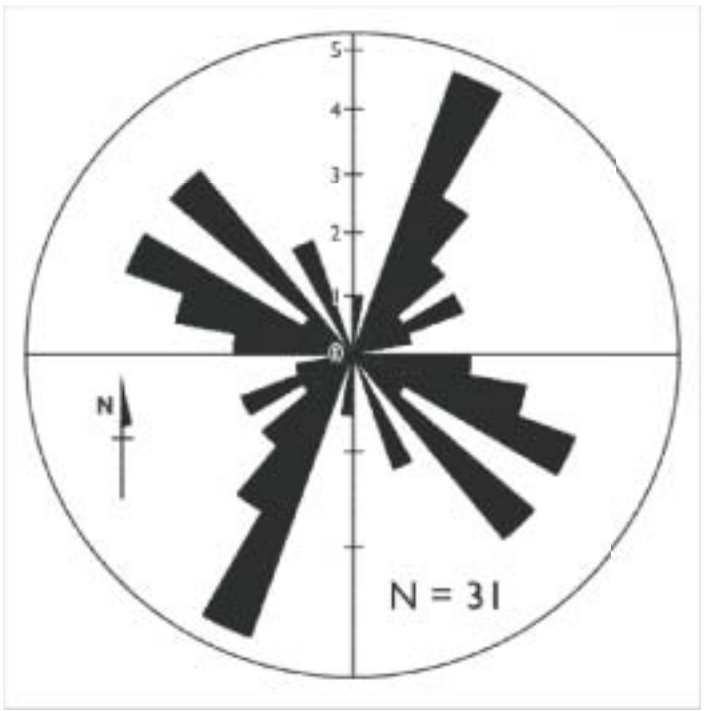

Figure 3.12. Rose diagram illustrating the dominant direction of lineation within Mazlin Creek, Atherton Tablelands. The major lineation direction is 25º, with minor directions of 290º and 315º. The lengths of the petals denote the number of lineations in each direction. (After Buck, 1999).

4. AQUIFER HYDRAULICS

4.1. Measurement of hydraulic head

Hydraulic head may be measured in piezometers, uncased boreholes or in intervals of uncased bores that have been isolated with packers. In all cases, the measured value applies to a finite interval of aquifer, which will usually contain a number of fractures as well as sections of unfractured rock. Different hydraulic heads may occur within different fractures, and differences in head may also occur between the fractures and the matrix. The measured hydraulic head will represent an average of the hydraulic heads within the sampled interval, but will usually be dominated by the larger fractures. In the case of packer systems, accurate measurements of hydraulic heads in low permeability zones may be difficult, because the time required for heads to stabilise (after the packers have been installed) may be weeks to months.

Measurement of variations in hydraulic head within individual boreholes or piezometer nests can provide useful information on the connectivity of fracture networks. Where hydraulic head within a borehole is uniform with depth, this might imply that fractures are vertically connected. Conversely, the presence of significant vertical variation in hydraulic head suggests poor vertical connection of fracture zones (Box 4.1). Also, if large vertical variations in hydraulic head exist, then construction of potentiometric surfaces becomes difficult. In porous media, potentiometric surface maps are usually constructed for individual aquifers, and by analogy it might be argued that potentiometric surface maps in fractured rock systems should be constructed for each fracture zone. Even where vertical variations in head are relatively small, potentiometric surface maps are not always able to be readily interpreted in terms of flow direction. In extreme cases, anisotropy of hydraulic conductivity may result in the groundwater flow direction differing from the direction of maximum hydraulic gradient by up to 90º (*see* Section 5.2). In heterogeneous systems, hydraulic gradients will usually be steeper in areas of low permeability and these tend to dominate potentiometric surface maps. High conductivity regions will appear as having little head gradient, even though they may be responsible for most of the flow.

Box 4.1. Vertical variations in hydraulic head, Clare Valley, South Australia.

Figure 4.1 shows the vertical distribution of hydraulic head measured in a piezometer nest in the Clare Valley, South Australia. A large decrease in head occurs between 35 and 45 m depth, and coincides with a zone of low hydraulic conductivity. It suggests that fracture zones at 30 m and 60 m depth are not vertically connected. An uncased borehole located only 20 m from this nest had a hydraulic head of 398.5 m, similar to that of the upper piezometers. The existence of large vertical stratification in hydraulic head in the piezometer nest, despite the presence of the nearby uncased borehole further suggests that there is little horizontal connection of fracture zones at this site. (In particular, the high hydraulic conductivity zone at 60 m depth must not be laterally extensive.)

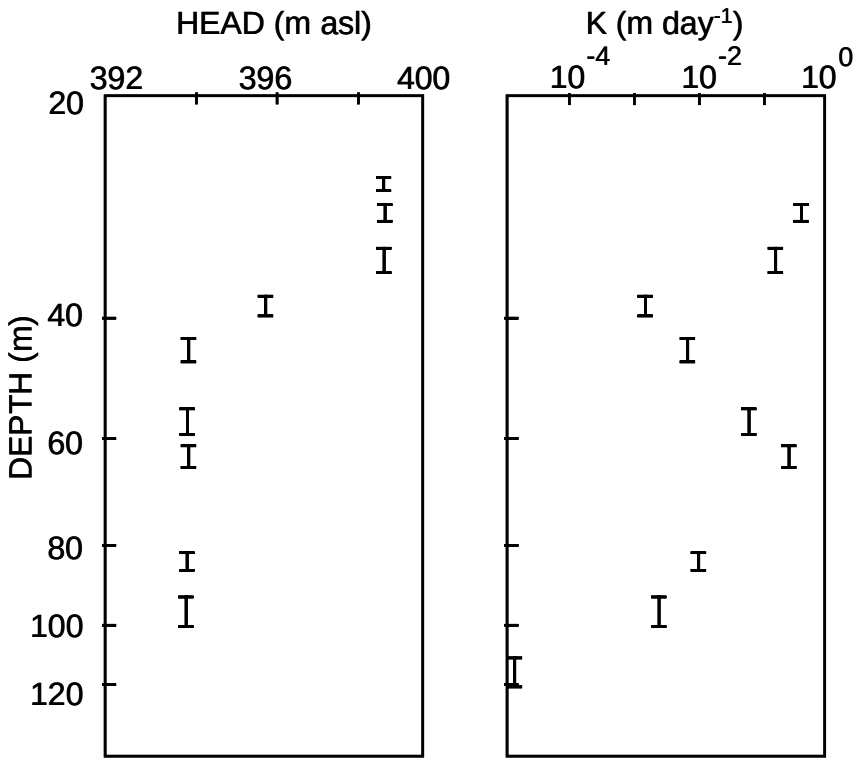

Figure 4.1. Vertical profile of hydraulic head measured in a piezometer nest in dolomitic marble, Clare Valley, South Australia. The hydraulic conductivity determined from single well pumping tests on the same piezometer nest is shown for comparison. A large decrease in head occurs between 35 and 45 m depth, and coincides with a zone of low hydraulic conductivity. (From Cook *et al.*, 1999).

Temporal variation in hydraulic head in fractured rock systems can also be more pronounced than in porous media systems. For example, water level rises of approximately 15 m in response to rainfall events of approximately 50 mm over 24 hours have been measured in fracture Cretaceous limestones and marly limestones in southern France (Bidaux & Drouge, 1993). Seasonal variations of up to 25 m are reported from fractured dolomite aquifers in Wisconsin (Bradbury & Muldoon, 1992; Fig. 4.2), and seasonal fluctuations of 15–30 m have been measured in fractured rock aquifers of the Dandenong Ranges, Victoria (Shugg, 1996). In some cases, this large seasonal variation in hydraulic head can result in large season variation in magnitude and direction of hydraulic gradients (Rayne *et al.*, 2001).

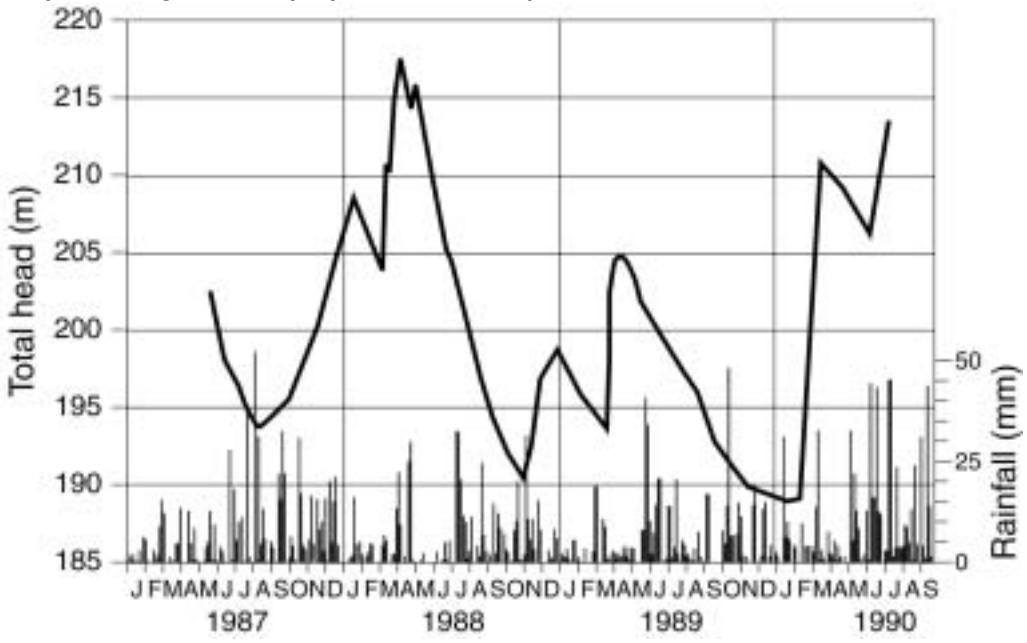

Figure 4.2. Hydrograph showing seasonal variations in hydraulic head for a piezometer in fractured dolomite of the Upper Door watershed, Wisconsin. (After Bradbury & Muldoon, 1992.)

The large variations in hydraulic head can be attributed to the low porosity and permeability of the aquifer matrix. In particular, the low permeability of the matrix means that the time required for it to fill and drain can be very long. Recharge through the vadose zone will usually occur rapidly along discrete, permeable fractures, which may become saturated during rain events, even though surrounding micropores remain unsaturated. Thus water levels in fractures may rise while most of the formation remains unsaturated (Fig. 4.3). In the case of a falling water table, it has been noted that the time for the matrix to drain may be extremely slow, so that the aquifer matrix may supply water as baseflow to streams for many months after the water table (as

reflected in fractures and piezometers) has declined (Price *et al.*, 2000). Where the rate of water level rise is slower, however, such as may be the case for deeper water tables displaying only seasonal variations in water level, then the water level in fractures and matrix may rise together. Of course, where the pore sizes within the matrix are very small, the matrix may not drain under gravity, and may remain saturated at all times (Healy & Cook, 2002).

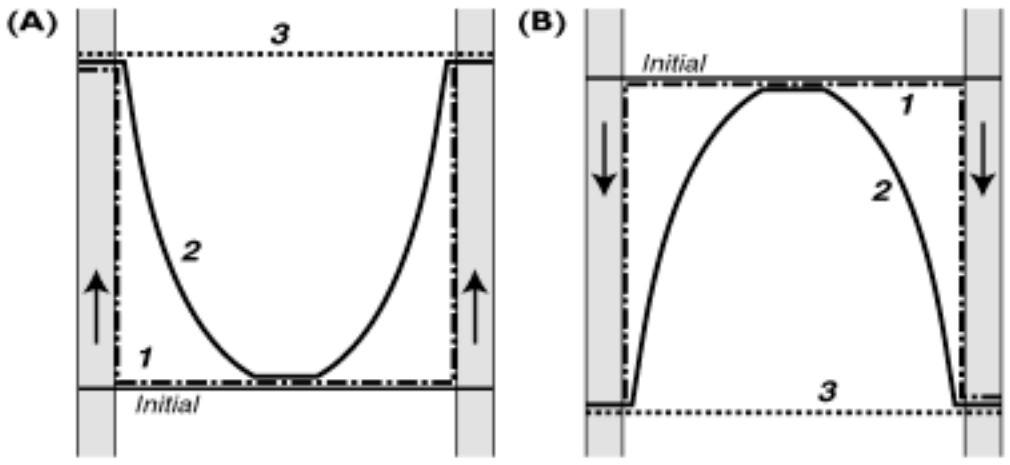

Figure 4.3. Schematic representation of saturation of a fractured rock matrix under rising (A) and falling (B) water tables. The initial water table position is indicated by the solid horizontal line. Where the rate of water table rise is rapid relative to the matrix permeability (1), the matrix remains unsaturated as the water level in the fracture rises. Where the rate of water level rise is slow, and the matrix permeability is high (3), the water table rises evenly in both the fracture and matrix. More usually, the matrix will partially fill as the water table rises (2). Equivalent behaviour occurs for declining water tables. (From Healy & Cook, 2002.)

It has also been observed that hydrograph variations in piezometers installed in fractured rocks may provide a poor record of water level variations within the aquifer itself. This arises where the permeability of the aquifer is low, and the storativity of the aquifer is very low relative to the storativity of the piezometer or well. Simmons *et al.* (1999) noted that short-term variations in aquifer water level are significantly attenuated within a well, particularly where the well radius is large (Fig. 4.4). The degree of attenuation increases as the storativity of the aquifer decreases. Longer-term variations in aquifer water level (such as annual cycles) will be less attenuated. This effect sometimes manifests itself as very smooth hydrographs in low porosity aquifers, which do not show responses to daily rainfall events.

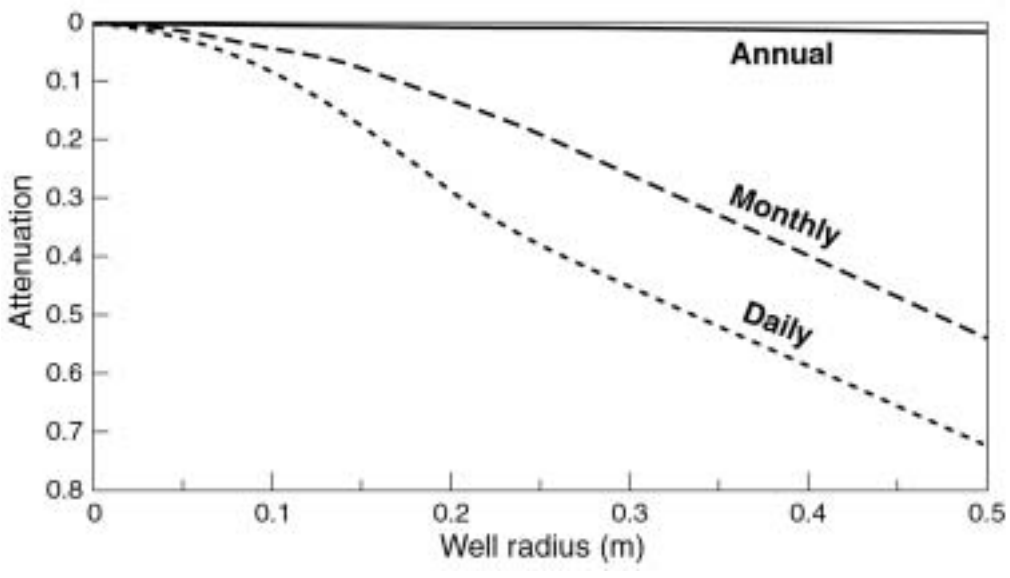

Figure 4.4. Attenuation of water level fluctuations in piezometers (defined as the difference between amplitude of water level fluctuation in the piezometer and in the aquifer, relative to that in the aquifer) as a function of well radius. (Values greater than zero represent attenuation of the signal within the piezometer.) Attenuation of daily, monthly and annual water level variations are compared. Simulations are for an aquifer hydraulic conductivity of 10 m/yr, and storativity of 0.005. (After Simmons *et al.*, 1999).

4.2. Measurement of aquifer hydraulic conductivity

4.2.1. Introduction

A number of methods are available for estimating the hydraulic conductivity of fractured rock aquifers. Pumping tests are one of the oldest tools for hydraulic characterisation. Single-well pumping tests enable an estimate of the average aquifer hydraulic conductivity in the vicinity of the borehole, but do not provide any information on its spatial variability. If single-well pumping tests are conducted on nested piezometers, or on intervals of uncased boreholes that are isolated using packers, then information on the vertical variation of hydraulic conductivity can be obtained. Multiple-well pumping tests can provide information on fracture connectivity and aquifer anisotropy, but are much more difficult and expensive to conduct. If the scales of heterogeneity are greater than the scale of the pumping test, then very irregular drawdown can occur, which can be difficult to interpret quantitatively. Borehole flowmeters and tracer tests are two additional tools that provide information on the vertical variation of hydraulic conductivity within a single uncased borehole.

4.2.2. Pumping tests

Pumping tests either inject or remove fluid from a borehole and measure the response (change in pressure) of the aquifer in the same or in nearby observation boreholes. A model is used to estimate aquifer properties (usually hydraulic conductivity and specific storage) from the hydraulic response. The values of the aquifer properties that are obtained will depend on the model that is used to interpret the test results.

Most models for interpreting pumping tests represent the aquifer as a homogeneous, isotropic porous medium, and adopt one of three basic geometries (Fig. 4.5; NRC, 1996). Spherical flow models describe fluid flow toward a spherical cavity in a homogeneous porous medium of infinite extent in all directions (Fig. 4.5a). Flow is three-dimensional, and equipotential surfaces are concentric spheres around the spherical cavity. This geometry might be used where the length of the test interval is not very different from the well radius. Radial flow geometry (Fig. 4.5b) describes flow toward a well that pumps from a homogeneous layer of infinite lateral extent (bounded above and below by impervious materials). Flow is two-dimensional, and equipotential surfaces are cylinders centred about the well axis. This geometry might also represent a horizontal fracture zone or a single horizontal fracture bounded by impermeable rock. Linear flow geometry describes flow that is uni-directional, such as linear flow towards a highly transmissive vertical fracture that intersects a well (Fig. 4.5c). Combinations of these three basic geometries are also possible. Methods for interpreting single well pumping tests using these various models are described in a number of texts.

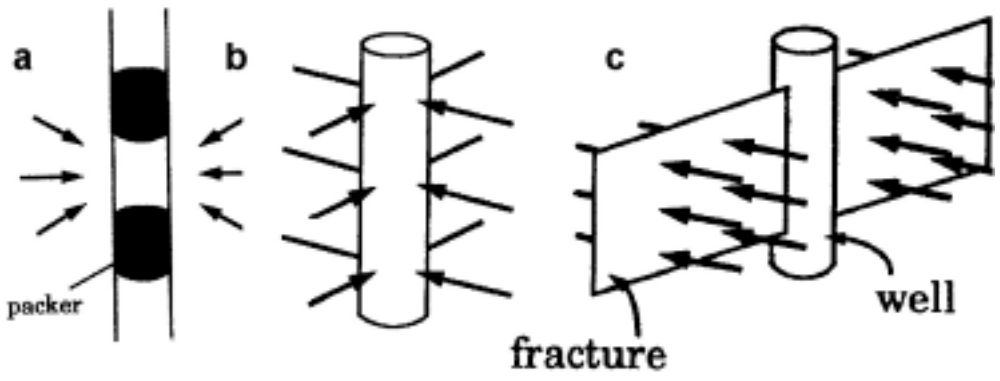

Figure 4.5. Contrasting models of groundwater flow to a well, that are used for interpreting single well hydraulic tests. (a) Flow to a short test interval in a borehole that approximates spherical geometry (interval length β borehole radius); (b) Radial flow to a cylinder; and (c) Linear flow to a well that intersects a highly transmissive vertical fracture. (From NRC, 1996.)

There are a number of reasons why pumping tests are unlikely to provide useful continuum estimates of aquifer hydraulic conductivity in fractured rocks. Firstly, the estimate of hydraulic conductivity is highly sensitive to the model chosen to analyse the data. Often none of the simplistic models represented by Figure 4.5 are appropriate, yet this may not be obvious from test results. Observed hydraulic head data may still superficially resemble one of these models. Because hydraulic conductivity is highly spatially variable in fractured rock systems, the hydraulic conductivity of the test interval is likely to change during a hydraulic test as the area of influence of the test increases. It is also common for the model that most closely approximates the test data to change throughout the test (e.g., from radial flow at short time to spherical flow at late time). Well-bore storage effects and well-skin effects can also have a pronounced effect on the results of hydraulic testing, depending on the type of test that is carried out. While their effects can be included in the model, to do so appropriately requires a high level of expertise on the part of the hydrogeologist. For these reasons, hydraulic conductivity values determined using different methods may sometimes differ substantially (Sidle & Lee, 1995). It is similarly difficult to accurately determine storativity or specific storage from single-well pumping tests. During constant flow and constant head tests, storage effects are dominant only for a relatively short period of time at the start of the test. The data during this period are commonly affected by a number of other factors, so that the storage effect can be very difficult to determine (NRC, 1996).

Multiple borehole tests offer a number of advantages over single borehole tests. In these tests, fluid is pumped from (or into) one well and drawdown is observed in the pumped well and in one or more nearby observation wells. If the test is conducted over a sufficiently large scale, then it may be able to treat the rock mass as a porous medium, and so determine both vertical and radial anisotropy. In other cases, multiple borehole pumping tests allow the interconnection between fractures to be investigated. In heterogeneous systems, it is frequently observed that nearby observation wells show little or no drawdown, while more distant wells may show large drawdown (Fig. 4.6). In some cases, this may occur even though the bores lie in the same direction from the pumping well.

Unless it can be demonstrated that the system is behaving as an equivalent (albeit anisotropic) porous media, estimation of model parameters from multiple borehole pumping tests may be difficult. It may be tempting to analyse the response in each observation well separately, using methods developed for isotropic porous media. This approach leads to a range of hydraulic properties being estimated, which might be interpreted as

representing the range of hydraulic properties of the rock mass. However, this approach can be very misleading, as pointed out by NRC (1996):

> Each separate analysis must be based on the assumption that the drawdown in the observation interval is due to the total rate of fluid removal at the pumping well. However, in a heterogeneous formation, the low-permeability regions yield less fluid and consequently suffer less drawdown than higher-permeability regions. A separate analysis of observation intervals situated in low-permeability regions will yield erroneously high permeability values because total fluid production is erroneously ascribed to a low drawdown.

The alternative is to use a numerical model to attempt to simulate pumping test results. However this will usually require the use of geophysical and other fracture mapping techniques to help constrain the location of high conductivity zones in the model, or otherwise issues of non-uniqueness are likely to arise (e.g., Hsieh, 2000). Nevertheless, despite the difficulty of quantifying hydraulic parameters from multiple well pumping tests, such tests often provide valuable information on aquifer behaviour, and help constrain conceptual models (Box 4.2).

Figure 4.6. Drawdown cone after five days continual pumping in a crystalline bedrock aquifer. The pumping well is 100 m deep, and was pumped at 20 L s^{-1}. Pumping induced drawdown in wells 700 m to the northeast, but had no effect on water levels in a well 150 m to the north. The cone is strongly anisotropic in the northeast-southwest direction. (After Caswell, 1992).

Box 4.2. Multiple well pumping test in fractured basalt, Atherton Tablelands.

In December 1999 a 4-day pumping test was performed in fractured basalt aquifers in Tolga, Atherton Tablelands, Queensland. The pumping bore was open to the aquifer between 44 and 91 m depth, and was pumped at approximately 40 L s^{-1} for the duration of the test. Drawdown in the pumped bore had stabilised at approximately 6.1 m by the end of the test. Water levels were measured in nine observation bores within a radius of 650 m (Fig. 4.7). At two observation bores, rises in water levels were recorded, presumably the result of irrigation activities nearby. For the remaining seven bores, drawdowns were between zero and 31 cm (Table 4.1). Figure 4.8 shows the drawdown plotted against depth of the screen interval, where this information was known, and for those bores not affected by irrigation. (Unfortunately, two of the observation bores were domestic wells for which screen depth information was not available.) Significant drawdown is observed in those bores that are screened at similar depths to the pumping bore, with negligible drawdown in bores with screens at shallower depths. The decrease in drawdown with distance for bores screened between 60 and 70 m depth is consistent with a horizontal (radial) transmissivity of approximately 10^4 m^2 day^{-1} (Theim solution). However none of these bores are located northwest or southeast of the pumping bore, and so the test is not able to characterise any radial anisotropy. The absence of drawdown in shallow bores suggests that the radial hydraulic conductivity is much greater than the vertical hydraulic conductivity (G. Herbert, unpublished data).

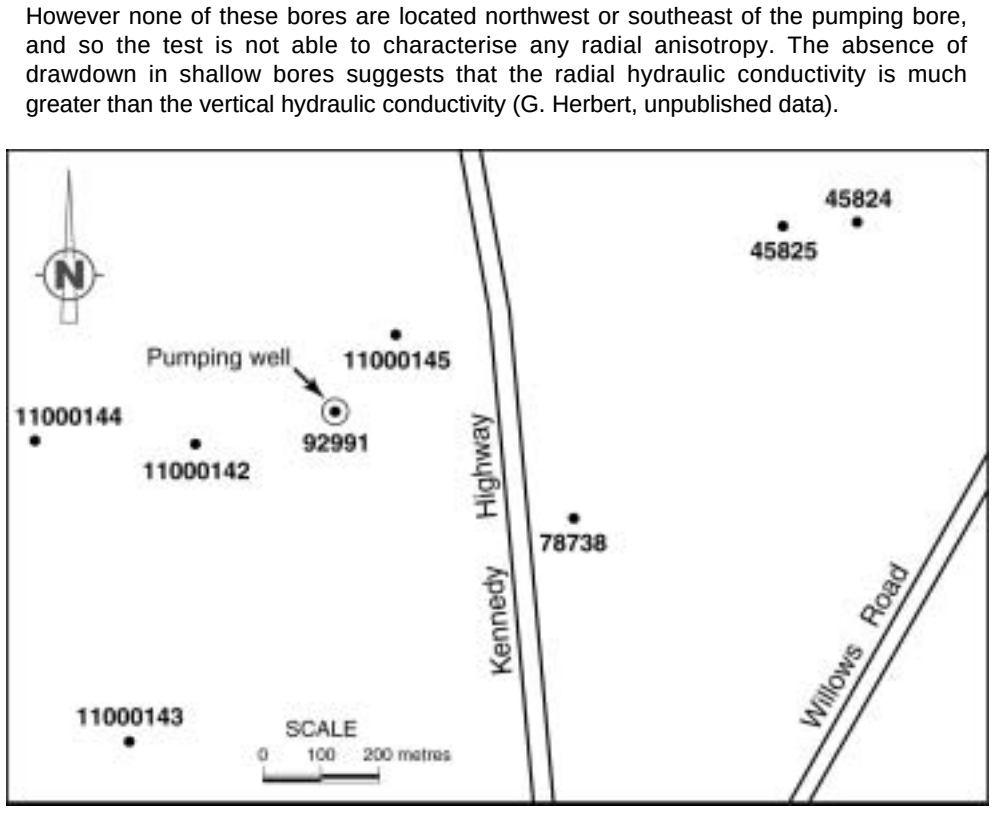

Figure 4.7. Location of pumping bore and observation bores for a 4-day pump test in fractured basalt, Tolga, Queensland.

Box 4.2 continues next page

Box 4.2 (continued).

Table 4.1. Details of drawdown in pumping bore (92991) and observation bores.

Bore No.	Drawdown (m)	Distance from Pumping Well (m)	Screen Depth (m)
11000142	0.18	164	64 – 70
11000143A	0.12	450	61 – 67
11000143B	<0.01	450	38 – 44
11000144	0.13	345	63 – 69
11000145	0.29	115	61 – 67
45824	0.31	640	Unknown
45825	<0.01	560	1 – 21
78738	0.22	305	Unknown
92991	6.1	0	44 – 91

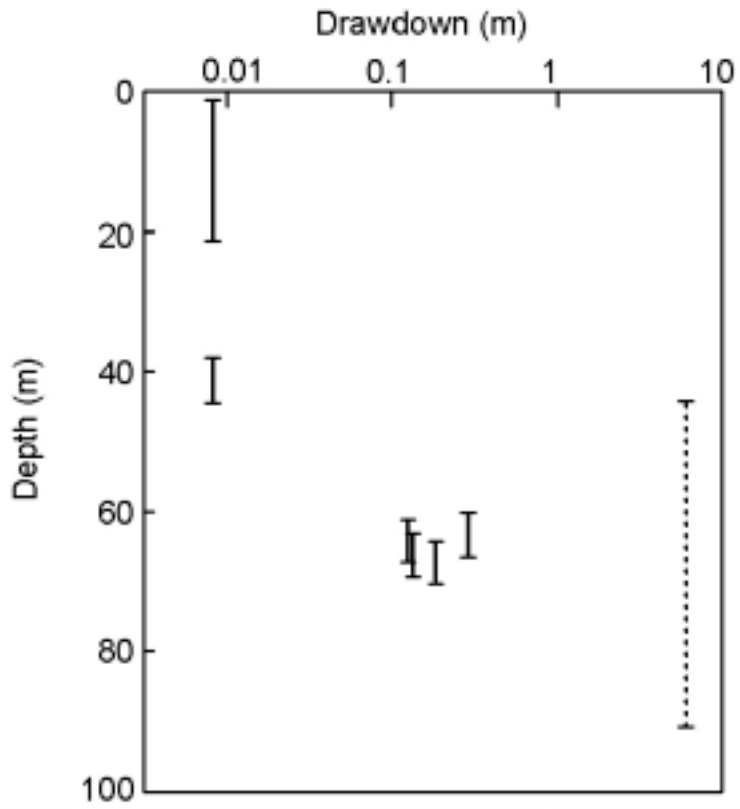

Figure 4.8. Drawdown versus depth of screened interval during a 4-day pumping test in fractured basalts, Tolga, Queensland. Vertical lines indicate the vertical extent of the well screens, and the broken line indicates the pumping well.

4.2.3. Borehole flowmeters

A borehole flowmeter is a device for measuring vertical flow within a borehole. A packer arrangement is usually used to seal against the sides of the borehole, and restrict vertical flow to within a small passage through the middle of the packer assembly, where it is measured. Spinner, heat pulse, or electromagnetic methods can be used to measure the flow rate. The groundwater is pumped (with the pump inlet located near the watertable), and this causes water to flow upwards through the borehole towards the pump inlet. Measurements of the vertical flow rate are made as the borehole flowmeter is lowered and/or raised, and this can be used to determine vertical variations in aquifer hydraulic conductivity.

Figure 4.9 shows the type of results that are produced from borehole flowmeter tests. Figure 4.9b shows the results for a homogeneous aquifer. When the flowmeter is located immediately below the pump inlet, the flow rate recorded will be equal to the pumping rate. As the flowmeter is lowered, the flow rate through the flowmeter will linearly decrease, as an increasing proportion of the flow to the pump is sourced from the aquifer above the flowmeter. At the bottom of the well, the flow through the flowmeter will be zero. In contrast, a fractured media typically displays a ‘stepped’ profile, with flow decreasing abruptly when the flowmeter is lowered beneath a major flowing fracture. The plot of flow rate versus depth can then be used to determine aquifer hydraulic conductivity as a function of depth, as described by Molz *et al.* (1994). Borehole flowmeter surveys can also be measured under ambient flow (without pumping) to measure natural vertical flow within boreholes.

4.2.4. Tracer approaches

Relative hydraulic conductivities in uncased bores can also be estimated using a tracer approach. The technique described by Pedler *et al.* (1990) involves replacing the standing column of water in a borehole with a uniformly deionised fluid, then profiling the changes in fluid electrical conductivity in the borehole as the well is pumped. The natural bore fluid is replaced by deionised water by first inserting a tube to the bottom of the well, and pumping deionised water into the tube while simultaneously pumping from the watertable to remove existing bore fluid. Once this is complete, the addition of deionised water is stopped, and the fluid electrical conductivity is profiled as the well continues to be pumped from the watertable. The pumping of the well draws the formation fluid (with higher electrical conductivity) into the borehole, and the location of high hydraulic conductivity zones within the borehole can be determined from changes in the profile over time (Box 4.3).

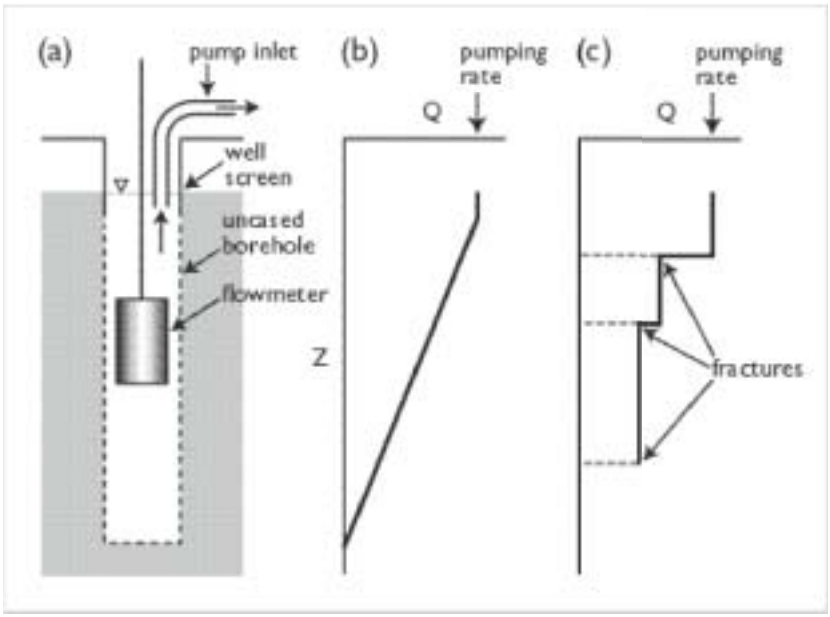

Figure 4.9. Typical data produced by borehole flowmeter surveys in porous media and fractured rocks. (a) survey set-up, (b) typical porous media results, (c) typical fractured rock results.

Figure 4.10. Preparing to carry out borehole flowmeter measurements. Photo courtesy of Paul Pavelic, CSIRO.

Of course, the test does not require the use of deionised water, simply that the water initially injected into the borehole is of sufficiently different concentration to the water in the aquifer. A model to estimate hydraulic conductivity based on the fluid logging data is described by Tsang *et al.* (1990).

Box 4.3. Measurement of aquifer hydraulic conductivity using wellbore fluid logging.

Figure 4.11 presents results of wellbore fluid logging during continuous well pumping in a fractured granite aquifer, Rhode Island, USA. Following addition of deionised water, a relatively constant electrical conductivity of 5-10 µS/cm was achieved over the entire profile. Due to mechanical difficulties, the well-bore fluid remained stagnant for an hour, and therefore a second logging was conducted prior to fluid extraction (log PA1345). This second logging already indicates natural flow of water into the bore at 16, 26 and 53 m. During pumping, formation water from these zones is drawn into the well, and then moves upwards towards the pump inlet (located close to the watertable). Based on this data, hydraulic conductivities for 3 m intervals centred at 15.7, 25.8, 29.4 and 53.8 m depth were estimated to be 2.1, 2.3, 2.0 and 0.6 m day^{-1} respectively (Pedler *et al.*, 1990).

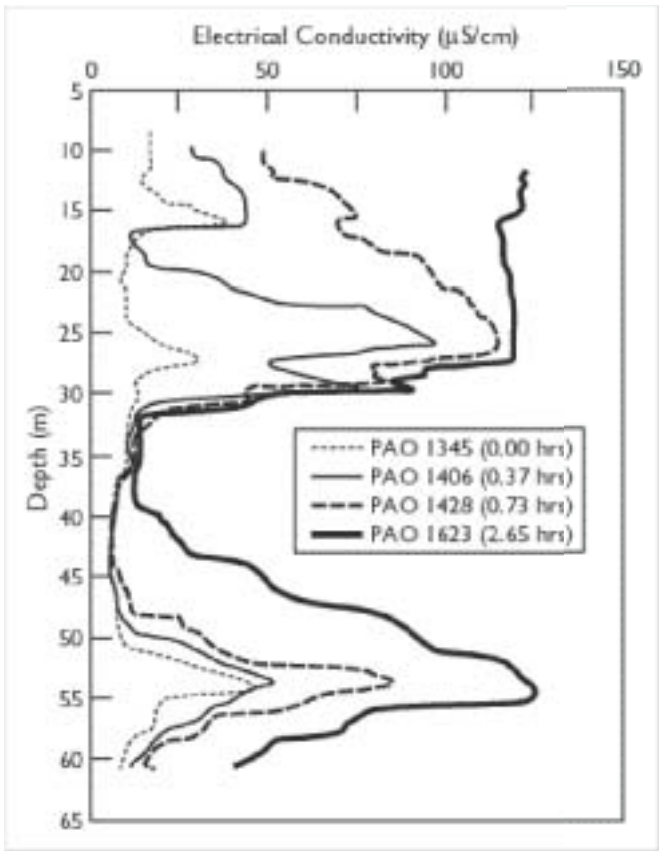

Figure 4.11. Time series of electrical conductivity profiles obtained from fluid logging during continuous pumping. (After Pedler *et al.*, 1990.)

4.3. Surface geophysics for mapping radial anisotropy

There are rarely enough observation bores surrounding a pumping well to accurately determine anisotropy in radial hydraulic conductivity. For this reason, surrogate measures of aquifer hydraulic conductivity can be extremely valuable. As the flow of electric current is analogous to fluid flow, high electrical current densities may indicate high hydraulic conductivities. Brown (1989) has shown that electrical current density varies with fracture aperture width, $2b$, whereas fluid flow depends on $(2b)^3$. In fracture analysis, a powerful survey technique is to conduct electrical measurements azimuthally around a central point in an attempt to measure anisotropy of hydraulic conductivity (Fig. 4.12). With collinear surveys (electrodes in a line) this is usually achieved by rotating the array around a fixed central point. The direction of dominant fracture orientation can be found from plotting the observations as a rose diagram.

Figure 4.12. Carrying out an azimuthal resistivity survey, centred on a borehole, in the Clare Valley. Photo courtesy of Graham Heinson, University of Adelaide.

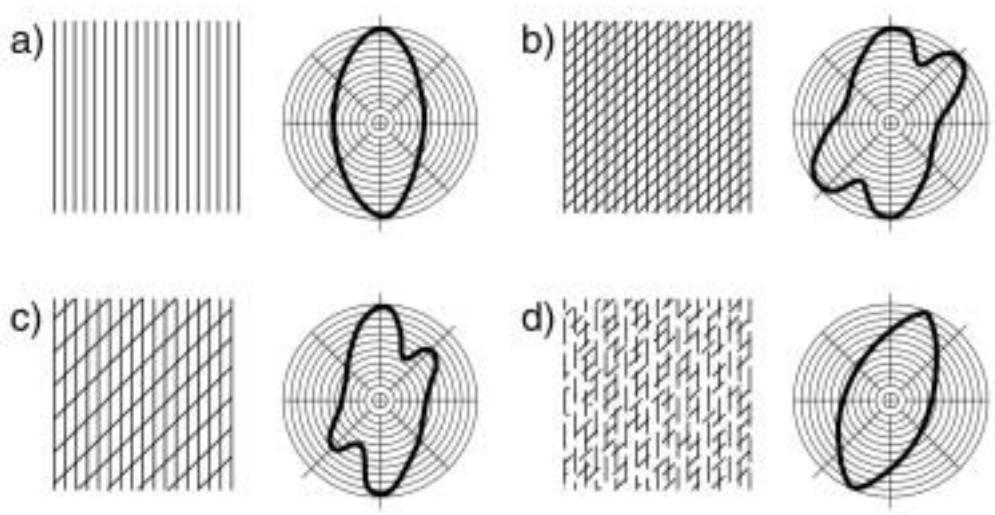

Figure 4.13. Hypothetical results of azimuthal resistivity measurements above vertically fractured rock using collinear arrays. Note that the maximum observed apparent resistivity is parallel to the direction of the fractures. (From Taylor & Fleming, 1988.)

Resistivity surveys can be made using a number of different current and potential electrode arrangements. For the Schlumberger, Dipole-Dipole and Wenner arrays, the maximum observed apparent resistivity is parallel to the direction of the fractures (Habberjam, 1972), while the true earth resistivity has a maximum at right angles to the fractures. This phenomenon is known as the *paradox of anisotropy* (Taylor & Flemming, 1988). The reasons for the paradox of anisotropy are complex, but relate to the non-uniform distribution of electrical current density in the direction of fracturing (Wilson *et al.*, 2000). Figure 4.13 shows schematic representations of different types of fracture systems and the resulting azimuthal resistivity plots. However, the preferred geometry for measuring fracture orientation is the square array (Lane *et al.*, 1995), because it is more sensitive to anisotropy in the subsurface, and it does not suffer from the paradox of anisotropy seen in co-linear arrays. This means that with a square array, the direction of maximum apparent resistivity will be perpendicular to fracture strike.

For electromagnetic induction, relating the azimuthal conductivity to fracture orientation is more complex. When the conductive targets (fractures) are shallower than about 10% of the coil separation, the EM equivalent of the *paradox of anisotropy* applies. For greater depths, the maximum conductivity is aligned parallel to the fractures (Wilson *et al.*, 2000).

Figure 4.14 shows results of an azimuthal resistivity survey at Mirror Lake, New Hampshire, using a square-array configuration, and with data collected every 15° about a central point. At this site, approximately 7 m of glacial drift is underlain by fractured crystalline bedrock, and so a relatively

large electrode spacing was chosen to minimise the impact of the overburden. Figure 4.14 shows a minimum resistivity oriented 30° from north, which is interpreted to be the principal fracture strike. The result is consistent with measurements of fracture orientation made at an outcrop within 250 m of the site (Fig. 3.5). If electrode spacings for azimuthal surveys are large relative to the spacing of the conductive fractures, then resistivity patterns should be similar at different electrode spacings, and if the survey is repeated nearby. However, if the spacing of conductive fractures is large relative to the area sampled by the geophysical survey, then different results may be obtained at different electrode spacings, and in different locations. In this case, interpretation of the results in terms of regional aquifer properties is difficult (Box 4.4).

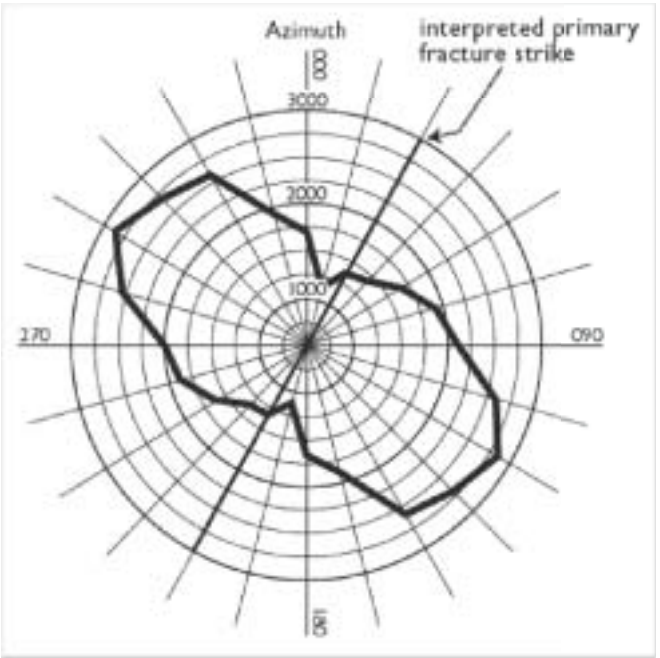

Figure 4.14. Square array resistivity data (ohm metres) from Mirror Lake, New Hampshire. The resistivity maxima occur at 120° and 300°, suggesting a primary fracture strike of 30°. (From Lane *et al.*, 1995.)

Box 4.4. Azimuthal resistivity surveys in the Clare Valley.

In the Clare Valley, South Australia, azimuthal resistivity surveys were performed to measure the orientation of major fractures. Figure 4.15 shows normalised apparent resistivity results for the DC Wenner array with electrode spacing of 20 m and 50 m carried out in Mintaro Shale. For the 20 m electrode separation, the ellipse has its major axis parallel to the bedding strike. As separation increases, the major axis of the ellipses gradually rotates, to be oriented 50º east of north at the 50 m electrode spacing. The reason for such changes is unclear, but may indicate changes in dominant fracture orientation with depth.

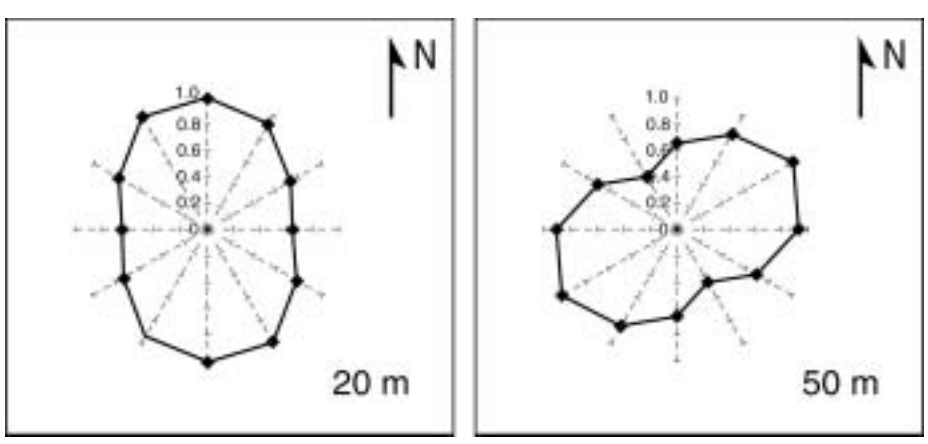

Figure 4.15. Normalised apparent resistivity polar plots for a Wenner array survey in the Clare Valley with electrode separations of 20 and 50 m. (After Wilson *et al.*, 2000.)

5. GROUNDWATER FLOW, AQUIFER RECHARGE AND DISCHARGE

5.1. Introduction

Determination of groundwater balances and calculation of aquifer sustainable yield usually require information on aquifer recharge and discharge, and groundwater flow rates and directions. Most traditional methods for calculation of groundwater flow rates and aquifer recharge and discharge rates cannot be directly applied to fractured rock systems. This chapter discusses a number of the methods that have been applied for calculation of volumetric flow rates of groundwaters, and how these might be applied in fractured rock systems.

5.2. Darcy's law

In porous media aquifers, horizontal groundwater flow rates are usually estimated from Darcy's law and measurements of aquifer hydraulic conductivity and hydraulic gradients. While Darcy's law is still theoretically applicable to fractured rock aquifers (*see* Section 1.3), there are a number of complications that make its practical application difficult. The large variability of hydraulic conductivity makes characterisation of average values very difficult, and preferential orientation of fractures will usually result in anisotropy. Even where a *representative elementary volume* can be defined (*see* Section 1.4), it may not be possible to measure hydraulic conductivity on this scale. Spatial variations in hydraulic conductivity and anisotropy can result in a flow direction that is not perpendicular to the potentiometric contours. In theory, flow direction may depart from the direction of maximum hydraulic gradient by up to 90º.

When applying Darcy's law in fractured rock, it is critical that hydraulic conductivity and hydraulic head gradients are measured over the same area of aquifer. Within a single borehole, for example, zones of highest hydraulic conductivity need not correspond with zones of highest ambient groundwater flow rate, because it should not be assumed that the horizontal hydraulic head gradient is the same at all depths. Furthermore, erroneous results may occur when regional groundwater flow rates are calculated by multiplying regional hydraulic head gradients with hydraulic conductivities determined from pumping tests that operate at a much smaller spatial scale (Box 5.1). For example, at Mirror Lake, multiple-well hydraulic tests indicate that the bedrock contains highly conductive fracture clusters, which are poorly connected regionally. Each cluster is believed to occupy a zone approximately

Box 5.1. Problems with applying Darcy's law to fractured rock aquifers.

Erroneous results can occur when regional groundwater flow rates are calculated by applying Darcy's law to hydraulic conductivity values and hydraulic head gradients that have been measured at different spatial scales. At Pearce Road, Clare Valley, the regional potentiometric surface suggests a hydraulic gradient of approximately 3 β 10^{-2} (60 m in 2 km). Between 35 and 38 m depth, the average aquifer hydraulic conductivity was measured to be in excess of 100 m day^{-1}, giving a flow rate in excess of 9 m^2 day^{-1} for this zone alone (Fig. 5.1). Based on a distance to the flow divide of only 2 km, the flow rate of 9 m^2 day^{-1} would suggest that recharge over this distance must be 1640 mm yr^{-1}, which is three times higher than the mean annual rainfall. This suggests that the hydraulic head gradient within the high conductivity zone is much less than the observed regional gradient. One reason for this might be that the fractures at this depth are not well-connected to the regional flow system.

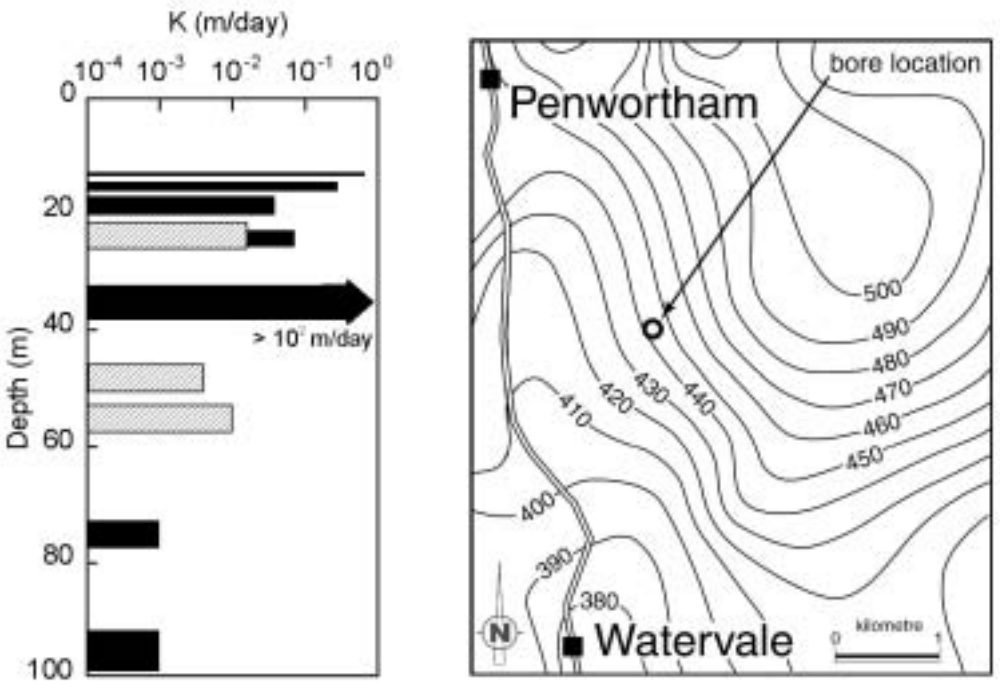

Figure 5.1. Potentiometric surface in one of the catchments of the Clare Valley, South Australia (contour interval 10 m), and the vertical distribution of hydraulic conductivity measured in a piezometer nest within the catchment.

1.5 m thick, and 20 to 50 m in horizontal extent, having a mean hydraulic conductivity of 6 β 10^{-5} m s^{-1}. Over distances of tens of metres, groundwater may travel through these highly permeable fractures clusters, but over distances of 100 m or more, groundwater must travel through less permeable regions which connect the clusters. The effective hydraulic conductivity at a scale of 100 m β 100 m has been estimated to be only 2 β 10^{-7} m s^{-1} (Tiedeman *et al.*, 1998). Problems can also result when potentiometric surfaces are constructed from sparse hydraulic head data, yet hydraulic conductivity is highly variable on a smaller scale.

Within the Clare Valley, South Australia, measurements of flow rate at different times throughout the year suggest a very large temporal variation in groundwater flow rate, despite relatively small seasonal variations in hydraulic head (Love *et al.*, 2002). A similar observation was made by Moore (1992) for the shale and limestone aquifers of Oak Ridge, Tennessee. In both cases, the observation can be ascribed to most of the flow occurring through a thin permeable weathered zone close to the land surface. While at any particular location, high hydraulic conductivity zones may occur at greater depth, on a regional scale these zones are only connected through the shallow zone. Thus, when the water table drops these fractures remain saturated but are no longer connected regionally, so flow through them decreases markedly (Fig. 5.2).

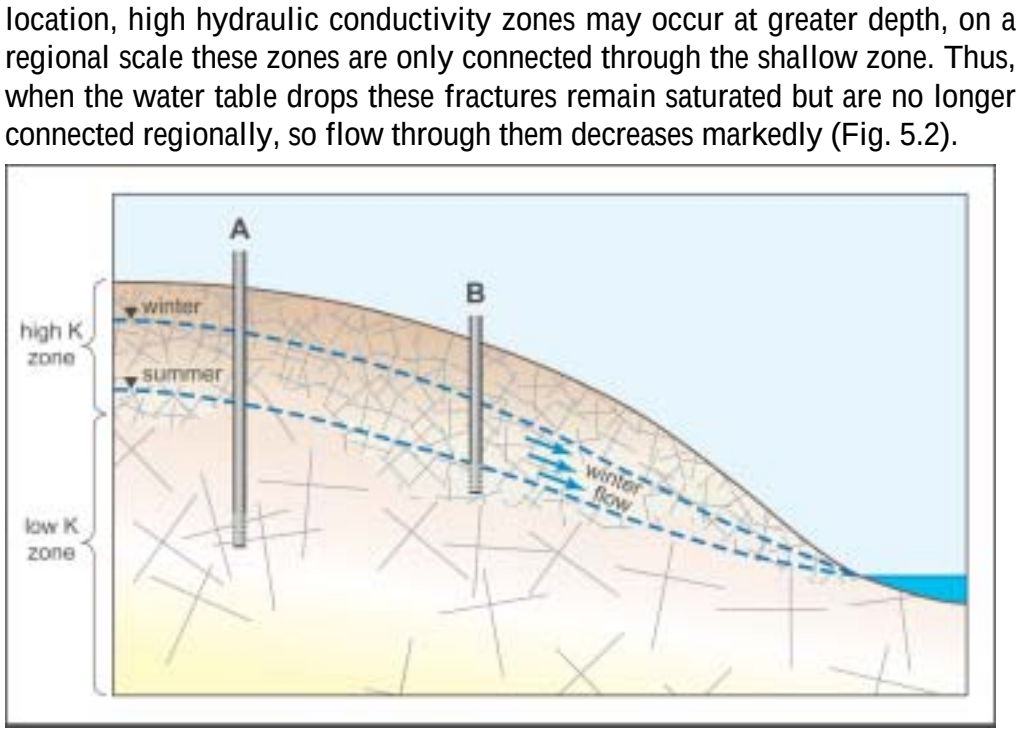

Figure 5.2. Schematic representation of regional groundwater flow through fractured rocks. A very high hydraulic conductivity is measured for well A, although very little flow occurs because the fractures are not connected to the regional flow system. Well B has moderate hydraulic conductivity. The flow rate through this well is extremely high when the water table is high, but approaches zero as the water table falls. On a regional scale, most of the fracture connections occur within the zone of water table fluctuation, and so connectivity decreases markedly as the water table falls.

5.3. Point dilution and well dilution methods

5.3.1. Introduction

Point dilution and well dilution methods seek to estimate the horizontal groundwater velocity through a well by measuring the rate at which the concentration of tracer that is injected into the well decreases over time. Measurement of radon concentrations in the well provides a natural analogue of these methods, which does not require the use of artificial tracers. However, while these relatively simple techniques provide direct information on groundwater flow rate, they do not provide any information on the flow direction. It should also be noted that because the well constitutes a local high hydraulic conductivity zone, convergence of groundwater flowlines near the well will mean that the flow rate within the well, per unit area, will be greater than the flow rate within the aquifer (Drost *et al.*, 1968). If no well casing is present, then the flow rate through the well will exceed that through the aquifer by a factor of two, so a correction can easily be applied. When casing is present, then the magnitude of this effect will vary with the bore geometry and with the hydraulic conductivity of the aquifer and the gravel pack (if present). Equations for calculating the correction factor required to convert flow rates through the well to those through the aquifer can be found in Drost *et al.* (1968).

5.3.2. Point dilution

In point dilution tests, packers are used in the well screen to isolate the portion of the aquifer to be tested. A tracer is introduced into the isolated part of the well, and this gets diluted over time due to mixing with groundwater flowing through the well. Throughout the test, the isolated portion of the well is mixed, so that variations in concentration within the isolated interval are minimised. The groundwater flow rate through the well is estimated from the rate of decrease of tracer concentration with time. If the isolated interval is well mixed, then the concentration of the added tracer in the chamber will decrease exponentially over time according to:

$$\frac{c \mid c'}{c_0 \mid c'} = \exp\left|\frac{\mid 2qt}{/r}\right| \qquad (5.1)$$

where c is the tracer concentration at time t, c_0 is the initial concentration, c' is the concentration naturally present within the groundwater, q is the flow rate through the well, and r is the well radius. Ideally, a tracer that is not naturally present within the groundwater is used ($c'=0$), so the analysis is simplified. The solution to Equation 5.1 for a well radius of 0.1 m, and for flow rates between 0.1 and 1.0 m day^{-1} is shown in Figure 5.3. At flow rates much below

0.01 m day^{-1}, diffusion may become important, and so Equation 5.1 will overestimate the advective water velocity. Figure 5.3 also shows results of a point dilution test carried out in fractured granites in Maine, USA. A 3 m interval of an uncased borehole was isolated using packers, and rhodamine was used as the tracer. Measurements were carried out over a period of 10 hours, during which time the concentration within the well decreased to 20% of its initial concentration. A flow rate through the well of between 0.3 and 1.0 m day^{-1} is inferred from this data. Point dilution tests carried out in fractured rocks in the Axe Creek catchment, Victoria, are described by Hodgson and Finlayson (1990).

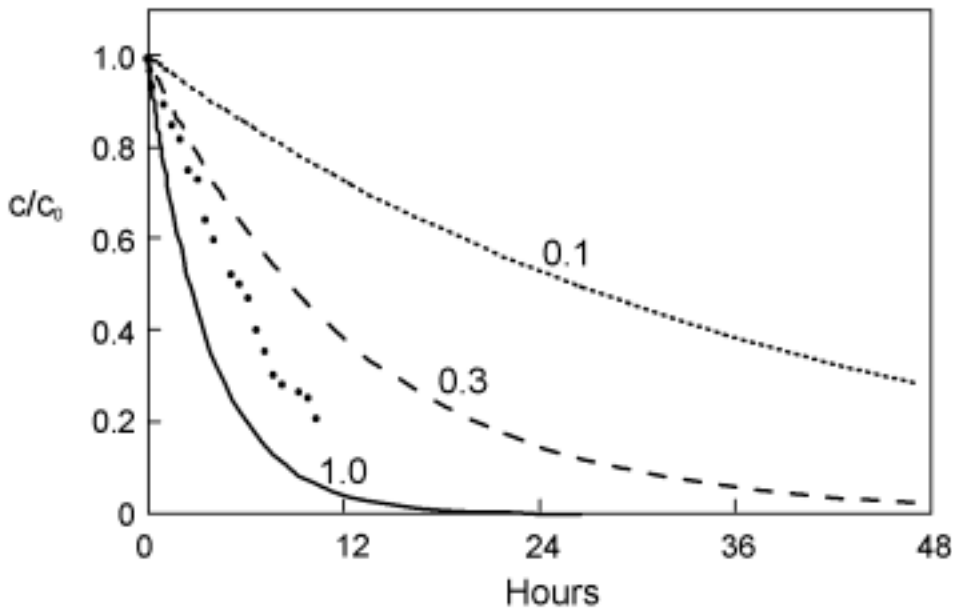

Figure 5.3. Theoretical concentration versus time curves for point dilution tests in a well of radius r = 0.1 m, and where the added tracer is not naturally present within the groundwater (c'=0). Flow rates of q = 0.1, 0.3 and 1.0 m day^{-1} are compared. Circles denote results of a point dilution test in fractured rock in Maine, USA (Sidle & Lee, 1995).

5.3.3. Radon

It has recently been shown that radon concentrations within wells can be interpreted as a natural version of a point dilution experiment. Radon has a half-life of 3.8 days, and is produced from radioactive decay of uranium-series isotopes within the aquifer. Radon concentrations in groundwater appear to be primarily controlled by aquifer mineralogy and the location of radon bearing minerals relative to the pore spaces. However, the ratio of radon concentrations in an undisturbed well to that in the groundwater (measured

after well purging) can be used to estimate the groundwater flow rate (Cook *et al.*, 1999; Hamada, 1999). If the flow rate through the well is very low, then the water in the well will be stagnant, and most of its radon will have decayed to background. Significant radon concentrations should be present in well water only if there is sufficient flow into the well to replenish the radon faster than it can decay.

Under conditions of steady groundwater flow, the flow rate can be determined from the ratio of radon concentration within the well to that within the aquifer:

$$q = \frac{c}{c_0 - c}\frac{--r}{2} \qquad (5.2)$$

where q is the flow rate into the well, c and c_0 are the radon concentrations in the well (measured before purging) and in the aquifer (measured after purging the well) respectively, r is the well radius and β is the decay constant for radon [0.18 day^{-1}]. Solutions to Equation 5.2 for well radii of 0.05, 0.1 and 0.15 m are depicted in Figure 5.4. The curves begin to flatten at flow rates greater than approximately 50 m yr^{-1}, which indicates that variations in radon concentrations in unpurged wells will be sensitive to groundwater flow rate only if the flow rate is less than about 50 m yr^{-1}.

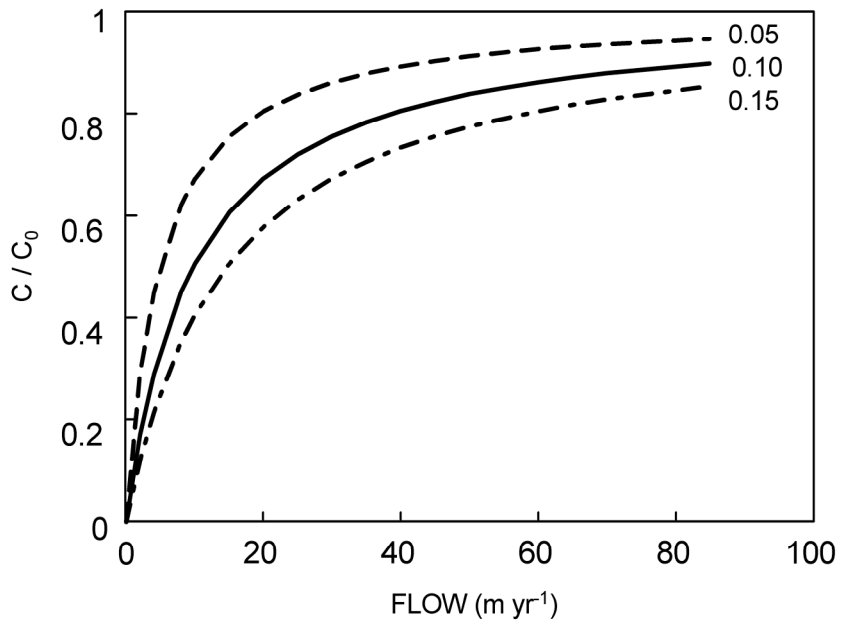

Figure 5.4. Theoretical relationship between radon concentration in an unpurged borehole, relative to that in the aquifer, and groundwater flow rate for bore radii of 0.05, 0.1 and 0.15 m. (From Cook *et al.*, 1999.)

Figure 5.5 shows the ratio of radon concentration measured before purging, to that measured after purging, versus depth of the well screen below

the land surface, for piezometers located throughout Atherton Tableland basalt aquifers, Queensland. For a large number of sites, $c/c_0 > 0.8$, indicating groundwater flow rates greater than approximately 50 m yr^{-1}, the upper limit of resolution of the method. (Values of $c/c_0 > 1.0$ are due to heterogeneity of radon concentrations within the aquifer, and indicate the radon concentrations are higher in the immediate vicinity of the well, than they are further away.) Figure 5.5 suggests consistently high groundwater flow rates above 30 m depth, but with highly variable flow rates below 30 m. This may be due to changes in the character of the basalt at depth, or to decreases in fracture apertures as a result of overburden pressure (Cook *et al.*, 2001a). In the Clare Valley, South Australia, radon concentrations have been measured in nested piezometers and used to identify flow zones at different depths within the aquifer (Box 5.2).

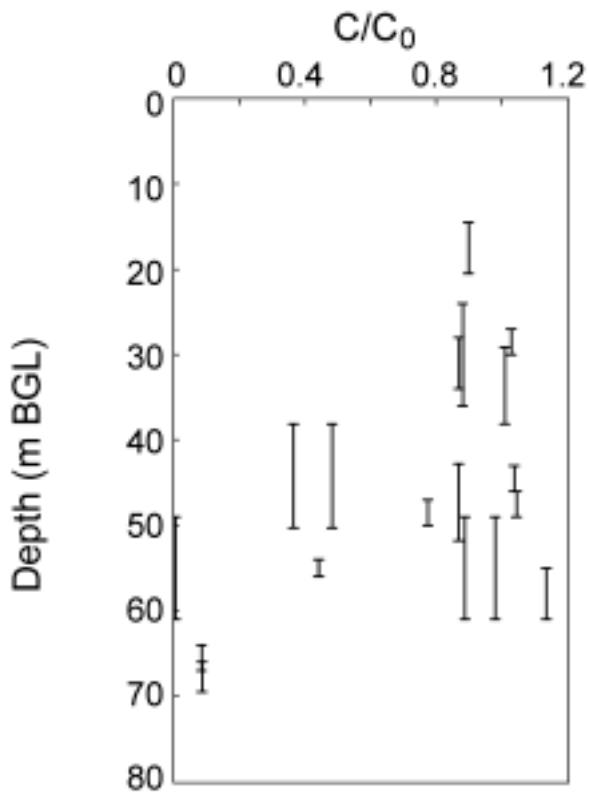

Figure 5.5. Ratio of radon concentration measured before and after purging, as a function of well depth (metres below ground level) for piezometers from the Atherton Tablelands, North Queensland. Vertical bars indicate the slotted intervals of the piezometers. (From Cook *et al.*, 2001a.)

Box 5.2. Measuring groundwater flow using radon, Clare Valley, South Australia.

Radon concentrations were measured both before and after purging a piezometer nest in the Clare Valley, South Australia (Fig. 5.6). Radon concentrations after purging increase from 20–40 Bq L^{-1} above 35 m depth, to 80–100 Bq L^{-1} below 50 m, which corresponds to a change in lithology from sandstone (above) to dolomitic marble (below). Concentrations measured before purging range between zero and 24 Bq L^{-1}. A vertical profile of the mean groundwater flow rate was determined from the ratio of the mean unpurged radon concentration at each depth, to the mean purged radon concentration (Equation 5.2). The mean flow rate through the borehole is calculated to be between 1 and 10 m yr^{-1} above 30 m, and between 0.3 and 3 m yr^{-1} between 40 and 70 m depth. Between 30 and 40 m, and below 80 m depth, it is estimated to be less than 0.3 m yr^{-1}. The flow rate through the aquifer would be approximately one-third of these values, because of the effect of flow convergence in the vicinity of the well.

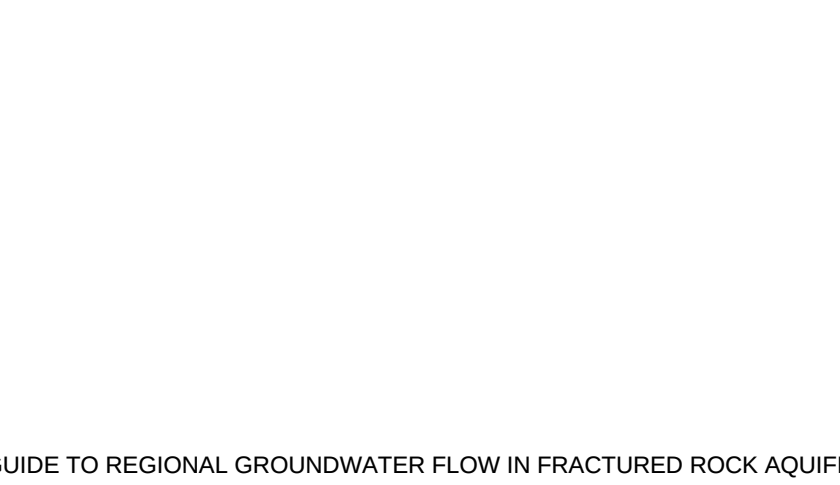

Figure 5.6. Radon concentrations before and after purging a nest of piezometers, Clare Valley, and inferred groundwater flow rates. a) Radon concentrations on samples obtained from the middle of the well screen on unpurged piezometers; b) Radon concentrations obtained after purging two well volumes; c) Ratio of unpurged to purged radon concentration; d) Inferred groundwater flow rates. (After Cook *et al.*, 1999.)

While its main advantage is its simplicity, there are a number of uncertainties in the radon method. Firstly, Equation 5.2 assumes complete mixing of water within the well, while this may not be the case in practice. (In the point dilution method, the water is mixed mechanically.) Secondly, the flow rate is determined from a single measurement of radon concentration in the well (or the ratio of this to inflow radon concentration), whereas in point dilution tests with artificial tracers the flow rate is determined by fitting a

number of observations made over time. Thirdly, it is possible that the radon concentration entering the well under ambient flow conditions is slightly different to that measured during well purging. For all of these reasons, the radon method is likely to be less accurate than point dilution experiments, and is probably best considered only to be semi-quantitative.

5.3.4. Well dilution

Well dilution tests are a modification of point dilution tests. However, the tests do not require isolation of an interval of well and mixing of the fluid within the interval during the test. Rather, measurements of tracer concentration are made over the length of the well, and information is obtained on vertical variations in the flow rate through the well. The technique involves replacing the standing column of water in a borehole with a fluid of a different concentration, then profiling the changes in fluid electrical conductivity as water from the aquifer flows into the well. The test is equivalent to that described in Section 4.2.4, except that in this case the well is not pumped, so natural groundwater flow rates rather than hydraulic conductivities are measured. Where horizontal flow rates through the well are low, circulation within the bore induced by density variations can complicate interpretation.

Cook *et al.* (2001a) carried out well dilution tests in fractured basalts of the Atherton Tablelands, North Queensland, by initially replacing the bore fluid with a more saline solution (Box 5.3). A pump is inserted to near the base of the bore, with the outlet of the pump located immediately above the water table, so that the pump does not remove water from the well, but recirculates it from the top to the bottom. At the same time, a concentrated salt solution is slowly poured into the top of the well. The concentrated solution is added for the whole time that the well is pumped, with the period of pumping chosen to be greater than that required to completely circulate the water in the well. Thus this process results in high salt concentrations mixed throughout the water column. Alternatively, where natural stratification of electrical conductivity exists within the well, the test can be performed by disturbing this natural stratification and then observing how long it takes to become re-established. In this case, there is no need to add tracer to the well, although interpretation of the test can be more difficult. If flow through the well is entirely horizontal, then the decrease in tracer concentration over time at each depth is given by Equation 5.1, and the groundwater flow rate at each depth is readily calculated.

Box 5.3. Measuring groundwater flow using well dilution, Atherton Tablelands.

Well dilution tests have been carried out in basalt and metamorphic aquifers on the Atherton Tablelands, Queensland (Cook *et al.*, 2001a). Figure 5.7 shows the results of a test on a bore that was drilled through basalt into metamorphic rock, clearly showing the difference in groundwater flow rates between these two units. The natural groundwater salinity at the site is approximately 0.1 mS cm^{-1}, whereas after injection, the electrical conductivity of the test zone ranged between 3000 and 6500 µS cm^{-1}. Within the basalt (above 20 m), the electrical conductivity decreases rapidly over time. Within the metamorphic rocks, the electrical conductivity changes only very slowly, and concentrations have decreased by less than 10 percent after 19 hours. Groundwater flow rates can be estimated from the rate of decrease of the concentration at different depths. Between 5–15 m depth (within the basalt), horizontal flow rates are estimated to be between 0.4 and 1.2 m day^{-1}. Within the metamorphic rocks, the horizontal flow rate is between 0.05 and 0.1 m day^{-1}. Correcting for flow convergence around the borehole would give flow rates through the aquifer of approximately half of these values.

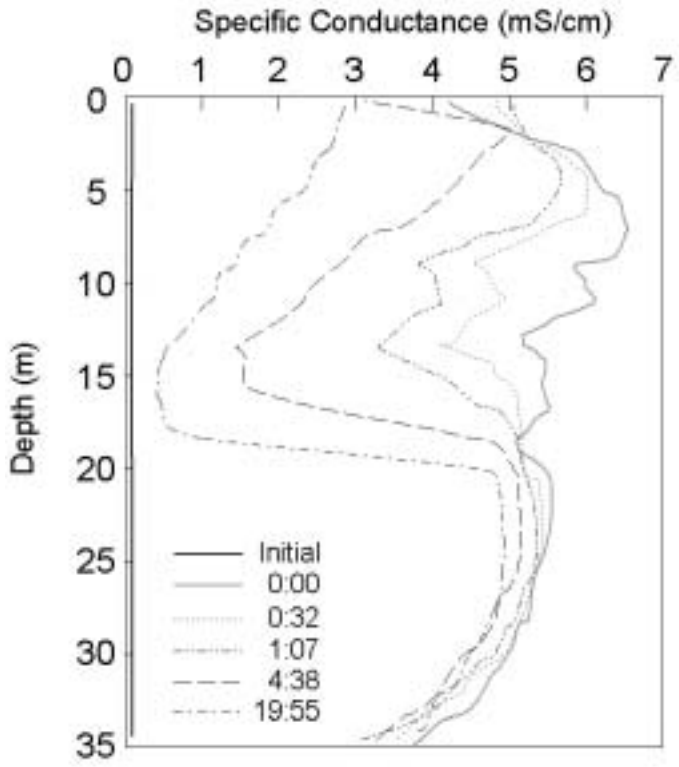

Figure 5.7. Results of well dilution experiment on a bore from the Atherton Tablelands. Depths are shown as metres below the water table. Times are in hours and minutes since the first profiling after injection. (From Cook *et al.*, 2001a).

Figure 5.8 shows a well dilution test carried out in fractured metasediments of the Clare Valley, without the addition of tracer. Natural stratification of electrical conductivity occurs in this well and was disturbed using a recirculation pump. Following recirculation, the electrical conductivity profile was measured at irregular intervals over a period of 16 days. The early-time data clearly shows the presence of individual fractures at approximately 17, 23, 30 and 38 m. In contrast, the fracture at approximately 72 m, apparent from the steady-state profile, does not appear to contribute a large flow into the bore. Semi-quantitative estimates of flow at all depths can be obtained from this data (Love *et al.*, 2002).

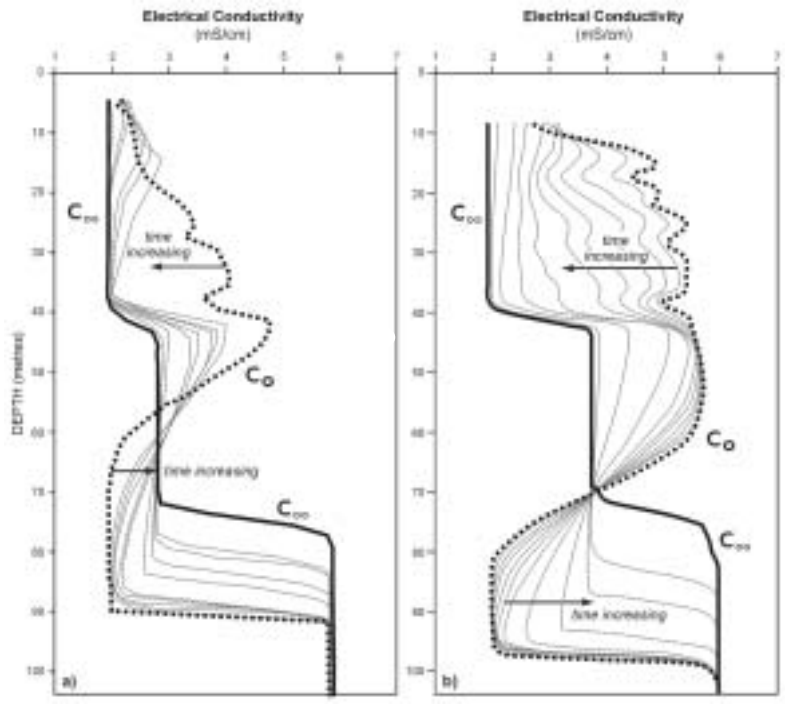

Figure 5.8. Results of well dilution experiments carried out in October 1998 (a) and May 2000 (b) on the same well, drilled into fractured metasediments in the Clare Valley, South Australia. The thick unbroken line shows the measured concentration in the well before mixing (assumed to be equal to that in the aquifer). The thick broken line represents the concentration in the well immediately after mixing. The thin lines represent transient EC profiles, while the arrow denotes increasing time since the well was originally mixed. For (a) the well was logged at 0.78, 0.95, 1.11, 1.81, 2, 6.2, 7.8, 13.9 and 15.8 days after mixing and for (b) the well was logged at 0.04, 0 .09, 0.15, 0.26, 0.4, 0.78, 1.7, 4.95 and 12.9 days after mixing. (From Love *et al.*, 2002).

5.4. Applied tracer tests

Applied tracer tests have commonly been used in fractured rock systems to investigate connectedness of fracture networks, and to characterise the fracture and matrix properties that affect solute transport. The tests can be performed either under the natural hydraulic gradient, or under an induced gradient. In natural gradient tests, tracer is injected into a well and the concentration of the tracer is monitored in a network of observation bores located down-gradient. The most obvious problem with these tests in fractured rock systems is that it is often difficult to predict the flow path of the injected tracer before the commencement of the test. In practice, this usually means that a large number of observation wells are necessary to ensure that the breakthrough of the tracer is observed. For example, Sanford and Solomon (1995) measured tracer concentrations in approximately 50 wells located in a fan-shaped area extending up to 200 m downgradient of their injection well, to ensure that the breakthrough of the tracer was detected (Fig. 5.9). Where breakthrough is observed, modelling of the concentration versus time data can often constrain a number of aquifer parameters.

While such intensively instrumented sites are beyond the scope of many investigations, tracer tests carried out with smaller numbers of wells sometimes provide valuable results. For example, Bradbury and Muldoon (1992) describe a natural gradient, applied tracer test in fractured dolomite using bromide and only two observation wells. Bromide was recovered from both observation wells (located 45 m from the injection well) after approximately 65 hours. The authors did not model the effects of matrix diffusion on bromide transport, or the effects of mixing within the borehole, and so the apparent tracer velocity of 16.5 m day^{-1} represents a minimum value for the groundwater velocity. In some cases, similar information can be obtained from groundwater contamination events, if observation bores are available to track the movement of the resulting plume.

While induced-gradient applied tracer tests (in which water is pumped into one well and/or removed from a second well) overcome the problem of uncertainty in flowpaths (because pumping forces water to move from one well to the other), these tests cannot be readily interpreted in terms of ambient groundwater flow. While they can be interpreted to help constrain fracture and matrix properties between the two wells, they are probably more suited to studies of contaminant movement than to regional groundwater investigations.

Figure 5.9. Part of the bore network for the natural gradient tracer test in fractured shale, West Bear Creek Watershed, Oak Ridge, Tennessee.
Photograph courtesy of William Sanford, Colorado State University.

5.5. Groundwater dating

In porous media aquifers, measurements of groundwater age obtained using environmental tracers can be used to quantify vertical and horizontal groundwater flow rates, and aquifer recharge rates. In fractured media, matrix diffusion means that apparent groundwater ages obtained with environmental tracers usually do not reflect the hydraulic age of the water. The water in the rock matrix is immobile, but tracer is able to diffuse between the mobile water in the fracture and the immobile water in the matrix. This affects the groundwater ages that we might measure using tracers.

Using the parallel plate model (Section 1.3), we can calculate how apparent groundwater ages measured with different environmental tracers may be affected by fracture characteristics. If an aquifer consists largely of vertical fractures, we can use this model to understand how groundwater ages should vary with depth. For an aquifer comprising parallel, vertical fractures at *large fracture spacings* (Section 1.3.2), apparent ^{14}C (carbon-14) and CFC-12 (chlorofluorocarbon-12) ages within the fractures as a function of depth can be approximated by:

$$t_a = \frac{z\theta_m D^{1/2}}{V_w b \theta^{1/2}} \qquad (5.3)$$

where t_a is the apparent age, V_w is the vertical groundwater velocity within the fractures, β_m is the matrix porosity, D is the effective diffusion coefficient within the rock matrix, $2b$ is the fracture aperture, z is depth, $\beta = 1.21 \beta 10^{-4}$ is the decay constant for ^{14}C, and $\beta = 0.06$ yr^{-1} is the atmospheric growth rate for

CFC-12 (Cook & Simmons, 2000).[5] According to this model, apparent groundwater age increases linearly with depth, as in the case for porous media. However, in a porous media the groundwater age at any depth is dependent only on the aquifer recharge rate and the porosity. In a fractured rock system it is dependent on the water velocity through the fractures, the fracture aperture, the matrix porosity and the matrix diffusion coefficient. Equation 5.3 shows that, other factors being equal, younger CFC-12 and ^{14}C ages (higher concentrations) will result from greater water velocities and fracture apertures, and lower matrix porosities and diffusion coefficients. In the case of ^{3}H (tritium) and ^{36}Cl (chlorine-36), the depth of the maximum concentration of these tracers as a function of depth can be approximated

$$z = V_w b \sqrt{\frac{2t}{D\theta_m}} \qquad (5.4)$$

where t is the time since maximum fallout.[6] (Maximum fallout occurred in approximately 1964 for ^{3}H and 1958 for ^{36}Cl.) This equation predicts that ^{3}H and ^{36}Cl will be present to greater depths as the water velocity or fracture aperture increases, and as the matrix porosity and diffusion coefficient decreases. We note also that the rate of movement of the maximum concentration is proportional to the square root of time, as discussed in Section 1.2.

Equations 5.3 and 5.4 are only approximations, based on idealised tracer input, and are also only appropriate for *large fracture spacings*. More generally, the distributions of environmental tracers within vertically fractured rocks can be determined using numerical modelling. Figure 5.10 depicts simulated vertical profiles of ^{3}H, ^{14}C and CFC-12 within fractures, in an aquifer comprising planar, parallel, vertical fractures in an impermeable matrix. Although the recharge rate used in the simulations is very low (R = 0.5

---

5 This is an approximation that assumes constant atmospheric activity of ^{14}C and exponential increase in atmospheric CFC concentration. More generally, for a fracture spacing $2B$, the apparent tracer age as a function of depth is given by

$$\frac{t_a}{z} = V_w^{-1}\left[1 + \frac{\theta_m D^{1/2}}{b^{1/2}} \tanh\left(BD^{-1/2}\right)\right]$$

(Neretnieks, 1981).

6 This equation is an approximate solution for the transport of a short pulse of solute through a single fracture, and is derived from the equation

$$\frac{c(x,t)}{c_0} = \frac{TD^{1/2}\theta_m t_w}{2b\pi^{1/2}t^{3/2}} \exp\left[-\frac{D\theta_m^2 t_w^2}{4b^2 t}\right]$$

where c_0 is the concentration of tracer during the pulse input (zero at other times), T is the length of the pulse, and t is the time which has elapsed since the commencement of the pulse (Lever & Bradbury, 1985).

mm yr^{-1}), ^{3}H is still present in fractures to more than 80 m depth. CFC-12 is present to approximately 70 m, with CFC-12 ages increasing linearly with depth. ^{14}C activities are greater than 100 pmc (percent modern carbon) above 32 m due to the presence of bomb ^{14}C, giving negative apparent ^{14}C ages. Below 32 m, ^{14}C ages rapidly increase. Figure 5.10 clearly shows that the groundwater ages obtained with the various tracers will be different. In particular, between 40 and 70 m depth, CFC-12 and ^{3}H are present, with ^{14}C ages greater than 100 years. This apparent discrepancy is due to enhanced retardation of ^{14}C by matrix diffusion, relative to CFC-12 and ^{3}H.

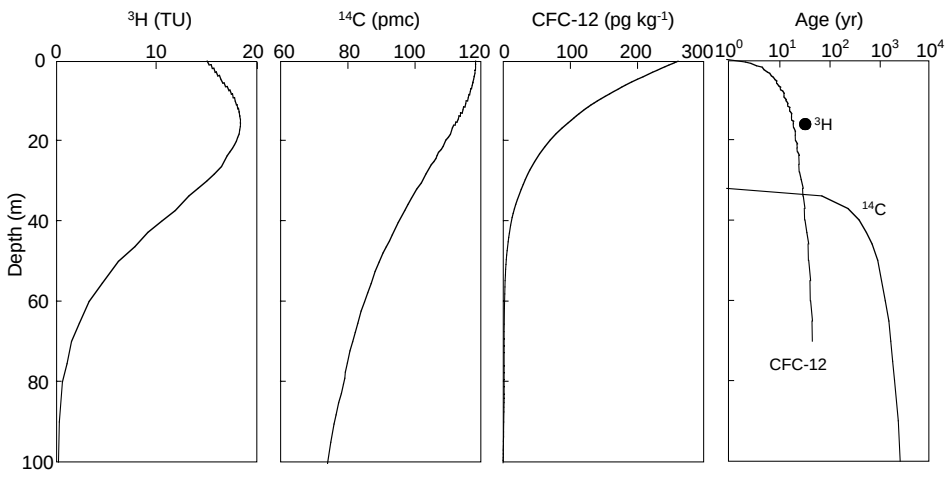

Figure 5.10. Simulations of ^{3}H, ^{14}C and CFC-12 concentrations and apparent ^{3}H, ^{14}C and CFC-12 ages, in an aquifer comprising planar, parallel, vertical fractures in an impermeable matrix. Profiles depict concentrations within the fracture, as would have been measured in 1996. The simulations are for aquifer parameters $D = 10^{-3}$ m^2 yr^{-1}, $\beta_m = 0.02$, $b = 40$ µm, $B = 4$ m, $V_w = 50$ m yr^{-1} and $R = 0.5$ mm yr^{1}. Apparent ^{14}C ages have been calculated assuming a constant input concentration of 100 pmc. The circle in the rightmost figure indicates the groundwater age of 32.5 years, indicated by the position of the maximum ^{3}H concentration in the profile. (After Cook & Simmons, 2000).

For the reasons discussed above, environmental tracers such as ^{14}C, CFC-12, ^{3}H and ^{36}Cl can be used to estimate groundwater flow velocities in fractured rocks only if fracture and matrix properties are known. In some cases, analysis of likely values of fracture and matrix properties may suggest that EPM conditions are likely to occur (Section 1.3.2). Where this is the case, then groundwater flow velocities can be calculated as if the aquifer were a porous medium (Cook *et al.*, 1996). However, this will not always be the case. If EPM conditions do not occur, it may be possible to place some bounds on flow velocities, but this will usually require accurate estimation of a number of fracture parameters (Cook & Simmons, 2000).

In systems that are not predominantly vertically fractured, vertical profiles of groundwater age can still provide useful information on fracture connectivity. In particular, they can be used to identify depths of circulation of groundwaters, or the depths to which vertical fractures transport significant amounts of water. Concentrations of ^{3}H, ^{36}Cl and CFC-12 in rainfall were very low before the 1950s, so the presence of these tracers in water samples provides clear evidence of active groundwater flow. Figure 5.11 depicts ^{3}H concentrations measured on groundwater extracted from piezometer nests installed in clayey till deposits of the St Clair Plain, southwestern Ontario, Canada (Ruland *et al.*, 1991). The tills have vertical fractures near the ground surface and observations in test pits showed that most weathering features along fractures reach a depth of only 2.5 m to 4 m, with isolated major fractures extending to depths of 5–6 m at some sites. ^{3}H concentrations exceeding 1 TU occurred to depths of 7.5 m at most sites, and the authors suggested that the ^{3}H had moved to the base of deep, open fractures by active groundwater flow, and travelled 1–2 m beyond that depth by molecular diffusion. Measurement of ^{3}H concentrations was thus able to identify the maximum depth of active groundwater flow in these deposits.

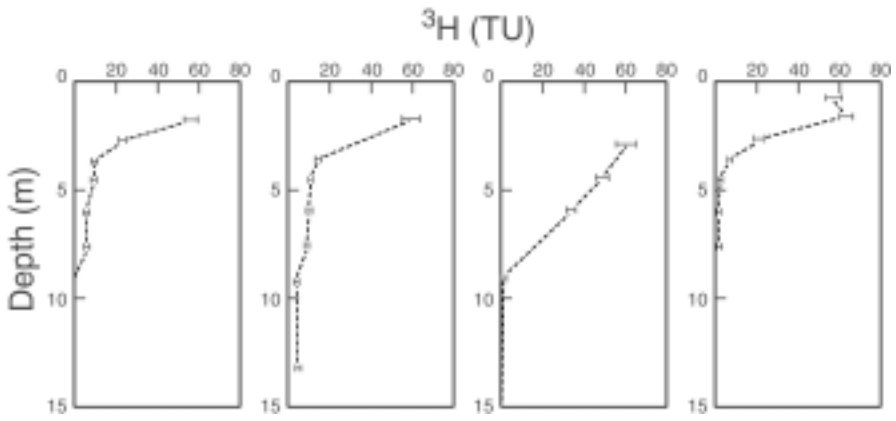

Figure 5.11. Tritium versus depth profiles in clayey till deposits of the St Clair Plain, southwestern Ontario, Canada. (After Ruland *et al.*, 1991).

5.6. Inferring recharge from hydrograph response

In porous media aquifers, observations of water level variations can sometimes be combined with measurements of specific yield to obtain information on aquifer recharge. There are a number of problems, however, associated with interpreting water level variation in fractured rocks in terms of recharge. Following Zuber and Motyka (1998), we may define the specific yield of a fractured rock as

$$S = \theta_f \beta_f + \theta_m (1 - \theta_f) \beta_m \qquad (5.5)$$

where β_f and β_m are the fracture and matrix porosities respectively, and β_f and β_m denote the fractions of these pore spaces that can be drained under the force of gravity. As fracture apertures greater than 4μm are empty at field capacity, β_f is usually close to one. $\beta_m\beta_m$ is simply the specific yield of the matrix blocks. Using Equation 5.5, Zuber and Motyka (1998) estimated the specific yield of karstic aquifers in southern Poland from measurement of fracture porosity from rock exposures and matrix specific yield measured in the laboratory.

Although this definition is consistent with the definition of specific yield for porous media, it does not necessarily facilitate routine use for interpretation of water level variations. As discussed in Section 4.1, the permeability of the aquifer matrix can control its ability to fill and drain as the watertable in fractures rises and falls in response to recharge events. If the rate of watertable rise in the fractures is very fast relative to the permeability of the matrix, then the specific yield will be close to the fracture porosity. Conversely, where the rate of watertable rise in the fractures is slow relative to the matrix permeability, then the specific yield will approach that given by Equation 5.5 (Fig. 4.4). This means that, in practice, we can only set bounds for the specific yield:

$$\leq_f \leq S \leq \leq_f + \leq_m \leq_m \qquad (5.6)$$

For the aquifer parameters given in Box 1.1, and assuming $\beta_m = 0.1$, this gives a possible range for the specific yield of more than an order of magnitude ($2.5 \beta 10^{-4} – 5.0 \beta 10^{-3}$).

The most successful approach for estimating specific yield in fractured rocks involves estimation of aquifer recharge and discharge by other means, and then using specific yield as a ‘fitting parameter’ when interpreting hydrograph responses. Gburek *et al.* (1999) compared the recession of bore hydrographs in interbedded shales, siltstones and sandstones from Pennsylvania with the baseflow recession curve over a 40-day period for a stream draining the aquifer. The specific yield was estimated to be 10^{-2} in the overburden, $5 \beta 10^{-3}$ in the highly fractured rocks at shallow depths, decreasing to 10^{-4} in poorly fractured material below 22 m depth. A sensitivity analysis suggested that the values of specific yield for each aquifer layer were accurate to better than an order of magnitude. Gburek and Folmar (1999) estimate a specific yield of $7 \beta 10^{-3} – 10^{-2}$ in the highly fractured zone at the same site, by comparing drainage rates from lysimeters with groundwater rises measured in bores. Similarly, Moore (1992) compared streamflow hydrographs with groundwater hydrographs from shale and limestone aquifers near Oak Ridge, Tennessee, and estimated a specific yield of approximately $2 \beta 10^{-3}$ from slopes of the recession curves. It remains unclear, however, whether such estimates of specific yield are sufficiently accurate to permit

their use in estimating recharge. Furthermore, as discussed in Section 4.1, piezometric records may not accurately reflect the rapid water level variations that occur in aquifers (Box 5.4). Thus the use of the watertable fluctuation for inferring aquifer recharge is unlikely to be successful in fractured rock systems.

Box 5.4. Water-level fluctuations and specific yield, Clare Valley, South Australia.

Figure 5.12 shows a hydrograph from a piezometer completed in the Mintaro Shale, Clare Valley, South Australia. The fracture porosity at this site has been estimated to be of the order of 10^{-3} based on outcrop mapping, and the matrix porosity 10^{-2} – 5 β 10^{-2} from helium porosimetry. The permeability of the matrix is extremely low (<10^{-12} m s^{-1}). (The specific yield of the aquifer has not been specifically determined.) The water table at this site varies relatively smoothly throughout the year, with most rainfall events not producing measurable changes in water level in the piezometer. This is not attributed to a lack of recharge, but rather attenuation of these short-term signals by the large storage capacity of the piezometer (Fig. 4.4). The only notable short-term rise in the water table occurred after 30 October 1997, when the water level rose by approximately 500 mm in response to 70 mm of rainfall. Although a large fraction of the rain that fell on this date probably reached the aquifer, the relatively small water level rise (relative to the aquifer porosity) is attributed to this attenuation. However, the annual cycle in water level is approximately 1.2–1.5 m, which is consistent with a recharge rate of approximately 60 mm yr^{-1} and a specific yield much closer to the total porosity than to the fracture porosity (4 β 10^{-2}).

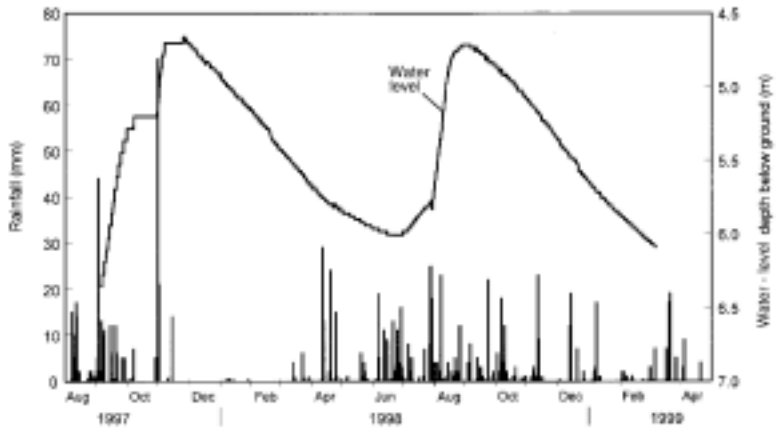

Figure 5.12. Water level fluctuations in a piezometer screened in Mintaro Shale, and daily rainfall at Clare, South Australia. The magnitude of the seasonal water level fluctuations and the independently estimated recharge rate are consistent with a value of specific yield close to the total porosity. Short-term fluctuations, in response to daily rainfall events, are generally absent, due to attenuation of short wavelength variations by the large storage capacity of the well.

5.7. Chloride mass balance

The chloride mass balance method has been widely used for estimating aquifer recharge in porous media aquifers (Scanlon *et al.*, 2002). If the chloride that occurs in groundwater is deposited by dust particles and precipitation, with negligible amounts contributed from rock weathering or anthropogenic sources (e.g., fertiliser), then at steady state we can express the chloride mass balance as:

$$C_P P = C_R R + C_Q Q \qquad (5.7)$$

where P is precipitation, R is recharge to groundwater and Q is surface water discharge (runoff), and C_P, C_R and C_Q are chloride concentrations in precipitation (wet and dry fallout), recharge and runoff, respectively. In many areas surface runoff (Q) is not significant, and the recharge rate can be estimated simply from

$$R = \frac{C_P P}{C_R} \qquad (5.8)$$

There are two major difficulties with use of the chloride mass balance in fractured rock systems. Firstly, residence times of water can be very long, particularly within the rock matrix, so weathering to produce chloride must be considered a possibility. However, the sources of chloride can often be examined by considering ratios with other ions. If additional sources of chloride are present, then the recharge rate derived from a chloride mass balance should be considered to be a minimum. Secondly, equilibrium conditions for chloride can take a very long time to develop following a change in environmental conditions. The time required for leaching of the stored salt and establishment of the new equilibrium will largely be determined by the rate of diffusion of salts from the matrix into the fractures. If fractures are widely spaced, then this time can be extremely long. Figure 5.13 shows the time required for chloride to leach from the rock matrix. It assumes that initially both fractures and matrix are in equilibrium at concentration C_m. A change in recharge then causes the chloride concentration in water flowing through the fractures to change to C_f. Figure 5.13 then plots the change in chloride concentration in the rock matrix mid-way between the fractures against time. The time required for the concentration in the matrix to become the same as that in the water flowing through the fractures can be approximated by

$$t = \frac{(2B)^2}{2D} \qquad (5.9)$$

where t is time, $2B$ is the fracture spacing and D is the effective diffusion coefficient for the aquifer matrix (Cook *et al.*, 1996).

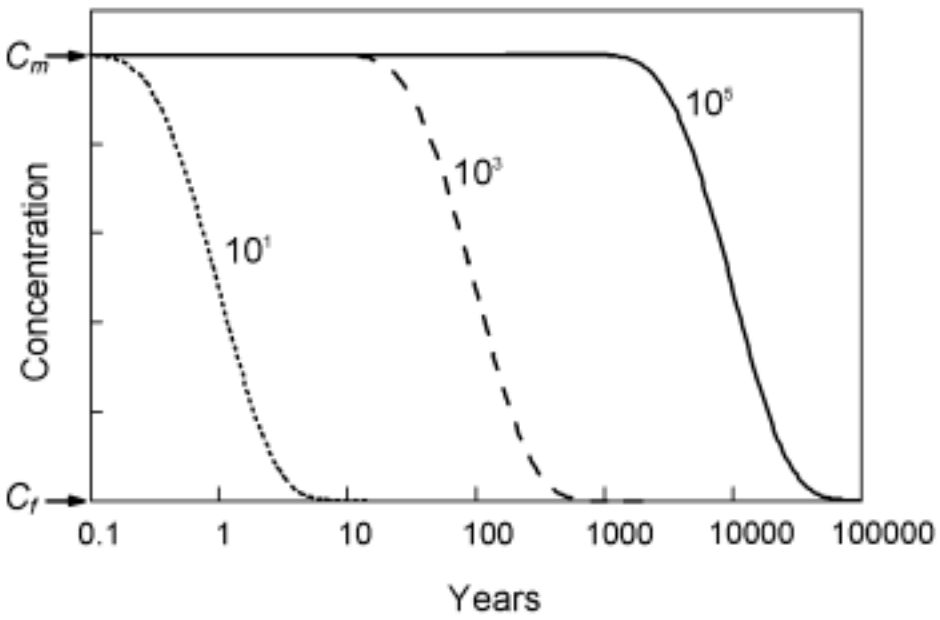

Figure 5.13. Time for solutes to diffuse from the aquifer matrix into the fractures. The decrease in solute concentration in the aquifer matrix mid-way between the fractures is plotted as a function of time. Numerals indicate values of $(2B)^2/D$ = 10, 1000, and 10^5 years.

In the Clare Valley and Playford Hills catchments of South Australia, steady state conditions for chloride may not have been re-established 100 years after clearing caused an increase in recharge (Box 5.5). In these areas, recharge rates derived from the chloride mass balance appear too low, and may indicate past recharge conditions, rather than current rates of recharge (Love *et al.*, 2002; URS, 2002). In the Willunga Basin, however, despite a similar clearing history, the chloride mass balance appears to provide reasonable estimates of recharge for both the hard rock and the sedimentary aquifers (Martin, 1998). Chloride mass balance methods have also been successfully used to estimate groundwater recharge rates to fractured basalt aquifers of the Atherton Tablelands, Queensland (Cook *et al.*, 2001a), and fractured sandstones and mudstones of the Karoo Sequence, South Africa (Sami & Hughes, 1996). Despite the above reservations, the chloride mass balance remains perhaps the most reliable means for quantifying recharge rates to fractured rock aquifers.

Box 5.5. Placing limits on recharge using the chloride mass balance, Clare Valley.

In the Clare Valley, South Australia, clearing of native Eucalyptus vegetation took place approximately 100 years ago, and aquifer recharge rates would have increased at that time. It has been suggested that much of the chloride present within the groundwaters in the Clare Valley represents residual chloride which pre-dates clearing of the native vegetation (Love and Herczeg, 2001), and that this chloride is only very slowly leaching out. The increases in electrical conductivity with depth observed at a number of sites throughout the valley (e.g., Fig. 3.11) may thus reflect a decrease in leaching with depth, perhaps due to lower flow rates and larger fracture spacings.

Based on a matrix diffusion coefficient $D = 10^{-4}$ m^2 yr^{-1} and a fracture spacing $2B = 1$ m, it is estimated that diffusive leaching of the stored salt would take in excess of 5000 years (Equation 5.9). Only where the fracture spacing is very small, such as in the shallow weathered zone, should leaching be complete. (For a fracture spacing of $2B = 0.1$ m, the leaching time is approximately $t = 50$ years.) If this is the case, then the chloride mass balance should provide a lower bound on the recharge rate. At one site, the chloride concentration in shallow groundwater is approximately 65 mg L^{-1}, giving a recharge rate of $R > 50$ mm yr^{-1} ($P = 650$ mm yr^{-1}, $C_P = 5$ mg L^{-1}). At another site, the chloride concentration in shallow groundwater is approximately 350 mg L^{-1}, giving a recharge rate of $R > 9$ mm yr^{-1}. The higher measured chloride concentration at the second site may indicate a slower rate of flushing of salt, which might result from a larger fracture spacing or smaller matrix diffusion coefficient.

It is also possible to calculate a pre-clearing recharge rate, based on the chloride concentrations that occur at depth within the aquifer. Some leaching of this chloride may have occurred since clearing, and so the original chloride concentration (which we assume to have been in equilibrium with the pre-clearing recharge rate) may have been greater than that which is observed today. Chloride concentrations at depth are in the range of 2000–5000 mg L^{1}, which corresponds to a pre-clearing recharge rate of < 2 mm yr^{-1} (Love *et al.*, 2002).

5.8. Groundwater discharge

Groundwater discharge from fractured rock aquifers can be estimated by measuring the discharge of streams that drain fractured rock catchments, or from measuring concentrations of various solutes within streams and applying solute mass balance methods (e.g., Ellins *et al.*, 1990). Provided that it can be assumed that solute concentrations measured within the groundwater reflect the concentration draining from the aquifer into the streams, then these methods can be applied in fractured rock aquifers as they would in porous media. It should be noted, however, that the spatial variability of groundwater inflows may be increased by water inputs from irregularly spaced fractures.

In some cases, estimates of recharge may be derived from this data, although some caution needs to be applied. Firstly, in fractured rock areas it can be very difficult to determine the area of land drained by streams. Surface water catchment boundaries need not correspond to groundwater flow boundaries (*see* Box 5.6). Secondly, surface water response to rainfall in fractured rock aquifers can be extremely rapid, and river flow rates may be extremely variable. This may cause some practical difficulties in accurate stream gauging, particularly during high flows. Since watertable variations in fractured rocks can be very large, groundwater inflows to streams can also be extremely variable, which can cause difficulties in calculation of average annual values. These difficulties may in part explain the apparently large discrepancies between estimated recharge and discharge rates to fractured rock aquifers in the Clare Valley, South Australia (Love *et al.*, 2002). In contrast, in the Atherton Tablelands, Queensland, estimates of recharge derived from a chloride mass balance approach are similar to baseflow estimates averaged over the catchment (Box 5.7).

Box 5.6. Catchment areas for groundwater discharge, Oak Ridge, Tennessee.

In a forested, karstic dolomitic catchment in Oak Ridge, Tennessee, Genereux *et al.* (1993) found that groundwater recharge from outside the catchment is a significant contributor to streamflow within the catchment. Figure 5.14 shows the apparent depths of runoff over a 12-month period for five subcatchments in Walker Branch Watershed. These were calculated by dividing the estimated inflow rates to various stream reaches by the size of their surface catchment areas. The largest watershed (above weir WB300) appears to generate 55 cm of runoff, whereas the area between weirs WB60 and WB0 (catchment area 1.24 hectares) appears to generate over 1000 cm of runoff, despite an annual rainfall of only 168 cm. These apparent runoff values clearly reflect the movement of subsurface water across surface topographic divides.

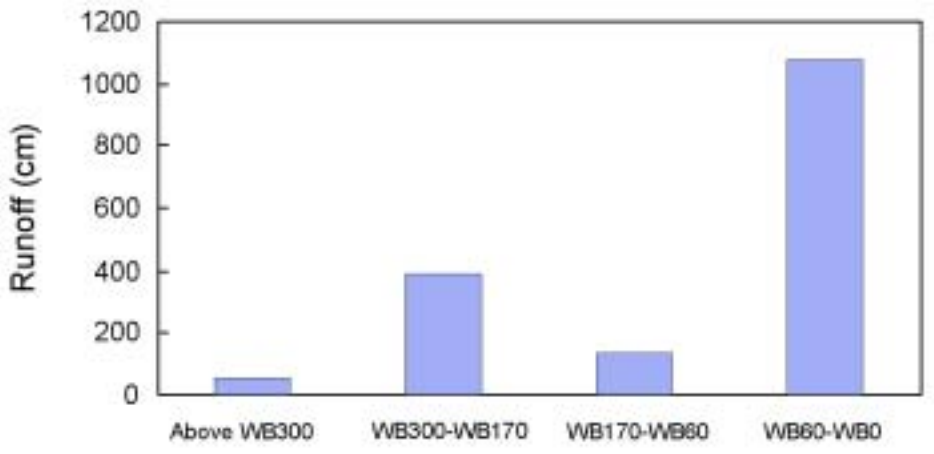

Figure 5.14. 'Apparent runoff' from four subcatchments of the Walker Branch Watershed, Oak Ridge, Tennessee. The sizes of the four catchments are: above WB300: 29.5 ha; WB300-WB170: 4.47 ha; WB170-WB60: 3.15 ha; WB60-WB0: 1.24 ha. (After Genereux *et al.*, 1993).

Box 5.7. Groundwater recharge and discharge, Atherton Tablelands, Queensland.

In the Atherton Tablelands, long term records of surface flows are available from gauging stations on the Barron River and on the North Johnstone River. The surface catchment areas above the gauging stations have been estimated at 220 and 173 km^2, respectively, and consist of fractured basalts. Mean annual discharge for the Barron and North Johnstone Rivers at these gauging stations has been measured to be approximately 138 000 and 170 000 ML, respectively. Expressing these as equivalent depths over the catchment areas, the total discharges become 625 and 977 mm, respectively. Total runoff has been separated into surface runoff and baseflow by ascribing any daily flows in the Barron River averaging in excess of 12.55 $m^3 s^{-1}$ (1085 ML day^{-1}) to surface runoff, and the remainder to baseflow. For the North Johnstone River, daily flows averaging in excess of 10 $m^3 s^{-1}$ (865 ML day^{-1}) were ascribed to surface runoff. The estimates of baseflow are 372 mm and 745 mm respectively, which was similar to the estimates of recharge obtained from chloride mass balance, and suggests that (as a long-term average) all of the recharge enters the streams as baseflow.

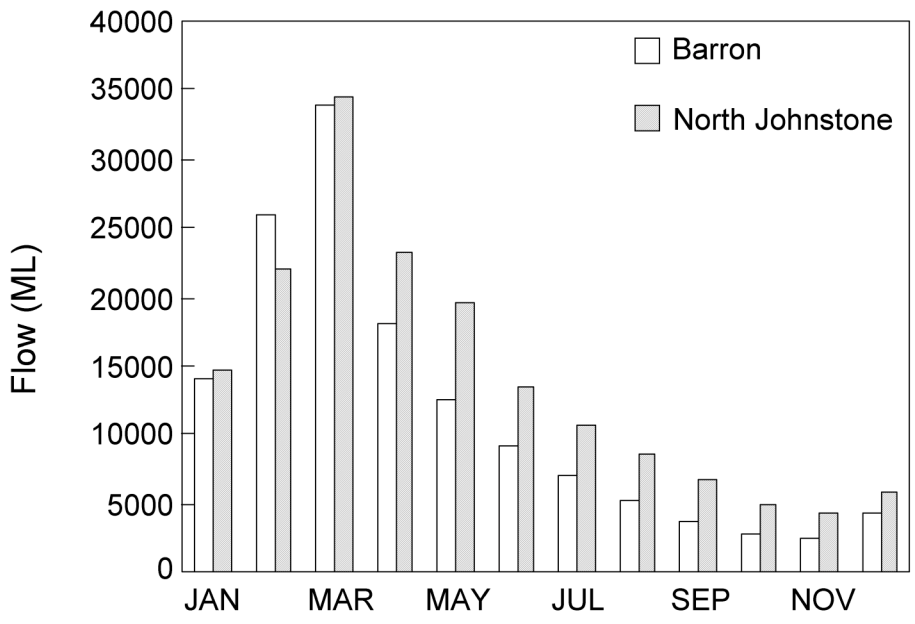

Figure 5.15. Mean monthly streamflows for the Barron River and the North Johnstone River, Atherton Tablelands. (From Cook *et al.*, 2001a.)

6. GROUNDWATER MODELLING

6.1. Introduction

This chapter describes the main approaches used for modelling groundwater flow and solute transport in fractured rock aquifers. Clearly, the main issue is how to describe the heterogeneity associated with fractures. A number of approaches exist, but most can be grouped into three classes: (i) the equivalent porous media approach, (ii) the dual porosity approach, and (iii) the discrete fracture network approach (Fig. 6.1). In the equivalent porous media approach, hydraulic properties of the system are modelled using equivalent coefficients such as permeability and effective porosity to represent the volume-averaged behaviour of many fractures within a fractured rock body. Thus, the details of individual fractures need not be known. This is in direct contrast to the discrete network approach where the details of individual fractures are explicitly accounted for in the model simulation. In the dual porosity approach, equivalent porous media properties are separately assigned for fracture and matrix elements, and an exchange coefficient based on a simplified fracture geometry is used for transfer between the two zones. The discussion that follows will provide a simple treatment of the advantages and limitations of each approach and the principles that guide the choice of modelling approach. It draws upon discussions presented by NRC (1996) and Thangarajan (2000), both of which present more exhaustive treatments of this topic.

6.2. Conceptual and mathematical models

Modelling is important for improving our understanding of system behaviour. It provides a framework for synthesising data from different tests and field investigations, and improving our conceptual understanding of flow and transport behaviour and the factors controlling them. Predictive modelling forms a basis for understanding longer-term behaviour of a system that may underpin management decision making. The development of a conceptual model is a key step in the modelling process. Key questions arise including: does the conceptual model provide an adequate representation of the hydrogeological system? Are the controlling features of the flow system accounted for? How does the model perform in comparison to field observations? Model non-uniqueness poses an interesting issue here. An important observation that has been made in fractured rock modelling

literature is that equally successful interpretations of both flow and transport data can be made by very different conceptual and mathematical models. This makes it even more important to understand from the outset what level of detail is needed to adequately represent the system being studied. As pointed out in NRC (1996), when constructing a conceptual model of a fractured rock aquifer, three factors necessarily must come into play. These are (i) the geology of the fractured rock, (ii) the scale of interest and (iii) the purpose for which the model is being developed. We will briefly deal with each one in turn.

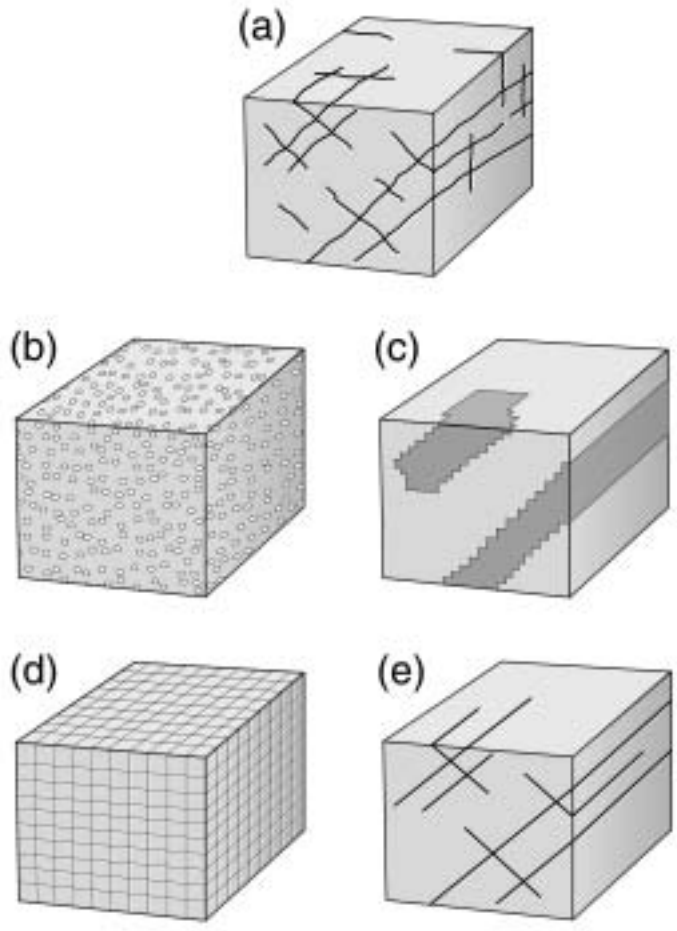

Figure 6.1. Different modelling approaches for fractured rock aquifers. (a) Actual fracture network; (b) Equivalent porous media model, using uniform aquifer parameters; (c) Equivalent porous media model in which highly fractured zones are represented by regions of higher hydraulic conductivity; (d) Dual porosity model; (e) Discrete fracture model, in which the major fractures are explicitly modelled. The discrete fracture model may have zero porosity in the matrix, porosity but zero flow, or may allow for flow.

Understanding the geology of a system helps to identify features that may be important in controlling the hydrogeology. As one end member, a fractured

rock system may be dominated by only a few major features in a relatively impermeable rock matrix. Alternatively, we may encounter a geologic system in which there is a complex network of highly interconnected fractures in a relatively permeable matrix. The *scale of interest* is very important. A fractured rock aquifer may be connected on a large scale but may be dominated by a small number of larger fractures on a smaller scale. The converse may also be true. The more traditional notion of dealing with fractured rock aquifers is that as the scale of interest increases the more appropriate it is to employ equivalent porous media modelling approaches, where extensive regions of an aquifer are represented by uniform hydrogeologic properties. How then do we determine these larger scale hydrogeologic properties from hydrogeologic tests carried out at significantly smaller scales? Finally and equally important is the *purpose or question* your model is intending to satisfy or answer. A distinction must necessarily be made at all times between hydraulic and solute transport modelling. Equivalent continuum approaches may be appropriate for answering questions that relate to averaged volume behaviour. However, more detailed modelling approaches are required when dealing with solute transport phenomena since the heterogeneity in the fractured rock aquifer explicitly controls migration pathways, rates and plume concentrations.

6.3. Equivalent porous medium approach

In this approach, individual fractures are not explicitly treated in the model but rather the heterogeneity of the fractured rock system is modelled using a small number of regions, each of which is modelled as an equivalent porous medium. The primary and secondary porosity and the hydraulic conductivity distribution are replaced with a continuous porous medium having equivalent hydraulic properties. An equivalent porous media approach makes the assumption that a *representative elementary volume* (*REV*) of material characterised by equivalent hydraulic parameters can be defined (*see* Section 1.4). Modelling results are only valid at scales larger than the *REV*. Modelling requires the definition of effective values for hydraulic conductivity, specific storage and porosity at the scale of the *REV*. These parameters can be determined from either aquifer testing or calculated from detailed field descriptions of fracture apertures, lengths and interconnections as well as unfractured rock volumes, porosity and permeability. However, field scale tests are often relevant at length scales on the order of tens of metres (which may be much smaller than the *REV*). Clearly, an issue is how to determine values at much larger scales on the order of hundreds of metres relevant to basin or sub-basin studies. At the scale of hundreds of metres or more, hydrogeologic simulation models calibrated to estimates of recharge rates,

watertable positions and/or potentiometric head data may be the most suitable and reliable way of estimating the large scale hydraulic conductivity of the fractured rock aquifer.

The single porosity approach is best used when predicting bulk average features of the flow system and may best be employed in steady state analyses. However, for problems that involve transient flow there is a need to account for fluid released from storage. Here, a clear distinction needs to be made between fluid present in the fractures and that present in the matrix. In the case where fracture densities are very high and intermediate matrix units are very small it may be possible to treat the system as one continuum where the hydraulic storage and transmissivity are represented by a lumped sum accounting for both fractures and matrix blocks. In such cases, conventional groundwater flow equations for the simulation of flow in porous media are used. The MODFLOW model (McDonald & Harbaugh, 1988) is an example of such an implementation for groundwater flow simulation, and has been successfully applied to fractured rock aquifers where hydraulic responses (and not transport) are important (Box 6.1, *see* pages 88 and 89). However, the model is limited in the way it can simulate anisotropy. (In particular, the maximum to minimum directions of the radial hydraulic conductivity must coincide with the model grid, and vertical anisotropy cannot be simulated within a layer.)

Simulation of solute transport is significantly more troublesome than flow. In the case of the equivalent porous media approach, adopting an approach based upon the advection-dispersion formulation is most uncertain. There is a need to define equivalent effective porosity and equivalent dispersive properties of the fracture network. The former is needed to predict average solute flow rates. The latter defines the extent along various directions of mixing. Whilst an equivalent and isotropic dispersion formulation may be employed, it is likely to be oversimplified and unrealistic. In most cases, spreading in a fractured rock aquifer is expected to be a highly anisotropic process. Whilst tracer tests can, in principle, yield estimates of effective porosity and dispersivity at smaller test scales, it is difficult to determine these parameters at the spatial scale required when considering large fractured rock bodies. While a calibrated flow model may adequately simulate observed hydraulic behaviour, significant errors are likely to occur in subsequent use of the flow model to predict solute transport.

6.4. Dual-porosity models

In cases where the matrix containing the fracture network has significant permeability dual-porosity models may be employed. This situation can be important when dealing with systems involving high matrix porosity as may

be encountered in some fractured sedimentary sequences (e.g., sandstone) or fractured clays. In such an approach, the fractured rock system is treated as two overlapping continuua and both are treated as porous media. The fractured network is represented by one flow equation and the matrix blocks are represented by another flow equation. This approach accounts for the exchange of water between matrix and fractures using a coupling term that represents the rate of mass transfer and the geometry of the fracture network is represented by a small number of geometric parameters. The main advantage of a dual porosity system is in transient flow modelling where the delay in hydraulic response of a fractured rock system caused by fluid resident in the less permeable matrix blocks can be simulated. In such cases, fluid is first released from the fractures and then from the matrix as a pressure gradient is created between the water contained in the matrix and the water contained in the fractures. The simple conceptual basis of the dual-porosity approach makes it appealing. Furthermore, when modelling solute transport, dual-porosity models are able to account for diffusive mass transfer between the fractures and matrix blocks.

There are a number of limitations of this approach that should be noted and these notably include the tendency to oversimplify and over-regularise the geometry of the fracture network as well as the difficulty in determining good parameter estimates needed as input to these models.

6.5. Discrete fracture network models

Discrete fracture network models allow for an explicit characterisation of fracture properties including aperture, orientation and length. Flow through each fracture is treated as being equivalent to flow between two uniform plates with separation equivalent to the aperture of the fracture (*see* Section 1.2). Some discrete fracture models only model flow and transport in fractures (i.e., they assume that the aquifer matrix has zero porosity). A few models allow for flow and transport in the porous matrix, as well as in the fractures, although the computational requirements of these models means that only relatively small numbers of fractures can be included. Also for computational reasons, in some cases, only regular fracture geometries are permitted (Fig. 6.2).

Because the discrete fracture network approach can explicitly account for flow path geometry and fracture properties it is suited to smaller-scale modelling studies. It can be used to study processes in a system where flow and transport occur principally within the discrete fractures or for developing an understanding of conceptual flow and transport processes within a more theoretical framework. The approach is generally limited by the data available on fractures as well as the ability to extrapolate properties from smaller scale tests to larger regions of interest. As fracture pattern complexity, intensity and

Box 6.1. Example of an equivalent porous media flow model.

Gburek *et al.* (1999) used the MODFLOW porous media model to determine watershed-scale aquifer parameters in a fractured sedimentary aquifer system in east-central Pennsylvania. Seismic testing suggested that the aquifer could be characterised by four distinct hydrogeologic layers (overburden, highly fractured, moderately fractured and poorly fractured layers; Table 6.1). Hydraulic tests using packers and measurements of fracture spacing in cores showed that hydraulic conductivity decreased with depth. The MODFLOW model was used to determine both watershed-scale hydraulic conductivity values and specific yield for each of the layers. This was achieved by calibrating the model to watertable observations under steady-state springtime recharge. Baseflow from a five year data set was used to calculate an equivalent steady state areal recharge over the watershed of 3 mm day^{-1}, which was fixed in the model, and hydraulic conductivity was used as a fitting parameter. After obtaining a satisfactory steady state calibration, the authors then determine values of *Sy* by calibrating a transient solution of drainage from the watershed following cessation of recharge.

Table 6.1. Summary of aquifer geology and hydraulic properties.

	Overburden	Highly Fractured	Moderately Fractured	Poorly Fractured
Depth (m)	0 – 2.4	2.4 – 11.0	11.0 – 22.4	22.4 – 90
Fracture frequency (m^{-1})	n/a	> 30	20	< 5
Hyd Cond (m day^{-1})				
Regional pumping tests	n/a	n/a	n/a	0.03
Packer tests	6.0	1.14	0.41	0.38
Model calibration	20.0	5.0	0.1	0.01
Specific yield				
Regional pumping tests	n/a	n/a	n/a	0.0001
Model calibration	0.01	0.005	0.001	0.0001

Calibrated hydraulic conductivity values of the highly and moderately fractured layers were in good agreement with those from packer testing. However, the calibrated values of the lowest poorly fractured layer were more than an order of magnitude lower than that determined by packer testing but similar to that determined by regional pumping tests carried out within this layer. The most likely explanation for this discrepancy is that the packer tests can be influenced by local fracturing not representative of the larger scale aquifer properties because of the sparse fracture density. Clearly, field data from packer and slug tests are only comparable to model calibration values where the larger scale flow is controlled by a high density of interconnected fractures. In poorly fractured layers, they are less representative of regional scale estimates.

Box 6.1 continued on next page

Box 6.1 (continued)

This case study highlights the successful use of the MODFLOW model for a system where hydraulic responses (and not transport) are important. As the authors point out, further refinements in aquifer parameters would produce better matches between the simulated and observed water table distribution and baseflow recession curve. They conclude that the simple layer geometry developed along with consistent and supportable *K* and *Sy* values meet the study objectives. One limitation, as pointed out by the authors, is that the degree of anisotropy of the geologic layers has neither been measured nor implemented in the model.

This case study demonstrates that the MODFLOW model can be successfully used to simulate hydraulic behaviour at a catchment scale. It is an interesting example in that calibration is performed by the variation of hydraulic conductivity with recharge as determined by a catchment scale water balance, held fixed. Whilst the model appears to reasonably simulate the observed range of behaviour for baseflow recession in the watershed, the authors note that further refinements between the layer geometry, hydraulic conductivity and specific yields would produce better matches between the simulated and observed water table distribution. The model is only semi-calibrated at best and is therefore most useful for gaining a better understanding of controlling features of the system and not for making absolute predictions about, for example, the hydraulic head at a point in various aquifer layers at some time in the future.

In both the steady state calibration and the transient calibration, baseflow recessions have been used to determine average areal recharge and the specific yield of layers. This approach necessarily smears spatial variability since the simulation of baseflow recession integrates across large spatial scales and is therefore less sensitive to more local variations in hydraulic conductivity than observed water table distributions. Clearly, the baseflow response is determined by all four hydrogeologic layers in the system, with early response controlled by the highly fractured layers and the later response controlled by the less fractured layers. With 4 layers (each with associated *Sy* and *K*), model calibration is expected to be non-unique. It is also possible to match field observations without the need to add further complexity to the model (e.g., each layer can be modelled assuming homogeneous EPM without the need for dual porosity modelling of each layer). However, further work would be needed to study the behaviour of hydraulic head variations and water table fluctuations both in space and time. Here, further refinement of the model would be necessary.

transmissivity increase, growing computational power is required to simulate the discrete fracture network and inevitably requires a simplification of the detail especially where large-scale regions are being simulated. Faced with this dilemma, the key is then to define the important active and connected fracture pathways that control flow in the system. In general, the discrete fracture network approach is relatively new in comparison to the continuum approaches. A key use for this approach at this stage is in the advancement of our conceptual understanding of flow and transport dynamics in fractured rock aquifers. Furthermore, a major use of current DFN models is for determining equivalent porous media parameters required in continuum modelling approaches. Here, they can be used to derive equivalent hydraulic properties based upon an explicit characterisation of fractures.

Two of the better-known discrete fracture models are FRAC3DVS <http://www.flowpath.com/software/others/frac3d.html> and NAPSAC <http://www.aeat-env.com/groundwater/napsac.htm>. FRAC3DVS is a three-dimensional, finite element model for simulating steady-state or transient, variably saturated groundwater flow and advective-dispersive solute transport in porous or discretely fractured porous media. Flow can occur both within the matrix and within the fractures, and exchange of water between fractures and matrix can occur in response to head gradients. Matrix diffusion between the fractures and the matrix is explicitly modelled. In contrast, NAPSAC is a finite-element software package for modelling groundwater flow and transport within fracture networks. Because it does not include flow or transport within the matrix, NAPSAC is capable of simulating much larger networks of fractures than FRAC3DVS.

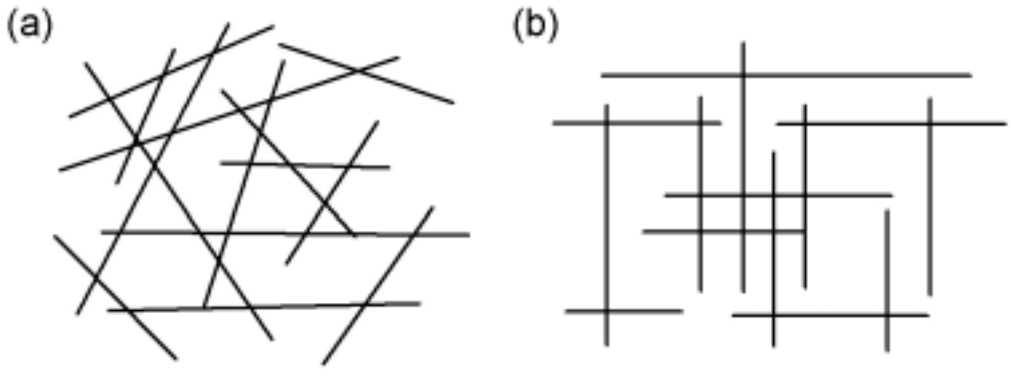

Figure 6.2. Networks of non-orthogonal discrete fractures that could be simulated using computer models. Because of problems with discretisation and computing times, fracture networks (such as those in (a)) are often simplified into orthogonal networks with similar fracture lengths, apertures and spacings (such as that shown in (b)) when models link fracture and matrix flow and transport.

6.6. Stochastic models

In the above discussion, the parameters relating to fluid flow and solute transport are assumed to be known with certainty, or that the most likely values of the parameters are used in the model. Such models are called deterministic models. However, in many cases we do not know all the controlling flow features at the appropriate spatial scales and we accept that a complete and accurate simulation of fluid flow or solute transport is not a realistic modelling objective (NRC, 1996).

In the stochastic approach (e.g., Neuman, 1987), the system is described in terms of physical parameters that are described by a spatially variable random field that is characterised by a probability density function. Thus, the stochastic continuum approach treats the parameter heterogeneity in the context of a statistical framework (Thangarajan, 2000). Multiple hydrogeologic and model realisations can be employed and run iteratively within a Monte Carlo framework so that uncertainty can be explicitly accounted for. In such approaches, the statistical parameters for the heterogeneous permeability field are determined and multiple realisations for the permeability field are then generated. The flow and transport problem is solved using a model for each realisation and a statistical analysis is carried out on the results from the simulations. Many tools have been developed for the geostatistical analysis of heterogeneous systems (e.g., Isaaks & Srivastava, 1989) and stochastic methods have been employed in numerous studies of hydrogeologic heterogeneity (e.g., Dagan, 1987; Neuman, 1987; Neuman *et al.*, 1985).

Both equivalent continuum and discrete fracture models can be applied stochastically. In stochastic continuum models, hydraulic conductivity and specific yield are described by statistical distributions, whereas in the stochastic discrete fracture approach, it is the fracture parameters that are statistically described, and varied accordingly. However, as NRC (1996) correctly points out, the validity of the stochastic approach is underpinned by the assumption that the equivalent statistics of the heterogeneous system do not vary spatially throughout that system.

6.7. Analytical solutions

Analytical solutions offer simple solutions for highly idealised systems. In these solutions, space and time are continuous variables, whereas in numerical models they are discretised into finite steps. However, simplifications are necessary and typically involve the need for very regular geometries, uniform material properties and simplified initial and boundary conditions. In many cases, these issues can limit the applicability of analytical solutions. However,

they are still very useful in providing quick and cheap solutions and in sensitivity analyses for determining the parameters that control system behaviour. Notably, they require minimal data for solutions, and in many studies there may only be enough data available to warrant the use of an analytical solution rather than a numerical one. It is suggested that where an analytical solution exists (e.g., for the concentration along a fracture with time after a solute slug is injected) that they be used either before or in parallel with more complicated numerical solutions to improve confidence in modelling predictions. In general, modelling should begin with simplest conceptual models and then add complexity as the collected data allows the refinement of the conceptual model. In this sense, analytical solutions can provide an excellent starting point for any modelling study. Furthermore, they can be very useful in bounding best and worst case behaviour in a system by quickly providing end-member responses (e.g., how long would it take for a slug of solute to move 100 m through a 2 mm fracture and the same distance in a 1 µm fracture?). Quick answers can be obtained using an appropriate analytical solution and can help to guide our understanding, as well as to provide guidance in the development of conceptual and numerical models.

In the context of flow and transport modelling in fractured rock, it should be noted that analytical solutions are probably most useful when dealing with discrete fracture approaches relating to solute transport phenomena. Existing ones for flow can be used when assuming EPM (e.g., Theis, Theim solutions for pumping tests) but their accuracy should be thought about carefully in relation to scale of application, and thus the assumption of an equivalent continuum existing at the scale of application.

6.8. Comparison of approaches

An important observation that has been made in fractured rock modelling literature is that equally successful interpretations of both flow and transport data can be made by very different conceptual and mathematical models. This is demonstrated by modelling of aquifer drawdown in fractured shale and phyllite at Wagga Wagga, NSW (Box 6.2, *see* pages 96 and 97). Two porous media models were used, which differed in the way they represented the heterogeneity. One used a seven-layer MODFLOW model (each layer being homogeneous and isotropic), while another used a two-layer fully 3D porous media model that incorporated both radial and vertical anisotropy. While both models were calibrated to the same pumping test data, they predicted very different drawdown distributions under operation of the dewatering scheme, which would operate at a much larger scale than the pumping test to which the models were calibrated. It should be emphasised that successful model

calibration does not mean that the model adequately reflects the distribution of aquifer properties. This is a major issue in fractured rock studies, because of the high spatial variability of aquifer properties.

Figure 6.3 compares simulations of flow in a fracture network with an impermeable rock matrix, carried out using equivalent porous media and discrete fracture network approaches. In the discrete fracture model, only selected fractures are included, in part because of our inability to accurately measure all the fractures in a system, and also due to computing requirements. The continuum model represents the fracture zone as a porous media with higher hydraulic conductivity. (Because the matrix blocks in the discrete fracture network simulation are impermeable, the hydraulic head is only defined in the fractures. Nevertheless, for the purpose of illustration, points of equal head in the fractures are connected using pseudo-contour lines that cross the impermeable matrix blocks.) Similar distributions of head are measured for both systems, which illustrates that both types of models can accurately simulate groundwater flow in fractured rock systems if adequately parameterised (Hsieh, 1998). Needless to say, the same cannot necessarily be said of solute transport.

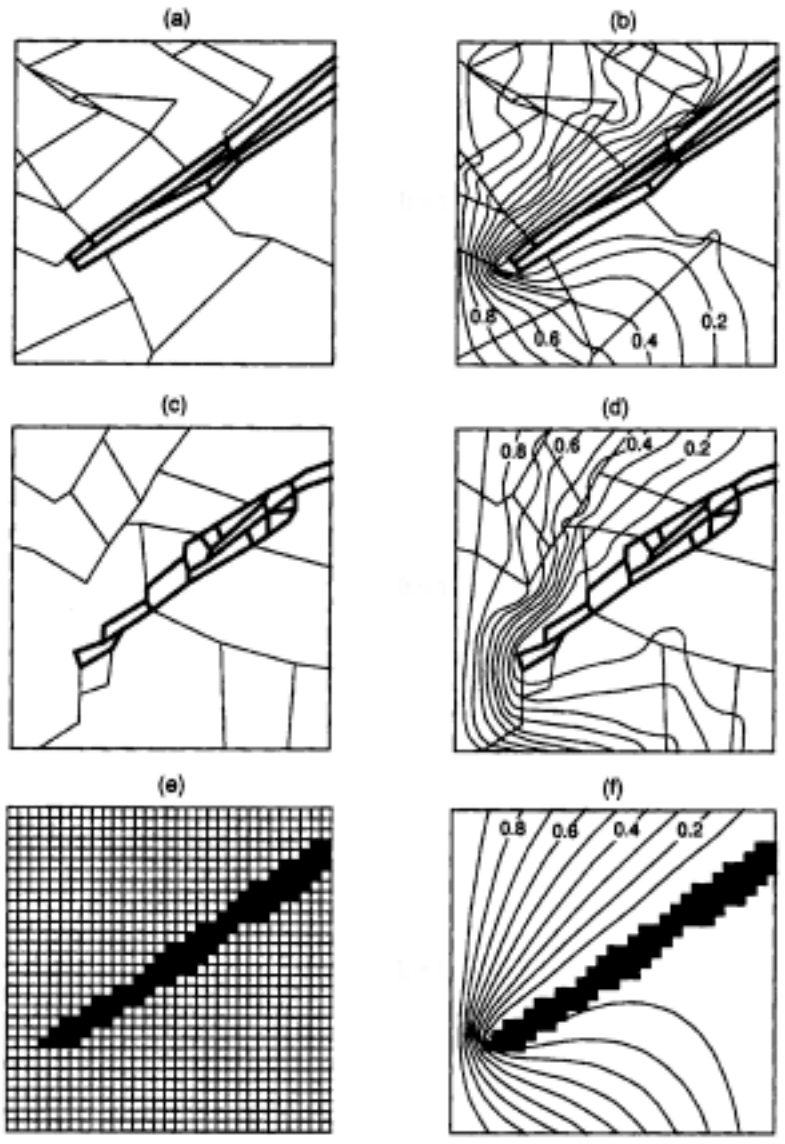

Figure 6.3. Simulation of flow in a fracture network with impermeable rock matrix. (a) The real fracture network. Thicker lines denote fractures that have a transmissivity that is 100 times greater than the rest of the network. (b) Distribution of hydraulic head in the fracture network, with constant head boundary conditions of 1 and 0 on the left and right hand boundaries, respectively, and linearly varying head (from 1 to 0) along the top and bottom. (c) Discrete fracture model. (d) Distribution of head in the discrete fracture model. (e) Continuum model. (f) Distribution of head in the continuum model. (From Hsieh, 1998).

Table 6.2. Advantages and disadvantages of different modelling approaches.

Model Type	Advantages	Disadvantages
Equivalent Porous Media	(i) Simplest approach, with lowest data requirements. (ii) If desired, high fracture zones can be simulated as zones with higher porosity and hydraulic conductivity. (iii) Most suitable for regional-scale applications of steady-state flow.	(i) Limited application to transient flow problems. (ii) Limited application when dealing with solute transport problems. (iii) Assumes that *REV* can be defined. Reliable predictions can only be made at scales greater than or equal to the scale of the assumed *REV*. Determination of aquifer parameters at these scales can be difficult.
Dual Porosity	(i) Suitable for systems where matrix has high porosity and permeability. (ii) Simplistic approach makes it appealing. (iii) Allows water and solute exchange between matrix and fractures. (iv) Can account for delayed hydraulic and solute responses caused by matrix storage.	(i) Tendency to over regularise and simplify the geometry. (ii) Difficult to quantify the parameters needed as input to DP model. (iii) Assumes that *REV* can be defined. Reliable predictions can only be made at scales greater than or equal to the scale of the assumed *REV*.
Discrete Fracture Network	(i) Explicit representation of individual fractures and fracture zones. (ii) May allow water and solute exchange between matrix and fractures. (iii) Good for conceptual process understanding within a simplified framework. (iv) Useful in determining equivalent continuum parameters based upon explicit characterisations.	(i) Requires the most detailed field knowledge, which is seldom available. (ii) Difficulty in extrapolating from smaller-scale parameter estimates to larger scales of interest. (iii) Computational power required to simulate complex networks requires the simplification of structure, especially where matrix diffusion is important.
Stochastic Approach	(i) Acknowledges uncertainty in the system. (ii) Possible to condition simulations with known data.	(i) Assumes that the equivalent statistics of the heterogeneous system do not vary spatially throughout that system.

Box 6.2. Example of a single continuum model incorporating anisotropy

To manage rising watertables and urban salinity at Wagga Wagga, NSW, a dewatering scheme has been constructed, and is now in operation. Two separate porous media models were produced to simulate the impact of dewatering. Paul (1997) employed a seven-layer MODFLOW model to simulate the vertical-horizontal anisotropy of the aquifer. However, given the expected sensitivity of this problem to aquifer anisotropy and the limited ability of MODFLOW to easily incorporate realistic anisotropy it was subsequently decided that another model would also be employed (Cook *et al.*, 2001b). FRAC3DVS, a discrete fracture network model, was applied in porous media mode (i.e., no fractures were simulated) for groundwater flow simulations because of its superior ability to handle anisotropy of hydraulic conductivity. Outcrop mapping in the Ordivician metasediments revealed that the aquifer was anisotropic along the bedding planes in a northwest to southeast orientation (maximum hydraulic conductivity at 330^{o}) and this information was easily incorporated into the FRAC3DVS simulations. A two-layer model was used: layer 1 representing a deeper unweathered shale and phyllite unit of 65m thickness and layer 2 representing a shallower weathered shale that extends from the surface to a depth of 36m. Both layers incorporated radial and vertical anisotropy. While the match between observed and predicted drawdown could be improved by the inclusion of additional layers in the model, the authors note that such a model would not necessarily have produced more reliable simulations for the dewatering test.

In order to calibrate the model, simulations were first found to reproduce drawdown observed during the seven-day pumping test described by Paul *et al.* (1996). FRAC3DVS was run in 2D mode with axisymmetric coordinates to simulate radial flow to a well. Vertical and radial hydraulic conductivity and specific yield values were varied until satisfactory fit with drawdown in seven observation wells was observed. These parameters were then used in a 3D model to simulate the proposed aquifer dewatering operation. Pumping is simulated for one year with nine wells each pumping at 0.6 L/s. The dewatering simulations predicted a drawdown of at least 2 m over an area of 55 hectares after one year of pumping (Fig. 6.4).

In contrast, the earlier MODFLOW simulation for the same pumping rate predicts a drawdown of 2 m over only 20.5 ha after one year of pumping (Paul, 1997). The difference between the previous modelling carried out by MODFLOW and that predicted by FRAC3DVS is due to the different ways in which the models incorporate heterogeneity. Both models were calibrated to the same pumping test data: the MODFLOW model used a seven layer system, whereas the FRAC3DVS model used a two layered system with vertical and hydraulic conductivity defined for each layer. It should be pointed out that the MODFLOW model is not a true 3D model and does not allow vertical conductivities (and hence anisotropy) to be specified (orthogonal to the layer rather than in the plane of the layer). As pointed out by Cook *et al.* (2001b), the large difference between the results of the two different modelling approaches is cause for concern and suggests that the pumping test was not sufficient to tightly constrain the models.

Box 6.2 continued next page

Box 6.2 (continued)

While the fit to the pumping test data achieved with the MODFLOW model simulations was noted to be superior to that achieved using FRAC3DVS, this was due to the large number of layers in the MODFLOW simulations. This model complexity is neither warranted nor justified on the basis of existing field data. There is no reason to believe that the superior fit to the pumping test data would lead to a more reliable simulation of the aquifer dewatering. It is not clear that pumping tests carried out over a small region would ever be sufficient to characterise a heterogeneous aquifer over a larger scale, and so accurate simulation of the small-scale data may not be of great value. For such a complex system, much larger-scale pumping tests with additional observation bores would be required to better characterise the aquifer on the scale of the dewatering test.

The case study clearly points out the limitations in modelling anisotropy in MODFLOW. Firstly, that in the plane of the layer, the anisotropy must be aligned with the numerical grid (along columns and rows oriented 90 degrees apart). Secondly, that because MODFLOW is not a true 3D model, vertical anisotropy (orthogonal to the plane of the layer) cannot be simulated. Furthermore, issues associated with scale are immediately apparent. The scale of the pumping test carried out to determine properties of the aquifer (and used in model calibration) is not consistent with either the scale of the dewatering test or the scale of the model domain. Thus it is likely that the hydraulic conductivity (and storativity) values used globally throughout the model based upon more local smaller-scale calibration are not representative of parameters at the dewatering scale or larger model domain. This is a potentially significant source of model prediction error. There is limited field data with which to determine the larger-scale applicability of this model.

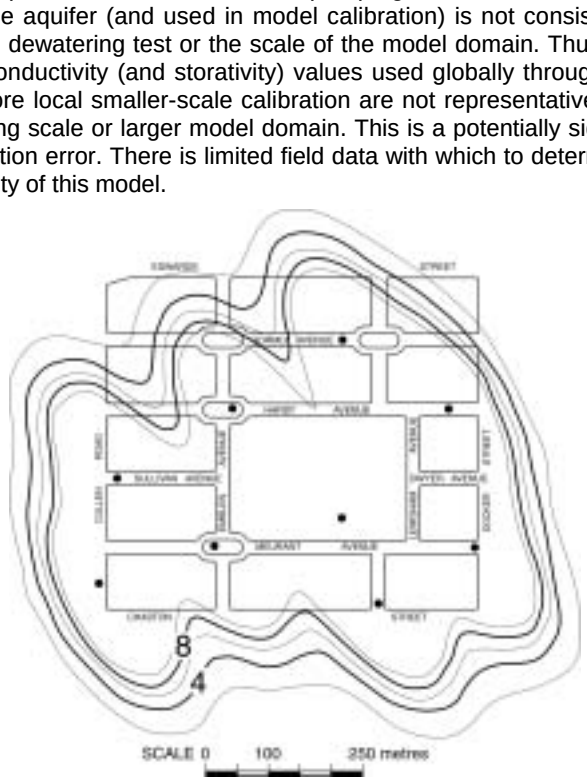

Figure 6.4. Predicted aquifer drawdown for the Wagga Wagga dewatering operation after 1 year of pumping. Circles denote pumping bore locations. Contour interval is 2 m, with drawdown contours between 2 and 10 m shown. (After Cook *et al.*, 2001b.)

6.9. Conclusion

There are numerous modelling approaches available for the simulation of flow and transport in fractured rock aquifers ranging from equivalent porous media (usually least data intensive) through to dual porosity and finally discrete fracture network models (usually most data intensive). Each offers advantages and disadvantages but the modelling approach taken will depend critically upon three key factors: (i) whether the study is concerned with bulk hydraulic (flow) or solute transport, (ii) the steady-state or transient nature of the problem and (iii) the scale of interest (near-well, local or regional).

For flow problems concerned with bulk average volumetric behaviour over larger spatial scales, an equivalent porous media approach will usually suffice. This approach works best for steady state flow systems but may also be adequate in some transient systems where the storage effects in the matrix are considered negligible. Where storage effects are not insignificant, a dual porosity approach, where fluid and solute exchange between matrix and fracture is allowed, is usually preferred. However, difficulties are typically encountered in over-regularising the geometry of the system and in determining the necessary parameters for this modelling approach. Difficulties in both these approaches can arise when working at very local scales (near-well) where important fractures controlling the flow system are not explicitly included in the model. In such cases, a discrete fracture network model may be employed as the smaller scale of the study usually permits the necessary conducting fractures to be identified and explicitly included in the model. One particular difficulty that has been noted is the use of equivalent porous media approaches in solute transport studies which tends to be highly problematic. In transport phenomena, the connected fractures control solute migration and these occur at scales much smaller than the associated representative elementary volume employed by the equivalent porous medium approach. Thus, a model may be successfully calibrated to match observed hydraulic behaviour (by varying recharge and/or hydraulic conductivity) but is most likely to be in significant error for subsequent application in the prediction of solute transport phenomena. In systems where solute transport is of primary interest, the conducting fracture pathways must be explicitly identified and incorporated into a discrete fracture network approach. Such approaches require more data but are typically employed within a stochastic framework by generating multiple realisations based upon field observations of fracture properties and a detailed analysis of model uncertainty. Analytical solutions may also be a very useful step in modelling studies where solute transport is of interest. They help to provide some ball-park estimates on system behaviour and may guide associated numerical modelling.

In all practical modelling, it is necessary to keep the complexity of the model consistent with the amount of data available. A key limiting factor in almost all hydrogeologic studies is data intensity and most importantly, a usual lack of it which typically limits the ability of discrete fracture network models to be applied at larger regional scales. A comparison of different conceptual models or models of different complexity can be a useful step in helping us understand the reliability, accuracy and inherent uncertainty in our model predictions. An inherent problem in all modelling is the scale at which the model is applied and the scale at which the input data collected in the field is relevant. Care must be paid to acknowledging both the relevant scale of field data and the scale of interest in the model. Difficulties are usually encountered in calibration and prediction where the scales of collected data and model application do not match. However, an awareness of these scaling issues allows us to be mindful of them in the calibration process. Depending upon regional connectivity of fractures, or lack of, and the near-well fracture intensity, there may be significant differences between the observed field estimates and calibrated model values. In such cases where there are significant scale discrepancies, we would not and should not expect the calibrated model values (for say hydraulic conductivity) to agree with those measured in the field.

7. REFERENCES

Andreola F., Leonelli C., Romagnoli M. and Miselli P. (2000) Techniques used to determine porosity. *Amer. Ceramic. Soc. Bull.*, July:49–52.

Banks D. (1998) Predicting the probability distribution of yield from multiple boreholes in crystalline bedrock. *Ground Water*, 36(2):269–274.

Barton C.C. (1996) Characterizing bedrock fractures in outcrop for studies of groundwater hydrology: an example from Mirror Lake, Grafton County, New Hampshire, In: Morganwalp D. and Aronson D.A. (ed.) U.S. Geological Survey Toxic Substances Program, U.S. Geological Survey, Water Resources Investigations Report 94–4015, 81–87.

Barton N. and Choubey V. (1977) The shear strength of rock joints in theory and practice. *Rock Mechanics*, 10:1–54.

Bidaux P. and Drouge C. (1993) Calculation of low-range flow velocities in fractured carbonate media from borehole hydrochemical logging data comparison with thermometric results. *Ground Water*, 31(1):19–26.

Bishop P.K. and Lloyd J.W. (1990) Chemical and isotopic evidence for hydrogeological processes occurring in the Lincolnshire Limestone. *J. Hydrol*., 121:293–320.

Bradbury K.R. and Muldoon M.A. (1992) Hydrogeology and groundwater monitoring of fractured dolomite in the Upper Door priority watershed, Door County, Wisconsin. Wisconsin Geological and Natural History Survey Open File Report 1992–2.

Bradbury K.R., Muldoon M.A. Zaporozec A. and Levy J. (1991) Delineation of wellhead protection areas in fractured rocks. Report EPA 570/9–91–009. United States Environmental Protection Agency, Washington, DC, 144pp.

Bradbury M.H. and Green A. (1985) Measurement of important parameters determining aqueous phase diffusion rates through crystalline rock matrices. *J. Hydrol.*, 82:39–55.

Brahana J.V., Thrailkill J., Freeman T. and Ward W.C. (1988) Carbonate rocks. In: Back W., Rosenheim J.S. and Seaber R.R. (ed.) *The Geology of North America*. Volume O–2, Hydrogeology. Geological Society of America, 333–352.

Bromley J., Mannström B., Nisca D. and Jamtlid A. (1994) Airborne geophysics: application to a ground-water study in Botswana. *Ground Water*, 32(1):79–90.

Brown S. (1989) Transport of fluid and electrical current in a single fracture. *J. Geophys. Res*., 94:9429–9438.

Buck L. (1999) Physical Features of Volcanism and their Relationship to Groundwater, Atherton Basalt Province, North Queensland. BSc Honours thesis, Queensland University of Technology. 178pp.

Cacas M.C., Ledoux G., de Marsily G., and Tillie B. (1990) Modeling fracture flow with a stochastic discrete fracture network: calibration and validation. 1: The flow model. *Water Resour. Resear*., 26: 479–489.

Caswell B. (1992) Protecting fractured-bedrock wells. *Water Well Journal*, 46(5):42–45.

Clauser C. (1992) Permeability of crystalline rocks. *EOS*, *Trans. Amer. Geophys. Union*, 73(21):233–240.

Cook P.G. and Herczeg A.L. (2000) Environmental Tracers in Subsurface Hydrology. Kluwer, Boston. 529pp.

Cook P.G. and Simmons C.T. (2000) Using environmental tracers to constrain flow parameters in fractured rock aquifers; Clare Valley, South Australia. In: Faybishenko B., Witherspoon P.A. and Benson S.M. (ed.) *Dynamics of Fluids in Fractured Rock*. Geophysical Monograph 122, American Geophysical Union, 337–347.

Cook P.G., Love A.J. and Dighton J.C. (1999) Inferring ground water flow in fractured rock from dissolved radon. *Ground Water*, 37(4):606–610.

Cook P.G., Solomon D.K., Sanford W.E., Busenberg E., Plummer L.N. and Poreda R.J. (1996) Inferring shallow groundwater flow in saprolite and fractured rock using environmental tracers. *Water Resour. Resear*., 32(6):1501–1509.

Cook P.G., Herczeg A.L. and McEwan K.L (2001a) Groundwater recharge and stream baseflow, Atherton Tablelands, Queensland. CSIRO Land and Water, Tech. Rep. 08/01.

Cook P.G., Stauffacher M., Therrien R., Halihan T., Richardson P., Williams R.M. and Bradford A. (2001b) Groundwater recharge and discharge in a saline, urban catchment; Wagga Wagga, New South Wales. CSIRO Land and Water, Tech. Rep. 39/01.

Dagan G. (1987) Theory of solute transport in water. *Annual Reviews of Fluid Mechanics*, 19:183–215.

Davis S.N. (1988) Sandstones and shales. In: Back W., Rosenhein J.S. and Seaber P.R. (ed.) *The Geology of North America*. Volume O–2, Hydrogeology. Geological Society of America, 323–332.

Davis S.N. and De Wiest R.J.M. (1966) Hydrogeology. John Wiley, New York, 463pp.

Dearborn L.L. (1988) Borehole geophysical investigation of fractured rock at an EPA superfund site in Massachusetts. Proc. 2nd National Outdoor Action Conf. on Aquifer Restoration, Ground Water Monitoring and Geophysical Methods, Dublin, Ohio. National Water Well Association, 875–895.

Drost W., Klotz D., Koch A., Moser H., Neumaier F. and Rauert W. (1968) Point dilution methods of investigating ground water flow by means of radioisotopes. *Water Resour, Resear*., 4(1):125–146.

Drury M.J. (1989) Fluid flow in crystalline crust: detecting fractures by temperature logs. In: Beck A.E., Garven G. and Stegena L. (ed.) Hydrogeological regimes and their subsurface thermal effects. Geophysical monograph 47. International Union of Geodesy and Geophysics and American Geophysical Union, Washington DC, 129–135.

Ellins K.K., Roman-Mas A. and Lee R. (1990) Using ^{222}Rn to examine groundwater/surface discharge interaction in the Rio Grande De Manati, Puerto Rico. *J. Hydrol.*, 115:319–341.

Engel R., McFarlane D.J. and Street G.J. (1989) Using geophysics to define recharge: and discharge areas associated with saline seeps in south-western Australia. In: Sharma M.L. (ed.) *Groundwater Recharge*. A.A. Balkema, Rotterdam, 25–39.

Faybishenko B., Doughty C., Steiger M., Long J.C.S., Wood T., Jacobsen J., Lore J. and Zawislanski P.T. (1999) Conceptual model of the geometry and physics of water flow in a fractured basalt vadose zone: Box Canyon site, Idaho. Lawrence-Berkeley National Laboratory, Report LBNL–42925, 51pp.

Feenstra S., Cherry J.A., Sudicky E.A. and Haq Z. (1984) Matrix diffusion effects on contaminant migration from an injection well in fractured sandstone. *Ground Water*, 22(3):307–316.

Fontes J.C., Bortolami G.C. and Zuppi G.M. (1979) Isotope hydrology of the Mont Blanc Massif. Isotope Hydrology 1978. IAEA, Vienna, 411–436.

Freeze R.A. and Cherry J.A. (1979) Groundwater. Prentice Hall, New Jersey. 604pp.

Gale J. E., Rouleau A. and Witherspoon P.A. (1982) Fundamental hydraulic characteristics of fractures from field and laboratory investigations. Papers of the Groundwater in Fractured Rock Conference; Canberra, Australia. Australian Government Publishing Service, Canberra, 95–108.

Gburek W.J. and Folmar G.J. (1999) A ground water recharge field study: site characterization and initial results. *Hydrol. Proc*., 13:2813–2831.

Gburek W.J., Folmar G.J. and Urban J.B. (1999) Field data and ground water modeling in a layered fractured aquifer. *Ground Water*, 37:175–184.

Genereux D.P., Hemond H.F. and Mulholland P.J. (1993) Spatial and temporal variability in streamflow generation on the West Fork of Walker Branch Watershed. *J. Hydrol*., 142:137–166.

Greswell R., Yoshida K., Tellam J.H. and Lloyd J.W. (1998) The micro-scale hydrogeological properties of the Lincolnshire Limestone UK. *Quarterly J. Eng. Geol*., 31:181–197.

Grisak G.E. and Pickens J.F. (1980) Solute transport through fractured media. 1. The effect of matrix diffusion. *Water Resour. Resear*., 16(4):719–730.

Habberjam G.M. (1972) The effects of anisotropy on square array resistivity measurements. *Geophysical Prospecting*, 20:249–266.

Halihan T., Mace R.E. and Sharp J.M. Jr. (2000). Flow in the San Antonio segment of the Edwards aquifer: matrix, fractures, or conduits? In: Wicks C.M. and Sasowsky I.D. (ed.) *Groundwater Flow and Contaminant Transport in Carbonate Aquifers*. AA Balkema, 129–146.

Hamada H. (2000) Estimation of groundwater flow rate using the decay of ^{222}Rn in a well. *J. Environmental Radioactivity*, 47:1–13.

Healy R.W. and Cook P.G. (2002) Using groundwater levels to estimate recharge. *Hydrogeology J*., 10(1):91–109.

Hendry M.J. (1982) Hydraulic conductivity of a glacial till in Alberta. *Ground Water*, 20(2):162–169.

Hodgson L. and Finlayson B. (1990) Single well dilution: its use in groundwater investigations for salinity management. *Aust. J. Soil Water Con*., 3(2):37–43.

Hsieh P.A. (1998) Scale effects in fluid flow through fractured geologic media. In: Sposito G. (ed.) *Scale Dependence and Scale Invariance in Hydrology*. Cambridge University Press, Cambridge, UK, 335–353.

Hsieh P.A. (2000) A brief survey of hydraulic tests in fractured rocks. In: Faybishenko B., Witherspoon P.A. and Benson S.M. (ed.) *Dynamics of Fluids in Fractured Rock*. Geophysical Monograph 122, American Geophysical Union, 59–66.

Isaaks E.H. and Srivastava R.M. (1989) An Introduction to Applied Geostatistics, Oxford University Press, New York, 561pp.

Kellgren N. and Sander P. (2000) Benefits of incorporating remote sensing techniques as a methodological approach for improving borehole siting in fractured rock aquifers. In: Sililo O. (ed.) *Groundwater: Past Achievements and Future Challenges*. Proc. 30th IAH Congress, Cape Town, South Africa, 26 Nov–1 Dec 2000. Balkema, Rotterdam, 175–180.

Kumar H., Sarma D. and Carlsson L. (2000) A geophysical perspective in siting high yielding boreholes in the lower Karoo aquifer in western Botswana. In: Sililo O. (ed.) *Groundwater: Past Achievements and Future Challenges*. Proc. 30th IAH Congress, Cape Town, South Africa, 26 Nov–1 Dec 2000. Balkema, Rotterdam, 193–198.

Lane J.W., Haeno F.P.J. and Watson W.M. (1995) Use of a square-array direct-current resistivity method to detect fractures in crystalline bedrock in New Hampshire. *Ground Water*, 33(3):476–485.

La Pointe P.R. and Hudson J.A. (1985) Characterization and interpretation of rock mass joint patterns. Geological Society of America Special Paper 199. Geological Society of America, 37pp.

Lawrence E., Poeter E. and Wanty R.B. (1991) Geohydrologic, geochemical, and geological controls on the occurrence of radon in ground water near Conifer, Colorado, USA. *J. Hydrol.*, 127:367–386.

Lee C.H. and Farmer I. (1993) Fluid Flow in Discontinuous Rocks. Chapman and Hall, London.

Liu K., Boult P., Painter S. and Paterson L. (1996) Outcrop analog for sandy braided stream reservoirs: permeability patterns in the Triassic Hawkesbury Sandstone, Sydney Basin, Australia. *AAPG Bull*. 80(12):1850–1866.

Love A.J., Herczeg A.L., Armstrong D., Stadter F. and Mazor E. (1993) Groundwater flow regime within the Gambier Embayment of the Otway Basin, Australia: evidence from hydraulics and hydrochemistry. *J. Hydrol*. 143:297–338.

Love A.J., Cook P.G., Harrington G.A. and Simmons C.T. (2002) Groundwater flow in the Clare Valley. Department for Water Resources, South Australia. Report DWR02.03.0002, 43pp.

McDonald M.G. and Harbaugh A.W. (1988) A modular three-dimensional finite-difference ground-water flow model. U.S. Geological Survey, Techniques of Water-Resources Investigations Book 6, Chapter A1, 586 pp.

McKay L.D., Cherry J.A., Bales R.C., Yahya M.T. and Gerba C.P. (1993) A field example of bacteriophage as tracers of fracture flow. *Environ. Sci. Technol*., 27(6):1075–1079.

McKay L.D., Sanford W.E. and Strong J.M. (2000) Field-scale migration of colloidal tracers in a fractured shale saprolite. *Ground Water*, 38(1):139–147.

Martin R.R. (1998) Willunga Basin – Status of Groundwater Resources 1998. Primary Industries and Resources SA, Report Book 98/28.

Merin I.S. (1992) Conceptual model of ground water flow in fracture siltstone based on analysis of rock cores, borehole geophysics and thin sections. *Ground Water Monit. Remediat*., 12(4):118–125.

Michalski A. (1990) Hydrogeology of the Brunswick (Passaic) formation and implications for ground water monitoring practice. *Ground Water Monit. Remediat*., Fall 1990:134–143.

Molz F.J., Boman G.K. and Waldrop W.R. (1994) Borehole flowmeters: field application and data analysis. *J. Hydrol.*, 163:347–3771.

Moore G.K. (1992) Hydrograph analysis in a fractured rock terrane. *Ground Water*, 30(3):390–395.

Moser H., Wolf M., Fontes J.-C., Florkowski T. and Payne B.R. (1989) Deuterium, oxygen-18, and tritium in Stripa groundwater. *Geochim. Cosmochim. Acta*, 53(8):1757–1763.

National Research Council (NRC) (1996) Rock Fractures and Fluid Flow: Contemporary Understanding and Applications. National Academy Press, Washington DC. 551pp.

Neretnieks I. (1981) Age dating of groundwater in fissured rock: influence of water volume in micropores. *Water Resour. Resear*., 17(2):421–422.

Neuman S.P. (1987) Stochastic continuum representation of fractured rock permeability as an alternative to the REV and fracture network concepts. In: Rock Mechanics, Proceedings of the 28th U.S. Rock Mechanics Symposium, Rotterdam, A.A. Balkema, 533–561.

Neuman S.P., Simpson E.S., Hsieh P.A., Jones J.W. and Winter C.L. (1985) Statistical analysis of hydraulic test data from crystalline rock near Oracle, Arizona. International Association of Hydrogeologists, Memoires, vol XVII.

Novakowski K., Lapcevic P., Bickerton G., Voralek J., Zanini L. and Talbot C. (1999) The Development of a Conceptual Model for Contaminant Transport in the Dolostone Underlying Smithville, Ontario. Unpublished.

Novakowski K.S. and van der Kamp G. (1996) The radial diffusion method. 2. A semianalytical model for the determination of effective diffusion coefficients, porosity, and adsorption. *Water Resour. Resear*., 32 (6): 1823–1830.

Parker B.L., Gillham R.W. and Cherry J.A. (1994) Diffusive disappearance of immiscible-phase organic liquid in fractured geologic media. *Ground Water*, 32(5):805–820.

Paul D. (1997) Wagga Wagga Urban Salinity. Implications for groundwater pumping: scenarios. Department of Land and Water Conservation. Report CNR97.001.

Paul D., Williams R.M. and Hamilton S. (1996) Wagga Wagga Urban Salinity. Implications for Groundwater Pumping. Department for Land and Water Conservation, Report TS96.071.

Pearce B.R. (1982) Fractured rock aquifers in central Queensland. Papers of the Groundwater in Fractured Rock Conference, Canberra, Australia. Australian Government Publishing Service, Canberra, 161–172.

Pedler W.H., Barvenik M.J., Tsang C.F. and Hale F.V. (1990) Determination of bedrock hydraulic conductivity and hydrochemistry using wellbore fluid logging method. In: Fourth National Outdoor Action Conference on Aquifer Restoration, Ground Water Monitoring and Geophysical Methods, Las Vegas, Nevada. NWWA, 39–53.

Prats M. (1972) The influence of oriented arrays of thin impermeable shale lenses or of highly conductive natural fractures on apparent permeability anisotropy. *J. Pet. Technol*., 24(10):1219–1221.

Price M., Low R.G. and McCann C. (2000) Mechanisms of water storage and flow in the unsaturated zone of the Chalk aquifer. *J. Hydrol*., 233:54–71.

Rayne T.W., Bradbury K.R. and Muldoon M.A. (2001) Delineation of capture zones for municipal wells in fractured dolomite, Sturgeon Bay, Wisconsin, USA. *Hydrogeology J*., 9:432–450.

Renshaw C.E. (1998) Sample bias and the scaling of hydraulic conductivity in fractured rock. *Geophys. Resear. Lett*., 25(1):121–124.

Robins N.S. and Buckley D.K. (1988) Characteristics of the Permian and Triassic aquifer of south-west Scotland. *Quarterly J. Eng Geol*, 21:329–335.

Ruland W.W., Cherry J.A. and Feenstra S. (1991) The depth of fractures and active ground-water flow in a clayey till plain in southwestern Ontario. *Ground Water*, 29(3):405–417.

Sami K. (1996) Evaluation of the variations in borehole yield from a fractured Karoo Aquifer, South Africa. *Ground Water*, 34(1):114–120.

Sami K. and Hughes D.A. (1996) A comparison of recharge estimate to a fractured sedimentary aquifer in South Africa from a chloride mass balance and an integrated surface-subsurface model. *J. Hydrol*., 179:111–136.

Sanford W.E. and Solomon D.K. (1995) Noble gas solute tracer experiment in a fractured, weathered shale near Oak Ridge, Tennessee. In: Intl Assoc. Hydrogeol. Solutions ’95 Conference, Edmonton, Canada.

Scanlon B.R., Healy R.W. and Cook P.G. (2002) Choosing appropriate techniques for quantifying groundwater recharge. *Hydrogeology J*., 10(1):18–39

Shevenell L. (1996) Analysis of well hydrographs in a karst aquifer: estimates of specific yields and continuum transmissivities. *J. Hydrol*., 174:331–335.

Shugg A. (1996) Hydrogeology of the Dandenong Ranges Fractured Rock Aquifers and the Comparison with Similar Aquifers in Victoria. MSc thesis, University of Technology, Sydney.

Sidle W.C. and Lee P.Y. (1995) Estimating local ground-water flow conditions in a granitoid: preliminary assessments in the Waldoboro Pluton Complex, Maine. *Ground Water*, 33(2):291–303.

Simmons C.T., Hee Hong Wye D., Cook P.G. and Love A.J. (1999) Signal propagation and periodic response in aquifers: the effect of fractures and signal measurement methods. In: Water 99 Joint Congress, Brisbane, Australia, 727–732.

Singhal B.B.S. and Gupta R.P. (1999) Applied Hydrogeology of Fractured Rocks. Kluwer, Dordrecht, 400pp.

Skagius K. and Neretnieks I. (1986) Porosities and diffusivities of some nonsorbing species in crystalline rocks. *Water Resour. Resear*., 22(6):389–398.

Snow D.T. (1968) Rock fractures spacings, openings and porosities. *J. Soil Mechanics and Foundations Division*, SM1:73–91.

Taylor R.W. and Fleming A.H. (1988) Characterizing jointed systems by azimuthal resistivity surveys. *Ground Water*, 26(4):464–474.

Thangarajan M. (2000) Approaches for modelling of hard rock aquifer system. *J. Geol. Soc. India*, 56:123–138.

Tiedeman C.R., Goode D.J. and Hsieh P.A. (1998) Characterizing a ground water basin in a New England mountain and valley terrain. *Ground Water*, 36:611–620.

Torgersen T., Benoit J. and Mackie D. (1992) Lithological control of groundwater ^{222}Rn concentrations in fractured rock media. In: Isotopes of Noble Gases as Tracers in Environmental Studies. IAEA, Vienna, 263–283.

Trainer F.W. (1988) Plutonic and metamorphic rocks. In: Back W., Rosenhein J.S. and Seaber P.R. (ed.) *The Geology of North America*. Volume O–2, Hydrogeology. Geological Society of America, 367–380.

Tsang C.F., Hufschmied P. and Hale F.V. (1990) Determination of fracture inflow parameters with a borehole fluid conductivity logging method. *Water Resour. Resear*., 26(4):561–578.

Tsang Y.W., Tsang C.F. and Hale F.V. (1996) Tracer transport in a stochastic continuum model of fractured media. *Water Resour. Resear*., 32(10):3077–3092.

URS (2002) State of the Catchment – Playford Hills. Unpublished report, prepared on behalf of Northern Adelaide and Barossa Catchment Water Management Board, City of Playford.

Van der Kamp G. (1992) Evaluating the effects of fractures on solute transport through fractured clayey aquitards. Proc. 1992 Conf. of the International Association of Hydrogeologists, Canadian National Chapter, Hamilton, Ontario.

Walker G.P.L. (1973) Length of lava flows. *Phil. Trans. R. Soc. Lond. A*., 274:107–118.

Waters P., Greenbaum D., Smart P.L. and Osmaston H. (1990) Applications of remote sensing to groundwater hydrology. *Remote Sensing Reviews*, 4(2):223–264.

Wilson T., Heinson G., Endres A. and Halihan T. (2000) Fractured rock geophysical studies in the Clare Valley, South Australia. *Exploration Geophysics*, 31(1–2):255–259.

Wood W.W. and Fernandez L.A. (1988) Volcanic Rocks. In: Back W., Rosenhein J.S. and Seaber P.R. (ed.) *The Geology of North America*. Volume O–2, Hydrogeology. Geological Society of America, 353–365.

Zuber A. and Motyka J. (1998) Hydraulic parameters and solute velocities in triple-porosity karstic-fissured-porous carbonate aquifers: case studies in southern Poland. *Environmental Geology*, 34(2/3):243–250.